1968

Flow Over a Rough Porous Flat Plate with Surface Mass Transfer

Francis K. King

FLOW OVER A ROUGH POROUS FLAT PLATE WITH SURFACE MASS TRANSFER

BY

FRANCIS K. KING

A thesis submitted
in partial fulfillment of the requirements for the
degree Master of Science, Major in
Mechanical Engineering, South
Dakota State University

1968

FLOW OVER A ROUGH POROUS FLAT PLATE

WITH SURFACE MASS TRANSFER

This thesis is approved as a creditable and independent investigation by a candidate for the degree, Master of Science, and is acceptable as meeting the thesis requirements for this degree, but without implying that the conclusions reached by the candidate are necessarily the conclusions of the major department.

Thesis Advisor — Date

Head, Mechanical Engineering Department — Date

ACKNOWLEDGMENT

The author is indebted to Dr. Edward Lumsdaine for his initiation, guidance and counseling which led to the work presented here.

The author wishes to thank Professor John F. Sandfort for his guidance throughout the author's graduate program.

Special thanks go to The Boeing Company, Seattle, Washington, for donating the acoustic panels used in the experiments.

This research was conducted as part of the project "Momentum Transfer for Flow over a Rough Porous Material with Variable Surface Mass Transfer", funds for which were awarded to Dr. Lumsdaine under a grant from South Dakota State University.

FKK

TABLE OF CONTENTS

TABLE OF FIGURES

LIST OF TABLES

CHAPTER I

INTRODUCTION

Flow over porous surfaces with suction or injection has been known for many years in practical applications. By injecting a fluid into the boundary layer to reduce the wall shear, the wall temperature of materials which are subjected to flow of hot gases or high-speed fluids is reduced; thus, relatively low-temperature materials can be used for turbine blades, combustion chambers and after-burners of gas turbines. By sucking a fluid from the boundary layer to prevent flow separation, wall drag as well as shear stress throughout the boundary layer are reduced, and, for example, higher airfoil lift can be obtained during take-off of an aircraft. Recently, with the increasing demands for a quiet engine by aircraft manufacturers as well as by the public, acoustic materials with tuned backing have been introduced into turbofan engines to damp out the noise emanating from the fan. With high-speed air flowing parallel to these rather rough and porous acoustic materials, alternative acoustic pressure acts as a force field to drive the air through the material. As a result, acoustic energy is consumed and the noise is damped out to some extent. This phenomenon can be simulated by using a porous surface under the alternating action of injection and suction. So far, the aerodynamic properties of these acoustic materials are not very well known.

Many studies in boundary layer theory have been concerned with flow over a porous surface through which fluid is injected or sucked. In 1936, Griffith and Meredith [1]* first obtained so-called "asymptotic suction profiles" for constant-velocity suction at the wall, stated as

$$U = U_o[1 - \exp(V_w\, y/\upsilon)] \qquad (1\text{-}1)$$

Later, Schlichting [2], Kay [3], Thwaites [4], and Ringleb [5] solved the problem by approximation methods. However, they restricted their studies to laminar boundary layer problems. Recently, Mickley and Davis [6] and Rotta [7] obtained solutions for turbulent flow, but did not take roughness into account. In general, it had been assumed that all material surfaces were to be made as smooth as possible; attention was focused on deriving the "law of the wall" formula for flow over smooth surfaces under injection or suction. In most practical flow applications, however, the Reynolds number is usually high enough that the surface must be considered rough and the flow must be considered turbulent.

Without considering surface mass transfer, Driest [8] derived an analytical solution for turbulent flow over a rough plate. To obtain a better understanding of the effect of roughness on shear stress, Lumsdaine** initiated a pro-

---

* Numbers in brackets refer to the References
**Author's thesis advisor

ject "Momentum Transfer for Flow over a Rough Porous Material with Variable Surface Mass Transfer". In the proposal to this project, he first stated the concept of combining roughness with injection or suction in a universal law of the wall. The present studies are a part of his project: to find, using theoretical analysis, empirical expressions for the velocity profile and the shear stress distribution and to substantiate this analysis with experimental data. In this study, Prandtl's boundary layer theory and turbulent mixing-length theory are assumed to hold. The governing equations for flow over a porous surface with injection or suction are the same as those for flow over an impermeable surface. The boundary conditions are modified to account for injection or suction. At the wall, the velocity component along the surface remains zero (no slip), but the velocity component perpendicular to the surface is assumed to be the injection or suction velocity V_w. When the fluid flows over a porous surface with injection or suction, the resultant flow at the wall is assumed to be wholly normal to the wall. This assumption can be justified by the fact that the pressure gradient across the porous surface is usually large.

Because this study assumes a turbulent boundary layer, all flow parameters are understood to be mean time-average values. As the first stage of Lumsdaine's project, the problem is also simplified by assuming a zero pressure gradient

and incompressible, steady, and homogeneous two-dimensional flow. According to the usual boundary layer theory assumptions, injection or suction across the porous surface is assumed to be small, of the order $U_\infty R_x^{-\frac{1}{2}}$; thus its "sink effect" or "source effect" on the main flow outside the boundary layer can be neglected and only its influence on the sublayer is considered. In practice, however, injection or suction may have considerable effect on the main flow, but these effects are very difficult to take into account.

A wind tunnel was designed by the author for studying the aerodynamic properties of porous plates; it was constructed and installed in the Heat Power Laboratory, Mechanical Engineering, South Dakota State University. With a total pressure tube, the velocity profile throughout the boundary layer and the average shear stress at the wall were determined. A Preston tube was used to measure local shear stress. There are only limited experimental data available on the relation between roughness and shear stress for flow over porous surfaces with injection or suction. Because of instrumentation problems, it proved difficult to obtain data in the sublayer. Nevertheless, the present study can be considered to be a first step toward further investigations into problems of this type.

NOMENCLATURE

Symbol		Units
A	= Van Driest constant	ft
A_*	= Dimensionless Van Driest constant	
C_f	= Local friction coefficient	
C_f'	= Average friction coefficient	
D	= Disturbance constant	ft
D_*	= Dimensionless disturbance constant, $\sqrt{\tau_w/\rho}\, D/\upsilon$	
DF	= Damping factor defined by Eq. (2-18)	
d	= Inside Preston tube diameter	in
E	= Average roughness height	ft
E_*	= Dimensionless average roughness height, $\sqrt{\tau_w/\rho}\, E/\upsilon$	
L	= Length of plate	ft
P	= Pressure	lb_f/ft^2
P_t	= Total pressure	lb_f/ft^2
P_s	= Static pressure	lb_f/ft^2
P_{t_o}	= Total pressure at free stream	lb_f/ft^2
RAYL	= RAYL number of acoustic panel	
RF	= Damping factor defined by Eq. (2-24)	
R_x	= Reynolds number, $U_o x/\upsilon$	
U	= Velocity component parallel to wall	ft/sec
U_o	= Free stream velocity parallel to wall	ft/sec
U_*	= Dimensionless velocity, $U/\sqrt{\tau_w/\rho}$ (shear velocity)	

Symbol		Units
U_{o*}	= Dimensionless free stream velocity, $U_o/\sqrt{\tau_w/\rho}$	
U'	= Fluctuation velocity of U	ft/sec
V	= Velocity component perpendicular to wall	ft/sec
V_*	= Dimensionless velocity, $V/\sqrt{\tau_w/\rho}$	
V_w	= Velocity component at the wall perpendicular to the wall	ft/sec
V_{w*}	= Dimensionless velocity, $V_w/\sqrt{\tau_w/\rho}$	
V'	= Fluctuation velocity of V	ft/sec
x	= Coordinate along the wall	ft
y	= Coordinate perpendicular to the wall	ft
y_*	= Dimensionless distance, $\sqrt{\tau_w/\rho}\ y/\upsilon$	

Greek Letters

σ	= Displacement thickness	ft
σ_s	= Thickness of the sublayer	ft
σ_{s*}	= Dimensionless thickness of the sublayer	
θ	= Momentum thickness	ft
ϵ	= Eddy viscosity, defined in Eq. (2-27)	lb_f-sec/ft^2
χ	= Universal constant from mixing-length theory	
μ	= Dynamic viscosity	lb_f-sec/ft^2
υ	= Kinematic viscosity, μ/ρ	ft^2/sec
ρ	= Density	lb_m/ft^3
τ	= Total shear stress	lb_f/ft^2
τ_t	= Turbulent shear stress (Reynolds' stress)	lb_f/ft^2

Symbol		Units
τ_l	= Laminar shear stress	lb_f/ft^2
τ_w	= Shear stress at the wall	lb_f/ft^2
ϕ	= Energy dissipation	lb_f^2/ft^4
Φ	= Total energy dissipation in the sublayer	lb_f^2/ft^3

CHAPTER II

ANALYSIS

A uniform stream flows over a flat plate at zero incidence with speed U_o. This free stream velocity is not to be affected by the presence of the plate and the fluid which is injected or sucked through the plate. The fluid is assumed to be unlimited in extent. The origin of the coordinates is taken at the leading edge of the plate, with x measured downstream along the plate and y measured perpendicular to and away from the plate (see Fig. 2-1). In the absence of a pressure gradient, the equation of steady motion and the equation of continuity in the boundary layer are reduced to

$$U\frac{\delta U}{\delta x} + V\frac{\delta U}{\delta y} = \frac{1}{\rho}\frac{\delta \tau}{\delta y} \qquad (2\text{-}1)$$

$$\frac{\delta U}{\delta x} + \frac{\delta V}{\delta y} = 0 \qquad (2\text{-}2)$$

where the appropriate boundary conditions are

$$\text{for } y = 0,\ x \geq 0 \ : \ U = 0,\ V = V_w(x) \qquad (2\text{-}3)$$

$$y \to \infty,\ \text{for all } x \ : \ U = U_o,\ V = 0 \qquad (2\text{-}4)$$

$$\text{for all } y,\ x = 0 \ : \ U = U_o \qquad (2\text{-}5)$$

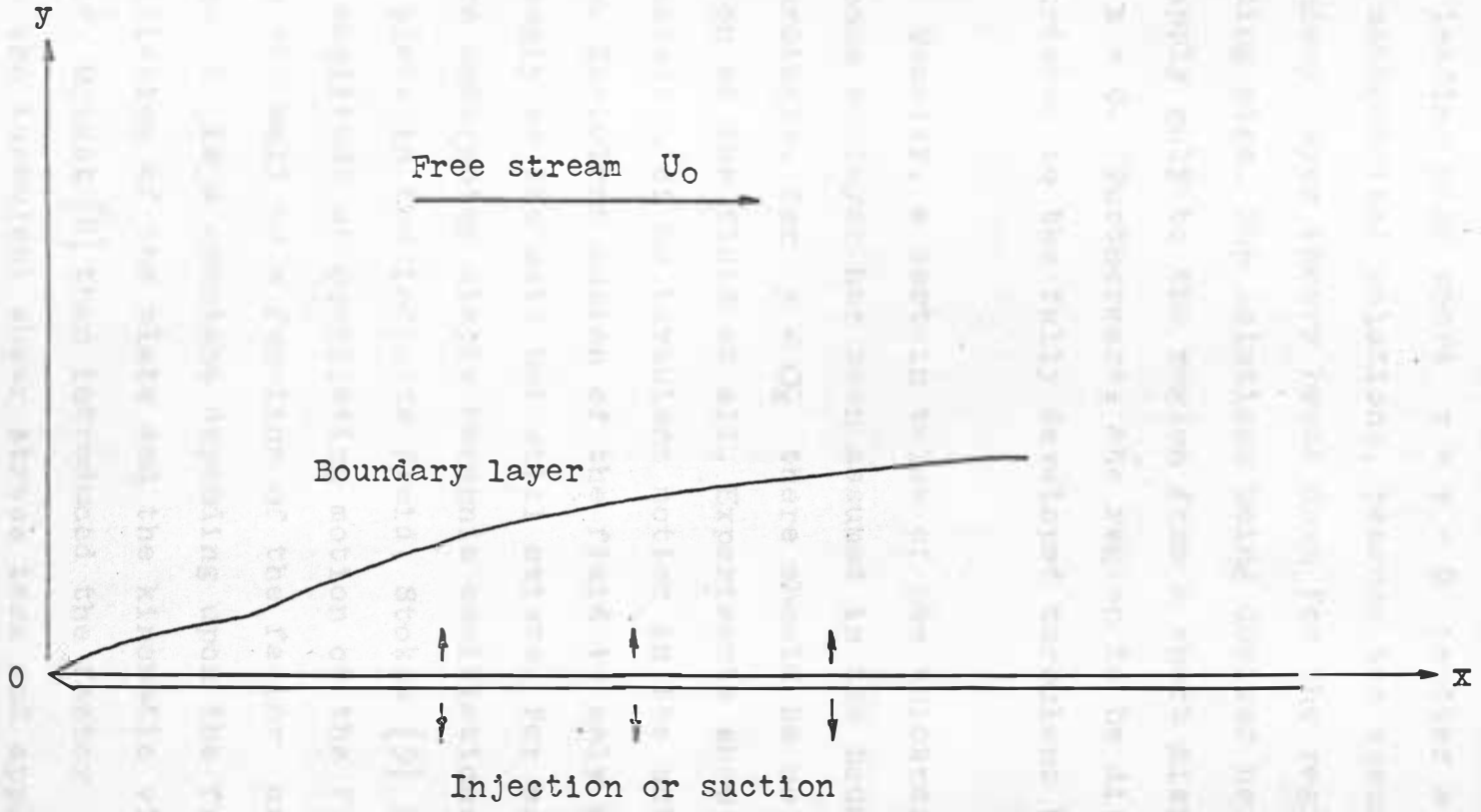

Fig. 2-1 Coordinates

The fact that these conditions indicate a discontinuity at the leading edge where $x = y = 0$ implies a singularity in the mathematical solutions, because the assumptions made in boundary layer theory break down for the region around the leading edge. The solutions being derived here must be taken to apply only to the region from a short distance downstream of $x = 0$. Furthermore, the region to be discussed is restricted to the fully developed turbulent boundary layer.

Usually, a certain value of the thickness σ_s of the viscous sublayer has been assumed in the boundary layer; accordingly, for $y < \sigma_s$ there should be no turbulent motion of the fluid at all. Experiments show that this expectation of no turbulent motion in the sublayer is not true. Turbulent motion of the fluid is only damped out strongly by the wall but still exists. For an infinite flat plate undergoing simple harmonic oscillations parallel to the plate in the infinite fluid, Stokes [9] indicated that the amplitude of oscillating motion of the fluid diminished from the wall as a function of the factor $\exp(-y/A)$, where A is a constant depending upon the frequency of oscillation of the plate and the kinematic viscosity of the fluid. Driest [8] then introduced the factor $[1 - \exp(-y/A)]$ into the turbulent shear stress term and applied it to the case in which the plate is fixed with the fluid oscillating relatively to the plate (i.e. turbulent fluid flow).

In the case of constant distribution of injection or suction along the plate, the derivatives of flow parameters with respect to x are so small that they can be neglected in the range very close to the wall. This can be written as

$$\frac{\delta}{\delta x} = \frac{d}{dx} = 0 \qquad (2\text{-}6)$$

The continuity equation (2-2) is then reduced to the form of

$$\frac{dV}{dy} = 0 \qquad (2\text{-}7)$$

After integration of Eq. (2-7) and substitution in the boundary conditions (2-3), this yields

$$V = V_W \qquad (2\text{-}8)$$

V_W is an arbitrary constant which is positive for injection and negative for suction. With the substitution of $V = V_W$ and $\frac{\delta}{\delta x} = 0$ into Eq. (2-1), the equation of motion becomes

$$V_W \frac{dU}{dy} = \frac{1}{\rho}\frac{\delta \tau}{\delta y} \qquad (2\text{-}9)$$

By integrating Eq. (2-9) and using boundary conditions (2-3) one obtains

$$V_w U = \frac{1}{\rho}(\tau - \tau_w) \qquad (2\text{-}10)$$

τ_w is the shear stress at the wall and is assumed constant along the plate. Dimensionless groups are defined for convenience as

$$\begin{aligned} U_* &= U/\sqrt{\tau_w/\rho} \\ V_* &= V/\sqrt{\tau_w/\rho} \\ y_* &= \sqrt{\tau_w/\rho}\, y/\upsilon \end{aligned} \qquad (2\text{-}11)$$

By rearranging Eq. (2-10), one gets

$$1 + V_{w*} U_* = \frac{\tau}{\tau_w} \qquad (2\text{-}12)$$

The total shear stress in turbulent boundary theory [10] is defined as

$$\tau = \mu \frac{dU}{dy} - \rho\overline{U'V'} \qquad (2\text{-}13)$$

Prandtl's mixing length theory [10] indicates that

$$-\rho\overline{U'V'} = \rho \chi^2 y^2 \left(\frac{dU}{dy}\right)^2 \qquad (2\text{-}14)$$

χ is a universal constant and is equal to 0.4 approximately. When the damping factor [9]

$$1 - \exp(-y/A) \tag{2-15}$$

is introduced, Eq. (2-13) becomes

$$\tau = \mu\frac{dU}{dy} + \rho\chi^2y^2\left[1 - \exp(-y/A)\right]^2\left(\frac{dU}{dy}\right)^2 \tag{2-16}$$

By non-dimensionalizing

$$\frac{\tau}{\tau_w} = \frac{dU_*}{dy_*} + \chi^2y_*^2\left[1 - \exp(-y_*/A_*)\right]^2\left(\frac{dU_*}{dy_*}\right)^2 \tag{2-17}$$

where

$$A_* = \sqrt{\frac{\tau_w}{\rho}}\,\frac{A}{\upsilon}$$

Rotta [7] showed that it is reasonable to generalize the damping factor as

$$DF = 1 - \exp\left(\frac{-y_*\sqrt{1+V_{w*}U_*}}{A_*}\right) \tag{2-18}$$

Then Eq. (2-17) is changed to

$$\frac{\tau}{\tau_w} = \frac{dU_*}{dy_*} + \chi^2 y_*^2 DF^2 \left(\frac{dU_*}{dy_*}\right)^2 \qquad (2\text{-}19)$$

Now, a substitution of Eq. (2-19) into Eq. (2-12) yields

$$\chi^2 y_*^2 DF^2 \left(\frac{dU_*}{dy_*}\right)^2 + \left(\frac{dU_*}{dy_*}\right) - (1 + V_{w*} U_*) = 0 \qquad (2\text{-}20)$$

which is a quadratic equation with $\left(\frac{dU_*}{dy_*}\right)$ as the variable. Solving Eq. (2-20) for this variable, one obtains

$$\frac{dU_*}{dy_*} = \frac{-1 + \sqrt{1 + 4\chi^2 y_*^2 DF^2 (1+V_{w*}U_*)}}{2\chi^2 y_*^2 DF^2} \qquad (2\text{-}21)$$

The other solution with the negative square root is not selected because it gives an impossible solution. The expression for $\frac{dU_*}{dy_*}$ cannot be negative unless flow separation occurs. For convenience of analysis, a multiplication by $1 + \sqrt{1 + 4\chi^2 y_*^2 DF^2 (1+V_{w*}U_*)}$ in the numerator and denominator of the right-hand term of Eq. (2-21) yields, after simplification,

$$\frac{dU_*}{dy_*} = \frac{2 (1 + V_{w*} U_*)}{1 + \sqrt{1 + 4\chi^2 y_*^2 DF^2 (1+V_{w*}U_*)}} \qquad (2\text{-}22)$$

This differential equation cannot be integrated directly;

however, it can be integrated numerically to obtain the dimensionless velocity profile.

So far, the roughness factor has not been mentioned. Roughness is considered as a vortex generator. The vortex-generation should grow with the size of the roughness. A disturbance constant D was introduced by Driest [9]. The damping factor should then be modified to

$$1 - \exp(-y/A) + \exp(-yD/AE) \qquad (2\text{-}23)$$

where E is the average height of roughness. Because the roughness is considered as a vortex generator, the factor $\exp(-y/A)$ should decrease its effect on the flow. The factor $\exp(-yD/AE)$ is introduced to counterbalance the factor $\exp(-y/A)$. As the vortex generation should grow with the size of roughness, the roughness damping factor is increased with increasing roughness E. Until the roughness is equal to the disturbance factor, the flow becomes fully turbulent. By writing the roughness damping factor in generalized form as

$$RF = 1 - \exp\left(\frac{-y_* \sqrt{1+V_{W*}U_*}}{A_*}\right) + \exp\left(\frac{-y_* D_* \sqrt{1+V_{W*}U_*}}{A_* E_*}\right) \qquad (2\text{-}24)$$

Equation (2-22) then becomes

$$\frac{dU_*}{dy_*} = \frac{2\,(1 + V_{W*}U_*)}{1 + \sqrt{1 + 4\,\chi^2 y_*{}^2 RF^2 (1+V_{W*}U_*)}} \qquad (2\text{-}25)$$

which now includes the effects of roughness. As the Reynolds' stress $\rho\overline{U'V'}$ is usually written as τ_t (turbulent shear stress), and since $\tau_l = \mu\frac{dU}{dy}$ for the laminar shear stress, the total shear is

$$\tau = \tau_l + \tau_t \qquad (2\text{-}26)$$

With the eddy viscosity ϵ defined as

$$\tau_t = \epsilon\frac{dU}{dy} \qquad (2\text{-}27)$$

Eq. (2-26) can be written as

$$\tau_t = \tau - \tau_w\left(\frac{dU_*}{dy_*}\right) \qquad (2\text{-}28)$$

or

$$\frac{\tau_t}{\tau_w} = \frac{\tau}{\tau_w} - \left(\frac{dU_*}{dy_*}\right) \qquad (2\text{-}29)$$

By the relation from Eq. (2-12), Eq. (2-29) finally reduces to

$$\frac{\tau_t}{\tau_w} = (1 + V_{W*}U_*) - \left(\frac{dU_*}{dy_*}\right) \qquad (2\text{-}30)$$

Since

$$\tau = (\mu + \epsilon)\frac{dU}{dy} \tag{2-31}$$

then, by non-dimensionalizing, one obtains

$$\tau = (\mu + \epsilon)\frac{\tau_w}{\mu}\frac{dU_*}{dy_*} \tag{2-32}$$

Therefore,

$$\frac{\epsilon}{\mu} = \frac{\frac{\tau}{\tau_w}}{\frac{dU_*}{dy_*}} - 1 \tag{2-33}$$

By substituting Eq. (2-12) into Eq. (2-33), one gets

$$\frac{\epsilon}{\mu} = \frac{1 + V_{w*}U_*}{\frac{dU_*}{dy_*}} - 1 \tag{2-34}$$

which is the relation between viscosity and eddy viscosity. By multiplying the numerator and denominator of the left-hand term of Eq. (2-34) by $\frac{dU}{dy}$, one finds that

$$\frac{\tau_t}{\tau_1} = \frac{1 + V_{w*}U_*}{\frac{dU_*}{dy_*}} - 1 \tag{2-35}$$

Equation (2-35) provides a relationship between turbulent shear stress and laminar shear stress throughout the boundary layer.

From the conservation of energy, Rotta [7] derived a relation for the sublayer:

$$\int_0^{\sigma_s} \tau_l \tau_t dy - \int_0^{\sigma_s} \rho \phi dy = 0 \qquad (2\text{-}36)$$

or

$$\int_0^{\sigma_s} \tau_l \tau_t dy - \Phi = 0 \qquad (2\text{-}36a)$$

In Eq. (2-36a), the first term is the production of energy and the second term is the total energy dissipation in the sublayer. The energy production can be written as

$$\tau_l \tau_t = \mu \frac{dU}{dy} \tau_t$$

or

$$\tau_l \tau_t = \frac{dU_*}{dy_*} \frac{\tau_t}{\tau_w} \qquad (2\text{-}37)$$

Equations (2-36) and (2-37) provide an understanding of how the energy dissipation acts in the sublayer.

There are two unknowns D_* and A_* which should be determined before solving Eq. (2-22) and Eq. (2-25). Driest [9] suggests that $D_* = 60$ is a good approximation. From Rotta's data [7], A_* can be represented approximately by

$$A_* = 26. - 25\ V_{W*} \qquad \text{(for the injection case)}$$

and

$$A_* = 26. - 200\ V_{W*} \qquad \text{(for the suction case)}$$

From Eq. (2-25), χ is assumed to have a value of 0.4. The boundary conditions used to solve Eqs. (2-22) and (2-25) are:

$$y_* = 0 \qquad U_* = 0 \qquad \frac{dU_*}{dy_*} = 1 \qquad (2\text{-}38)$$

and

$$y_* \to \infty \qquad \frac{dU_*}{dy_*} = 0 \qquad (2\text{-}39)$$

However, the integration constant of Eq. (2-22) or Eq. (2-25) is taken care of by numerical integration procedures. The IBM-360 Computer Program I (Fortran) is given in the Appendix; it was used to find the numerical results for

given values of E_* and V_{w*} in Eq. (2-22) or Eqs. (2-25), (2-30), (2-35), and (2-37). The results are discussed in Chapter IV.

CHAPTER III

EXPERIMENTS

A. Wind Tunnel

The wind tunnel used for the experiments is shown in Figs. 3-1 to 3-4. It was designed to simulate two-dimensional flow over porous plates with either suction or injection of a secondary fluid from or into the boundary layer. Referring to Fig. 3-1, the main-stream air is blown into the honeycomb section 2 by a cetrifugal fan 1. The honeycomb is constructed with six-inch long steel tubes one-half inch in diameter; it is used to damp out the rotational motion of the fluid produced by the fan. Screens 3 and 4 generate the turbulent motion in order to simulate a turbulent boundary layer. Ducts 5 and 6 suck the main flow into the air intake duct 15 so as to reduce the boundary layer thickness. A damper in each of the ducts 5 and 6 enables them to be fully closed. The back plate 7 in the test section is adjustable to allow simulation of uniform or accelerated flow. With plugged holes in the back plate 7, pressure tube probes 8 can be inserted into the test section to take data through the holes. Section 9 indicates the porous plate to be studied. Section 10 is a secondary air plenum to provide the injection or suction. The secondary air is supplied by a vacuum pump through air hoses and valves 13. Rockwool 12 is packed between test plate 9 and flexible plate 11. The

density of the rockwool is determined by the shape of the flexible plate at different locations. Since the varying density of the rockwool introduces a different pressure resistance to the air which passes through the rockwool, the desired distribution of injection or suction can be simulated. Bellmouth plug 14 was used to adjust the back pressure. The test cross-sectional area was 9 1/4 inches by 9 3/4 inches; the section was 48 inches long. The honeycomb section and the test section were constructed with quarter-inch mild steel plates. Ten-guage mild steel sheets were used to build the air return and intake sections. The heavy-guage steel plates and the flexible connections between fan and ducts were used mainly to prevent propagating the vibrations produced by the fan. The wind tunnel was designed for easy disassembly to allow further modifications.

B. Experimental Procedures

The basic experimental procedures are as follows:

1. Turn on air pump, set the desired distribution of injection or suction by adjusting the flexible plate.

2. Turn on the fan. Set the main-stream velocity by adjusting the intake duct damper and the bellmouth plug.

3. Adjust the boundary layer removal by means of the dampers in the return ducts.

4. Adjust the back plate to make $\frac{dU_o}{dx}$ or $\frac{dP}{dx}$ equal to zero or to any desired value.

5. Measure velocity prefiles at different stations along the test plate through the opening in the back plate. The wind tunnel should be operated at steady state.

C. Measurement and Calculation Technique

1. Velocity Profile

Boundary layer velocity profiles are measured at different x-stations along the top wall as desired. Static pressure is measured at each station by a static probe inserted into the main stream. No measurable pressure gradient was observed in the y-direction. A specially constructed probe was used to obtain total pressure in the boundary layer. The probe tip was made from a 22-guage steel needle with an outside diameter of 0.02915 inches. The total pressures used to calculate the velocity profile were measured by means of multi-tube manometers using 0.826 specific gravity oil as the measuring fluid. The reference pressure for the manometers is atmospheric.

2. Boundary Layer Thickness

The measured velocity profiles were used to calculate the boundary layer momentum thickness

$$\theta = \int_0^\infty \frac{U}{U_o}(1 - \frac{U}{U_o})dy \qquad (3\text{-}1)$$

and the boundary layer displacement thickness

$$\sigma = \int_0^\infty (1 - \frac{U}{U_o})dy \qquad (3\text{-}2)$$

at each station. There are two computer programs given in the Appendix for obtaining numerical results to Eqs. (3-1) and (3-2). Program II was used to plot velocity profiles approximately. The velocity profiles can be smoothed out by the operator. Program III was used to obtain numerical results for θ and σ.

3. Friction Coefficients

Average friction coefficients were evaluated by means of the Von Kármán momentum equation, with the terms involving products of the fluctuating velocity components neglected:

$$\frac{d\theta}{dx} - \frac{V_w}{U_o} + (2 + \frac{\sigma}{\theta})\frac{\theta}{U_o}\frac{dU_o}{dx} = \frac{\tau_w}{\rho U_o^2} = \frac{C_f}{2} \qquad (3\text{-}3)$$

It is believed that, except in the vicinity of a separation point or at very high blowing rates, the fluctuating terms may be safely neglected [6]. In the present experiments, $\frac{dU_o}{dx}$ or $\frac{dP}{dx}$ was approximately zero. Computer Program III was used to obtain average friction coefficients and shear stress at the wall besides solving Eqs. (3-1) and (3-2).

The local friction coefficient was measured by a Preston tube. This tube, with an external-to-internal diameter ratio

of 0.6 and an external diameter of 0.02915 inches, was mounted at the middle plane of the test duct, with a static pressure probe at the same vertical plane. Smith and Walker's calibration formula [11] was used to calculate the shear stress at the wall τ_w. This equation

$$\log_{10} \frac{\tau_w d^2}{4\rho U^2} = -1.396 + 0.875 \log_{10} \frac{(P_t - P)d^2}{4\rho U^2} \tag{3-4}$$

is good for Reynolds numbers up to 2.5×10^{10}. Thus the local friction coefficient is

$$\frac{C_f}{2} = \frac{\tau_w}{\rho U_o^2} \tag{3-5}$$

after τ_w is calculated from Eq. (3-4) and the collected pressure data. Program IV is given in the Appendix for Eqs. (3-4) and (3-5) to get numerical values from experimental data.

4. Roughness E

There are many mechanical devices to determine the roughness of a plate, but none were used in the present experiments because they were not available. Instead, a comparison method was utilized. All the equipment was checked out by running the test on a smooth flat plate without injection or suction. The calculated average friction coefficient for this smooth flat plate at certain Reynolds numbers

was compared to the graph obtained by Schlichting [10]. Then, by running the test under the same conditions on a panel of unknown roughness, the calculated local friction coefficient at certain Reynolds numbers was located on the Schlichting graph. The corresponding value of U_oE/υ was found. As U_o and υ are known properties during the test, E can easily be determined.

D. Acoustic Panels

There were four acoustic panels of RAYL 5, 16, 25, and 40 which were donated by The Boeing Company, Seattle, Washington, for the experiments. Each panel was run for three different cases:

1. No injection or suction
2. With injection
3. With suction

After all necessary data were collected and the velocity profiles and local friction coefficients were determined, the velocity profiles were transformed to non-dimensional shear velocity and shear coordinate form. Thus, the comparison between theoretical analysis and experimental results can be made. Computer Program V is given in the Appendix for this purpose. The experimental results are discussed in the following chapter.

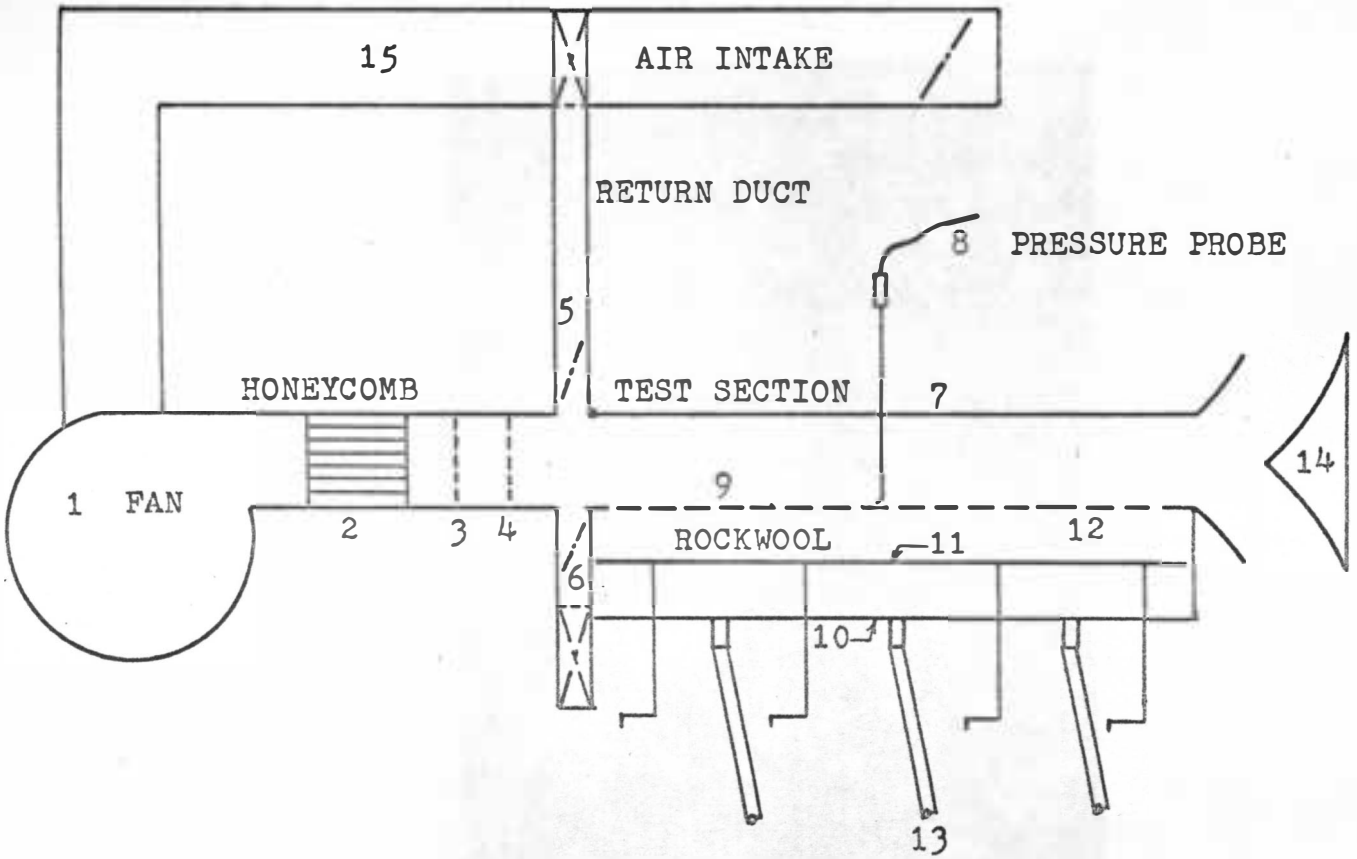

Fig. 3-1 Wind Tunnel

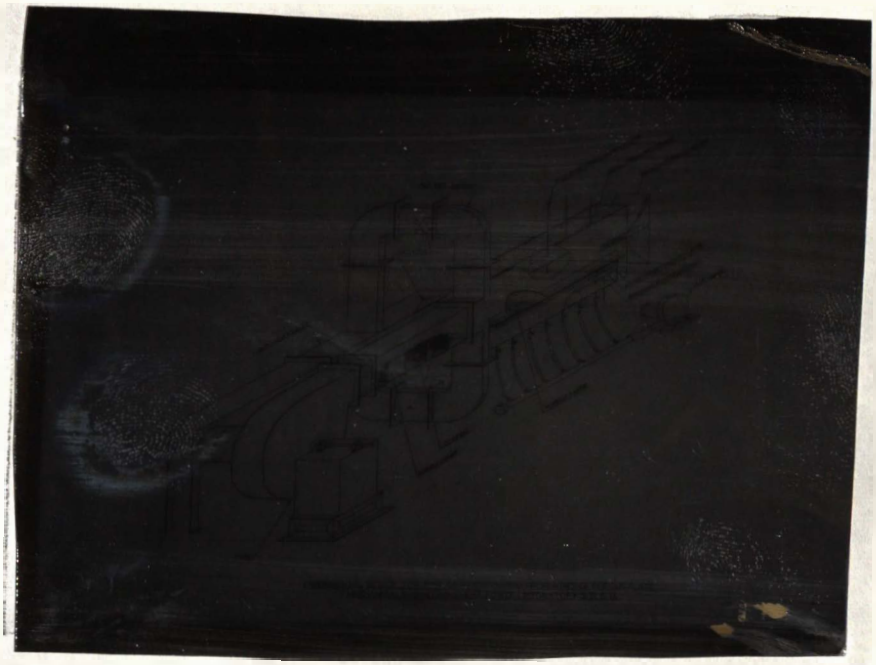

Fig. 3-2 Pictorial View of Wind Tunnel

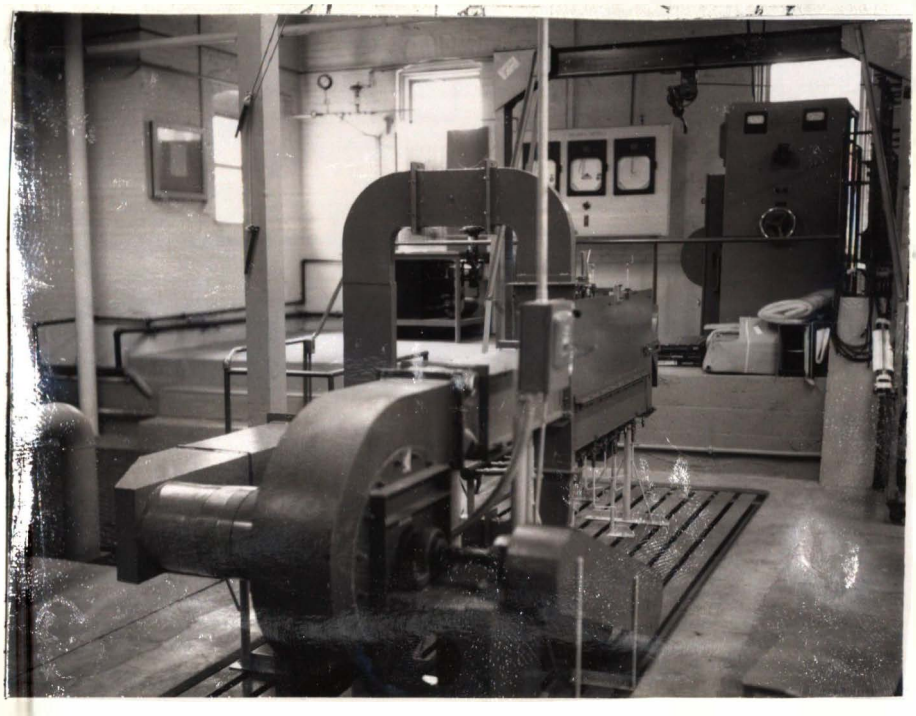

Fig. 3-3 Wind Tunnel

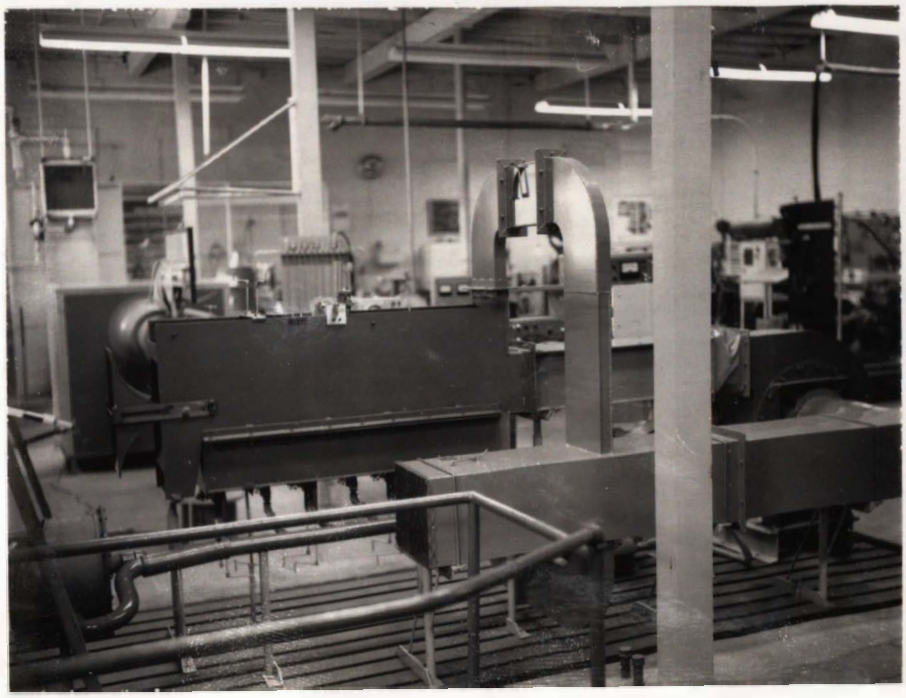

Fig. 3-4 Wind Tunnel

CHAPTER IV

DISCUSSION AND CONCLUSIONS

A. Theoretical Analysis

The combination of values for each parameter E_* and V_{w*} used in Program I to find numerical results for the theoretical universal velocity distribution, the turbulent shear stress distribution, the ratio of turbulent shear stress to laminar shear stress, and the energy production distribution are as follows:

$E_* = 0, 10, 20, 30, 40, 60, 100$

$V_{w*} = 0.12, 0.08, 0.04, 0, -0.04, -0.08$

Only partial results were plotted. The disturbance constant D_* which is equal to 60 is considered a criterion of the rough characteristics of the flat plate. When E_* is equal to zero, the plate is smooth. When E_* is larger than zero but less than or equal to D_*, the plate is partly rough. When E_* is larger than D_*, the plate is fully rough. In Fig. 4-1, curves show the universal velocity distribution of flow over a flat plate with different roughness but without injection or suction (i.e. various values of E_* and with $V_{w*} = 0$). Regions of roughness determined by the disturbance constant are also shown. Figs. 4-2 to 4-9 show the universal velocity distribution of flow over a flat plate with a fixed roughness but with various injection or suction; these curves are derived by solving Eq. (2-25). All universal velocity

distributions were plotted with U_* and y_* as coordinates on a semi-logarithmic chart. One can find that each curve in these figures has an inflection point at $10 < y_* < 50$. This inflection point is about at a distance where y_* is equal to A_*. Where y_* is less than A_*, the damping factor DF or RF has very little effect on Eq. (2-22) or Eq. (2-25). In other words, the viscosity effect dominates the fluid flow very near the wall. But as y_* approaches and gradually becomes larger than A_*, the damping factor increases its effect and turbulent motion becomes dominant. Equation (2-22) or Eq. (2-25) fails when V_{w*} is approximately less than -0.08. The square root in these equations becomes imaginary. It can be explained that fluid flow becomes laminar when $V_{w*} < -0.08$; Eqs. (2-22) and (2-25) hold only for turbulent flow. Another deficiency is that these two equations do not give any information about separation. Actually, at large values of V_{w*}, separation will occur.

From Eq. (2-30), the ratio of turbulent shear stress to shear at the wall in the sublayer for a constant roughness E_* with various injection or suction values V_{w*} was plotted versus y_* in Figs. 4-10 to 4-13. Since the turbulent shear stress is defined as

$$\tau_t = \rho \chi^2 y^2 DF^2 \left(\frac{dU}{dy}\right)^2$$

or

$$\tau_t = \rho \chi^2 y^2 RF^2 \left(\frac{dU}{dy}\right)^2$$

then at $y = 0$, τ_t is equal to zero and so is the ratio of τ_t/τ_w. However, with increasing y, the turbulent shear stress is increased until at very large y, $\frac{dU}{dy}$ becomes very small and τ_t/τ_w remains almost constant. Also, from Eq. (2-30), one obtains

$$\frac{\tau_t}{\tau_w} = 1 + V_{w*} U_* - \left(\frac{dU_*}{dy_*}\right)$$

This ratio of τ_t/τ_w is quite different from unity at large y_* which can be seen in Figs. 4-10 to 4-13, except at $V_{w*} = 0$. This implies that the conventional assumption that total shear stress τ is approximately equal to the shear stress at the wall τ_w fails for the sublayer when injection or suction exists.

Results from Eq. (2-35) were plotted in Figs. 4-14 to 4-17; in each figure, the roughness E_* is kept constant at either 0, 20, 60, or 100 and V_{w*} is shown for six different values. Notice that when E_* is equal to zero, the ratio τ_t/τ_l is small when y_* is small. But when roughness exists, this ratio becomes large. Roughness generates turbulent motion and increases turbulent shear stress. However, at large y_*, the ratio τ_t/τ_l is usually large because there the turbulent motion effects predominate over

the viscosity effects. For a rough plate, the ratio τ_t/τ_1 is larger than unity in the sublayer. In Figs. 4-15 to 4-17, the total shear stress τ can be considered approximately equal to τ_t.

In Figs. 4-18 to 4-22, the results of Eq. (2-37) were plotted. Energy production $\tau_1\tau_t$ is considerably smaller than energy dissipation very near the wall; it increases with increasing y_* to its maximum value and then decreases rapidly. Since energy dissipation [7] is written as

$$\Phi = \nu\frac{d^2}{dy^2}\left(\frac{U^2}{2}\right) = \frac{\tau_w^2}{\rho\mu}\frac{d^2}{dy_*^2}\left(\frac{U_*^2}{2}\right)$$

one can get

$$\Phi = \frac{\tau_w^2}{\rho\mu}\int_0^{\sigma_{s*}}\frac{d^2}{dy_*^2}\left(\frac{U_*^2}{2}\right)dy_*$$

The substitution of this expression into Eq. (2-36a) yields

$$\int_0^{\sigma_{s*}}\tau_1\tau_t dy_* = \left(\frac{\tau_w}{\rho}\right)^{\frac{3}{2}}\int_0^{\sigma_{s*}}\frac{d^2}{dy_*^2}\left(\frac{U_*^2}{2}\right)dy_*$$

The thickness of the sublayer σ_{s*} can be calculated when τ_w is known. Injection increases energy production because it adds energy into the sublayer; the opposite holds for suction. Roughness decreases energy production because more energy dissipates to the wall, thus increasing the value of

shear stress at the wall. In view of conservation of energy, with equal shear stress at the wall, the thickness of the sublayer is reduced by injection or roughness but increased with suction. However, the total boundary layer thickness is increased by injection or roughness and decreased by suction.

From the discussion and graphic variations in the figures, conclusions can be made as follows:

1. Knowing E_* and V_{w*}, the universal velocity distribution and the turbulent shear distribution can be predicted.

2. The total shear stress τ cannot be assumed equal to the shear stress at the wall τ_w in the sublayer when injection or suction exists.

3. Injection increases the dimensionless velocity profile, energy production and the ratio of turbulent shear stress to the shear stress at the wall. Suction has the opposite effect.

4. Roughness decreases the universal velocity profile and energy production. It also decreases the ratio of turbulent shear stress to shear stress at the wall when injection exists, but it has the opposite effect when suction esists.

5. The relation between roughness and shear stress throughout the boundary layer can be predicted, but there is still no way to obtain the shear stress at the wall by this analysis. However, the wall shear can be found experimentally.

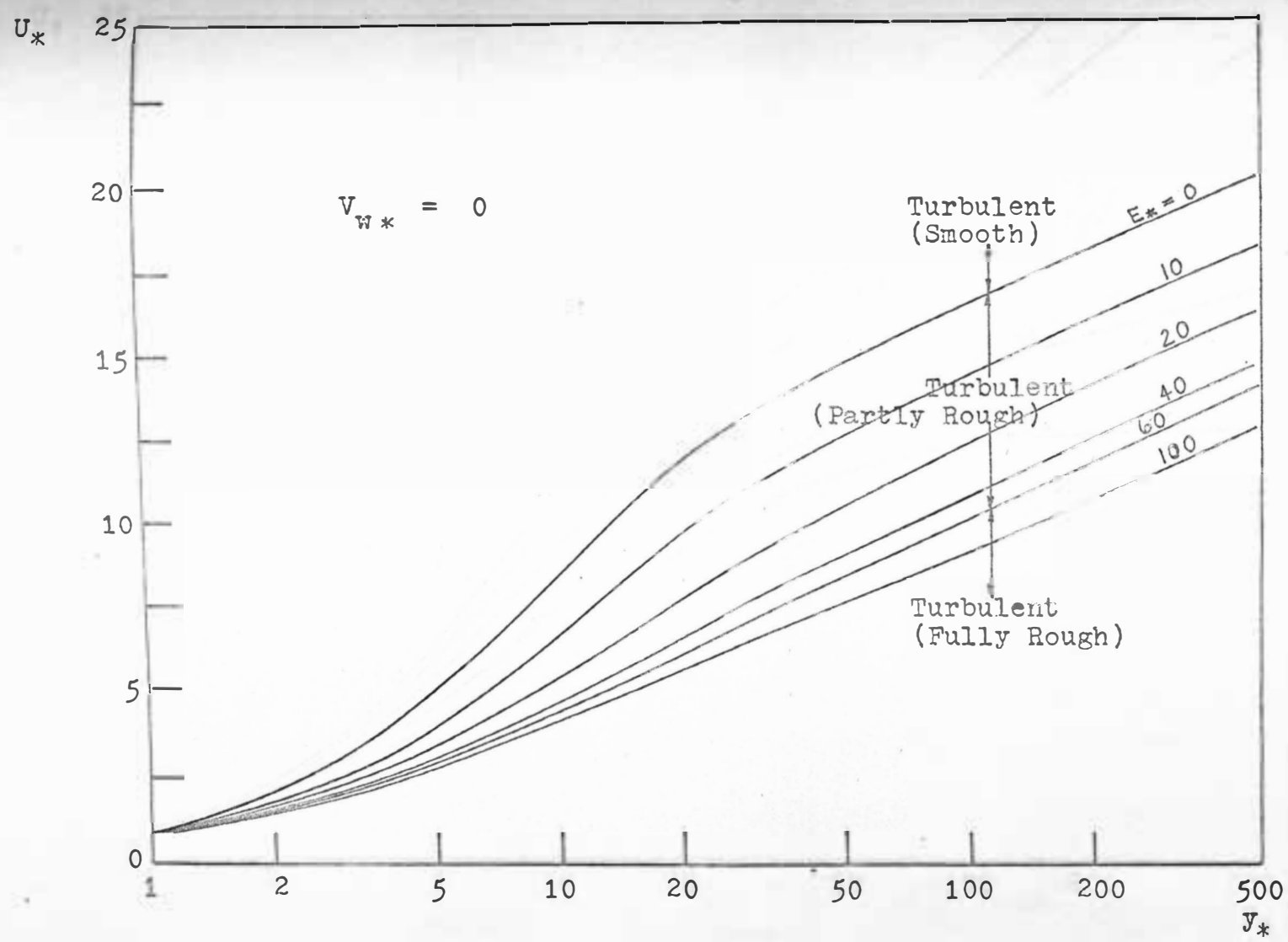

Fig. 4-1 Theoretical velocity distribution at constant V_{w*} with various E_*

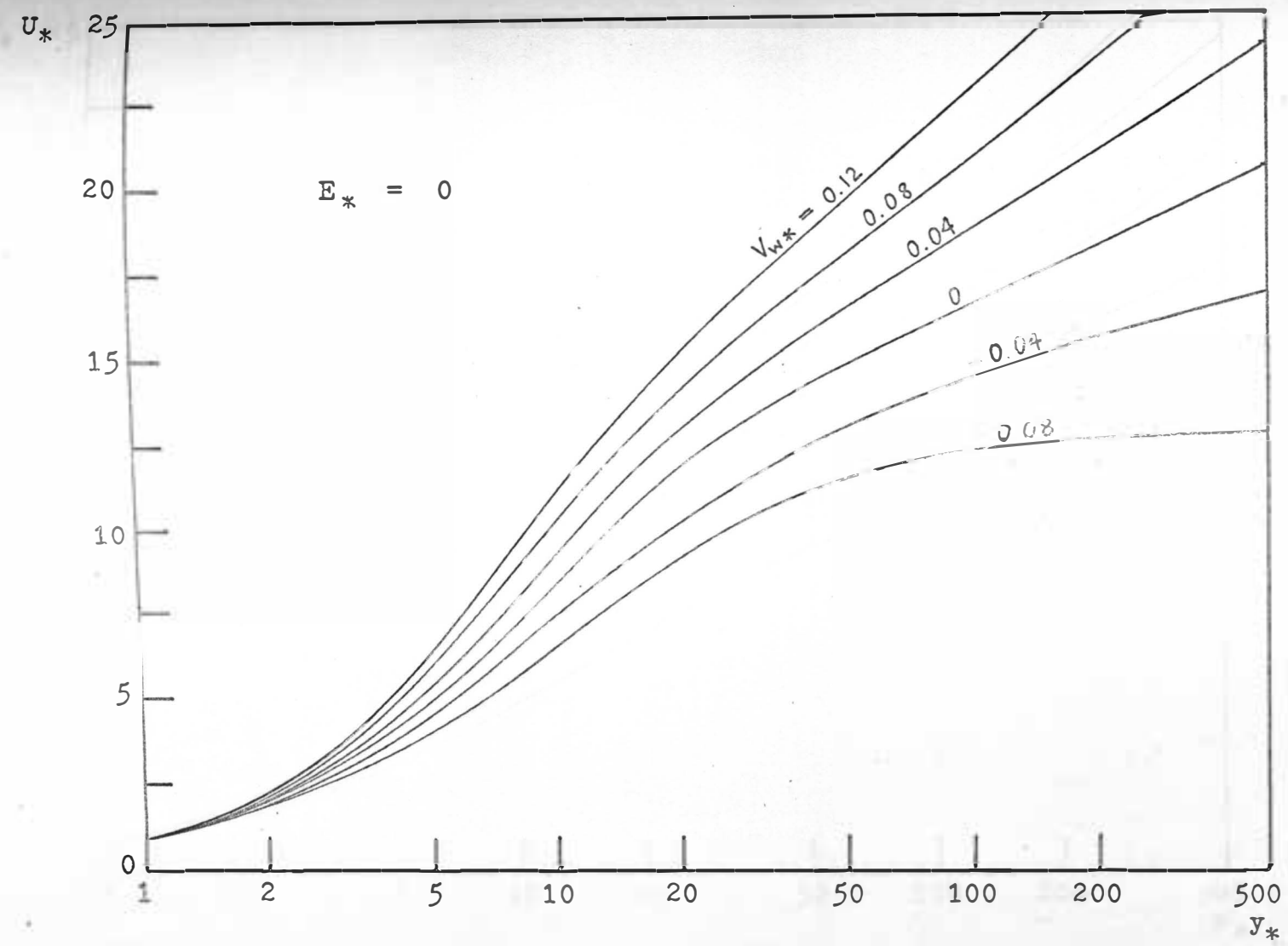

Fig. 4-2 Theoretical velocity distribution at various V_{w*} with $E_* = 0$

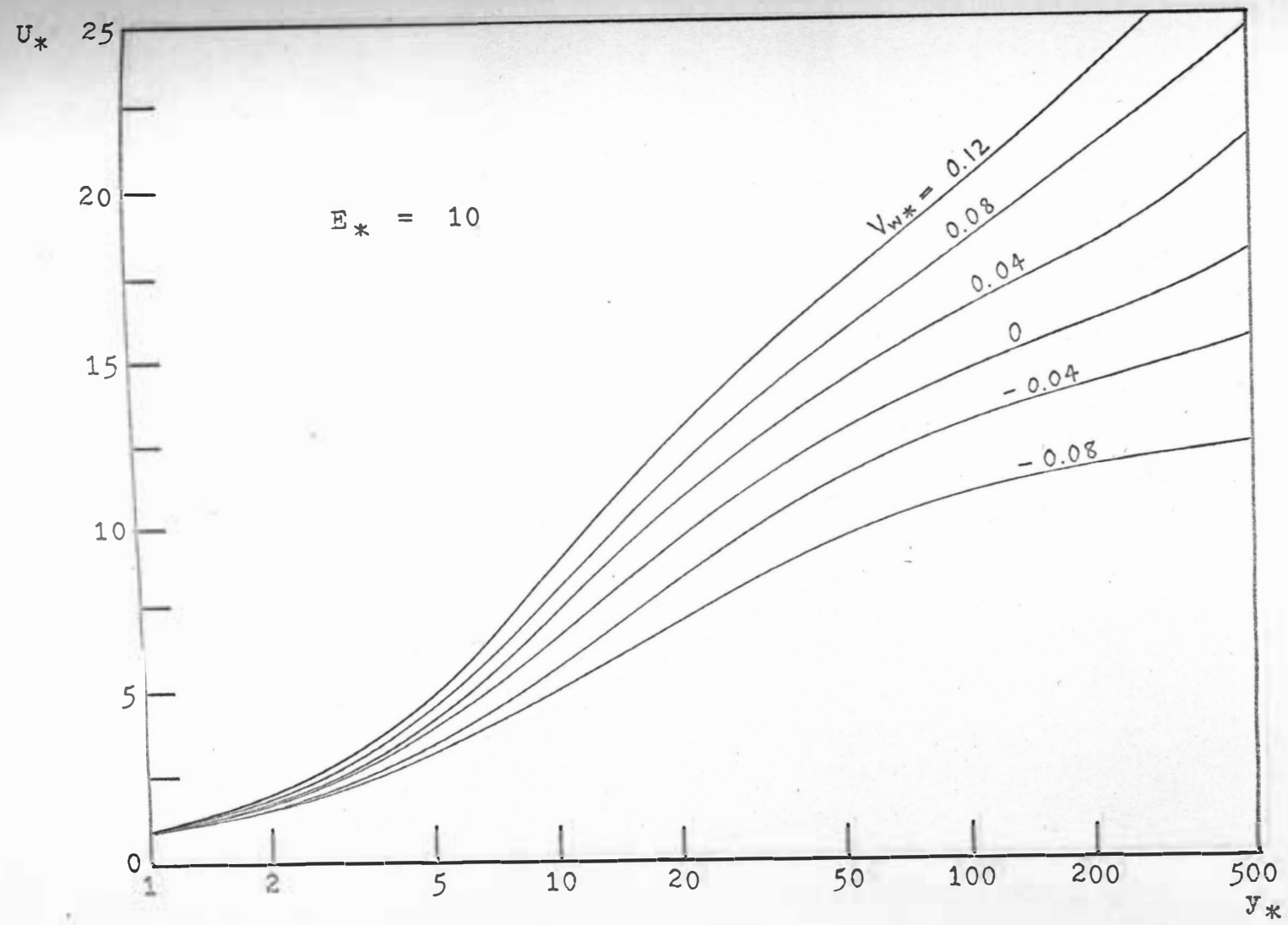

Fig. 4-3 Theoretical velocity distribution at various V_{w*} with $E_* = 10$

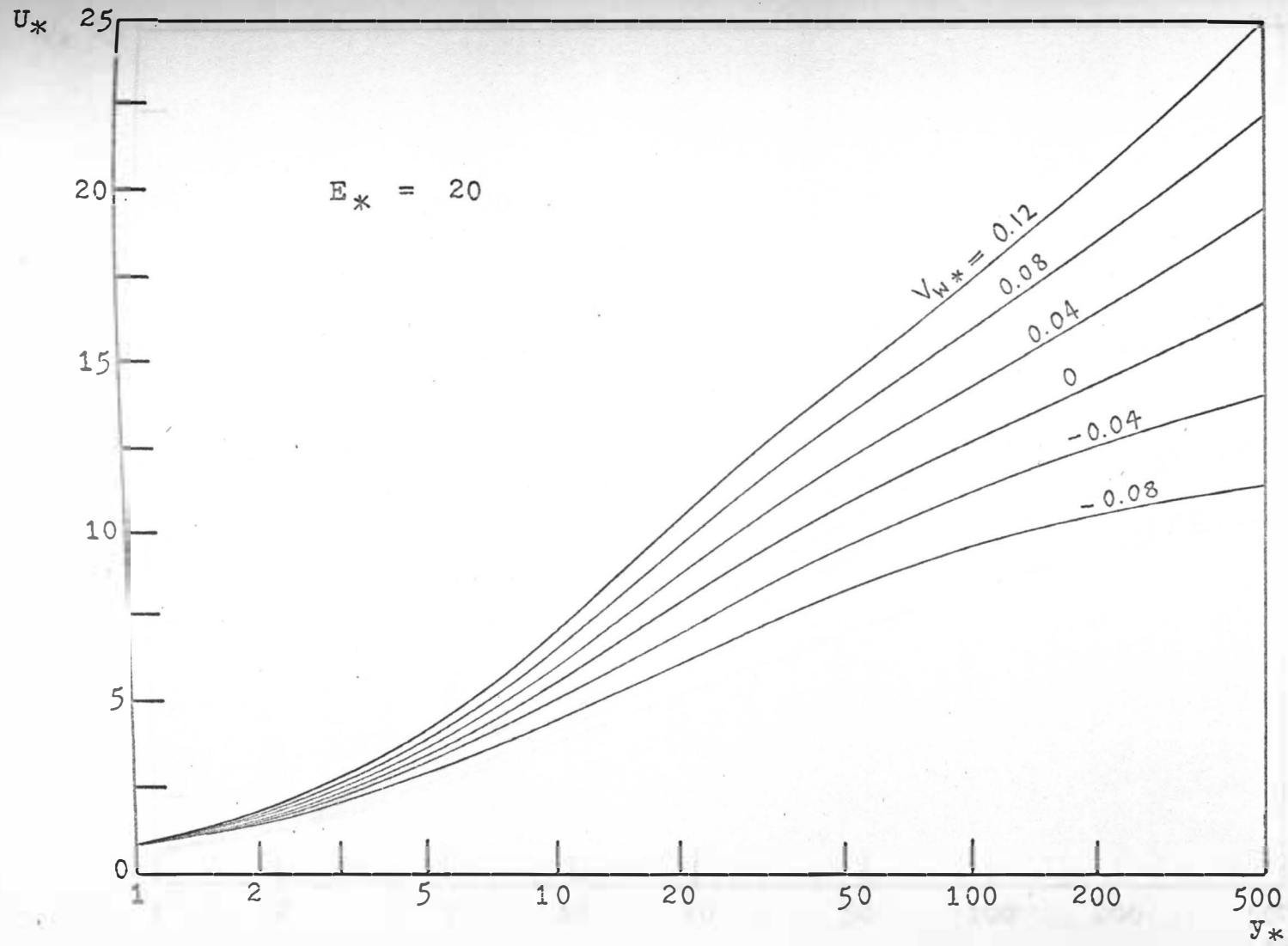

Fig. 4-4 Theoretical velocity distribution at various V_{w*} with $E_* = 20$

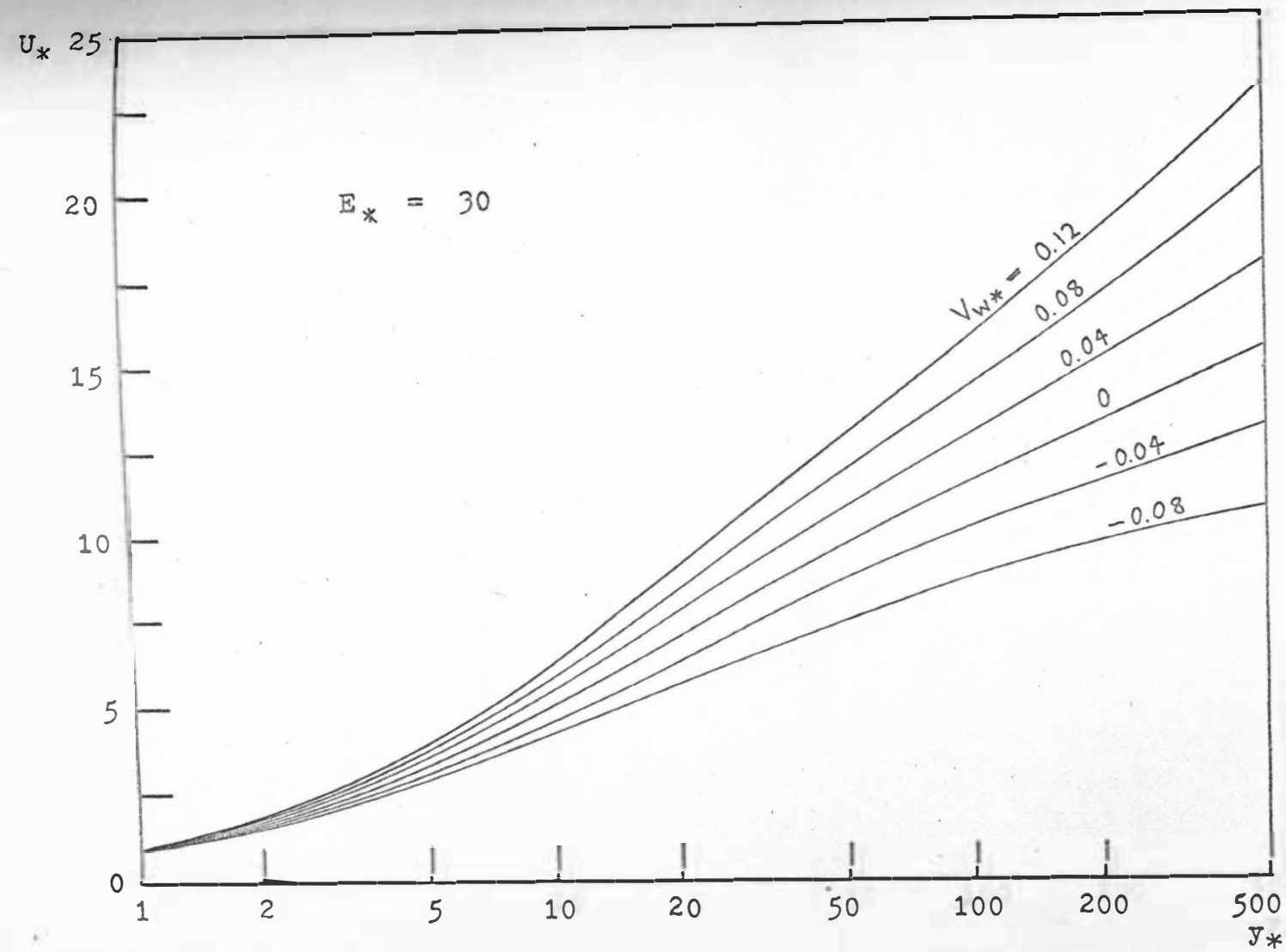

Fig. 4-5 Theoretical velocity distribution at various V_{w*} with $E_* = 30$

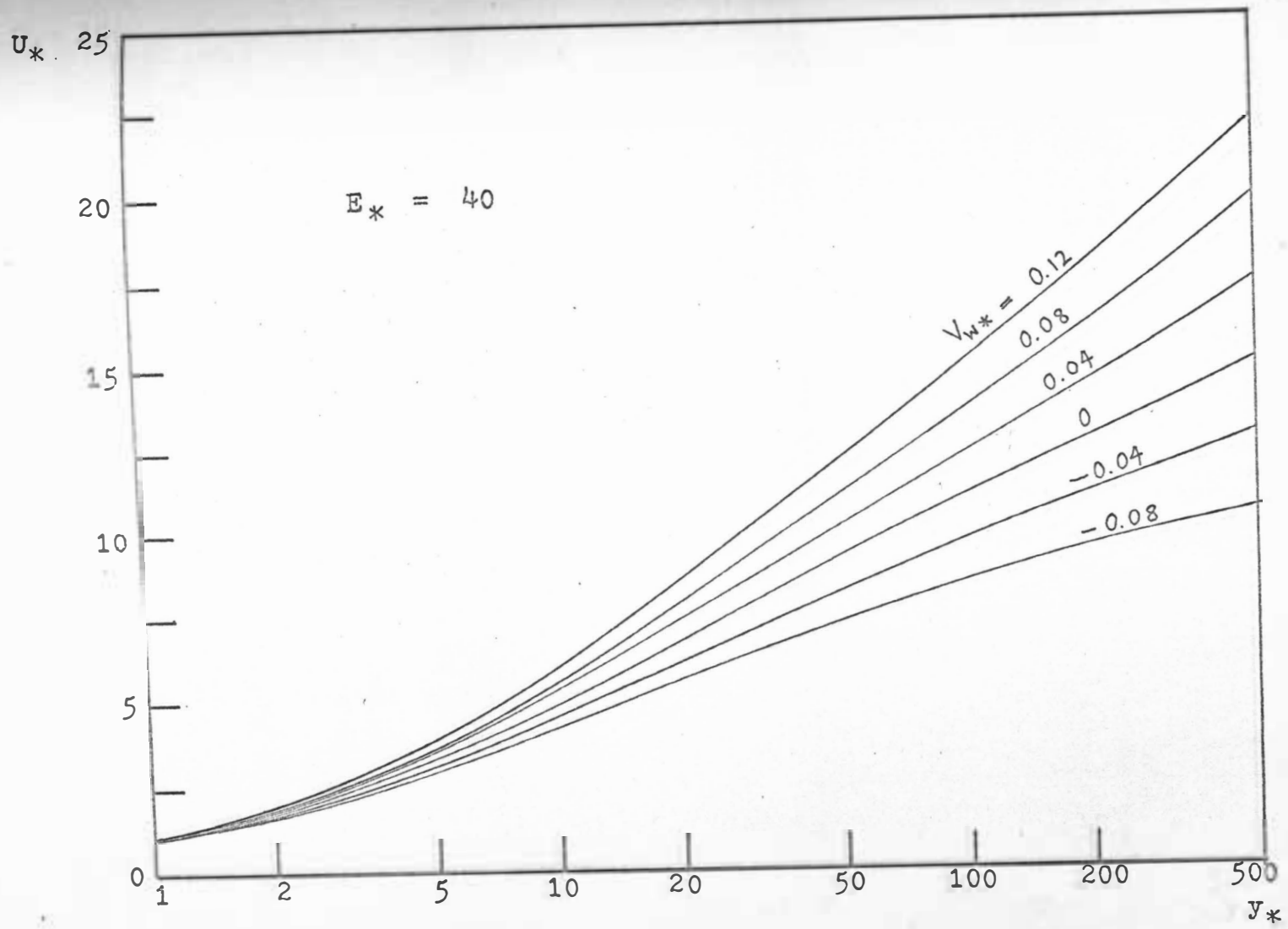

Fig. 4-6 Theoretical velocity distribution at various V_{w*} with $E_* = 40$

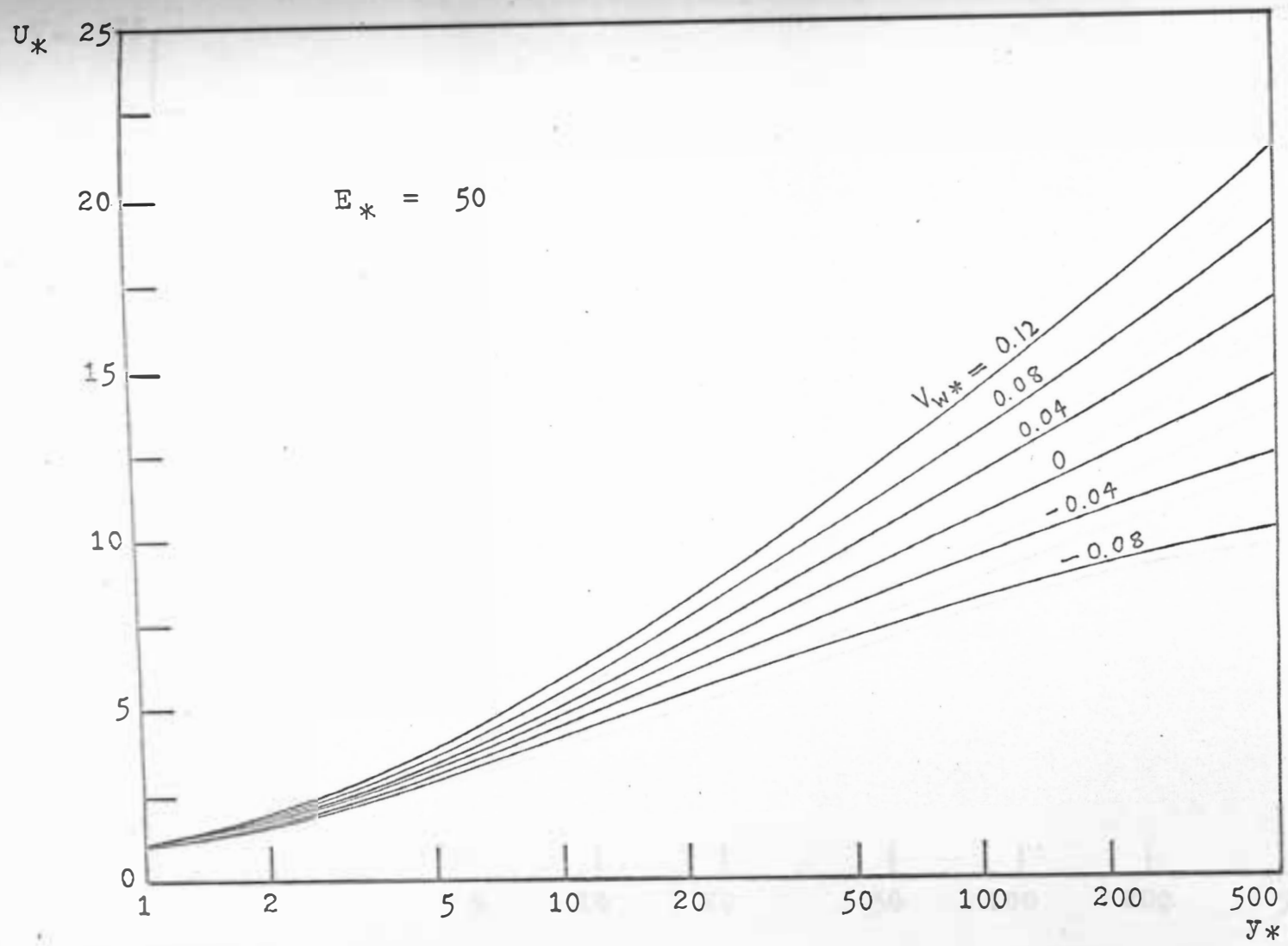

Fig. 4-7 Theoretical velocity distribution at various V_{w*} with $E_* = 50$

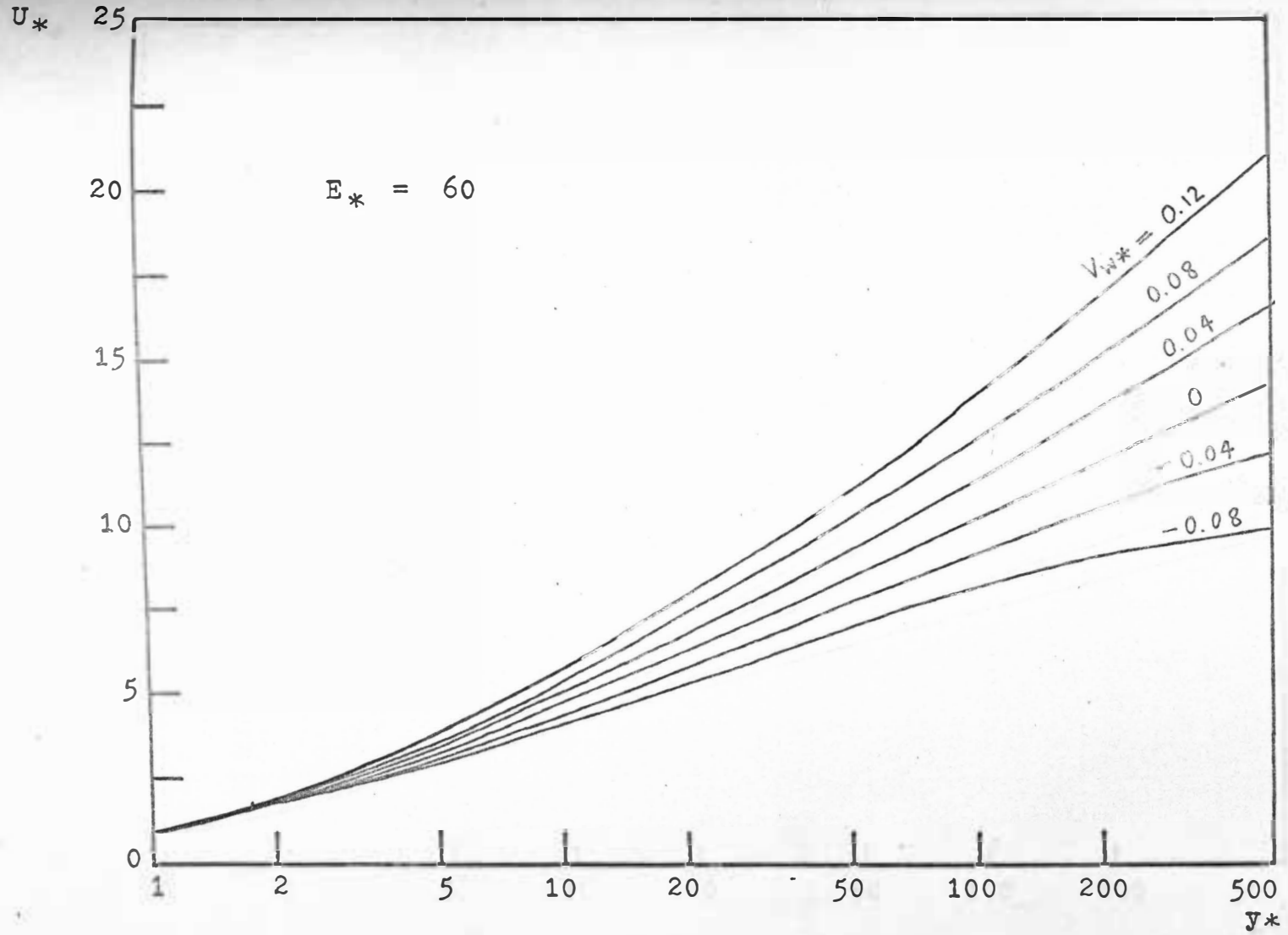

Fig. 4-8 Theoretical velocity distribution at various V_{w*} with $E_* = 60$

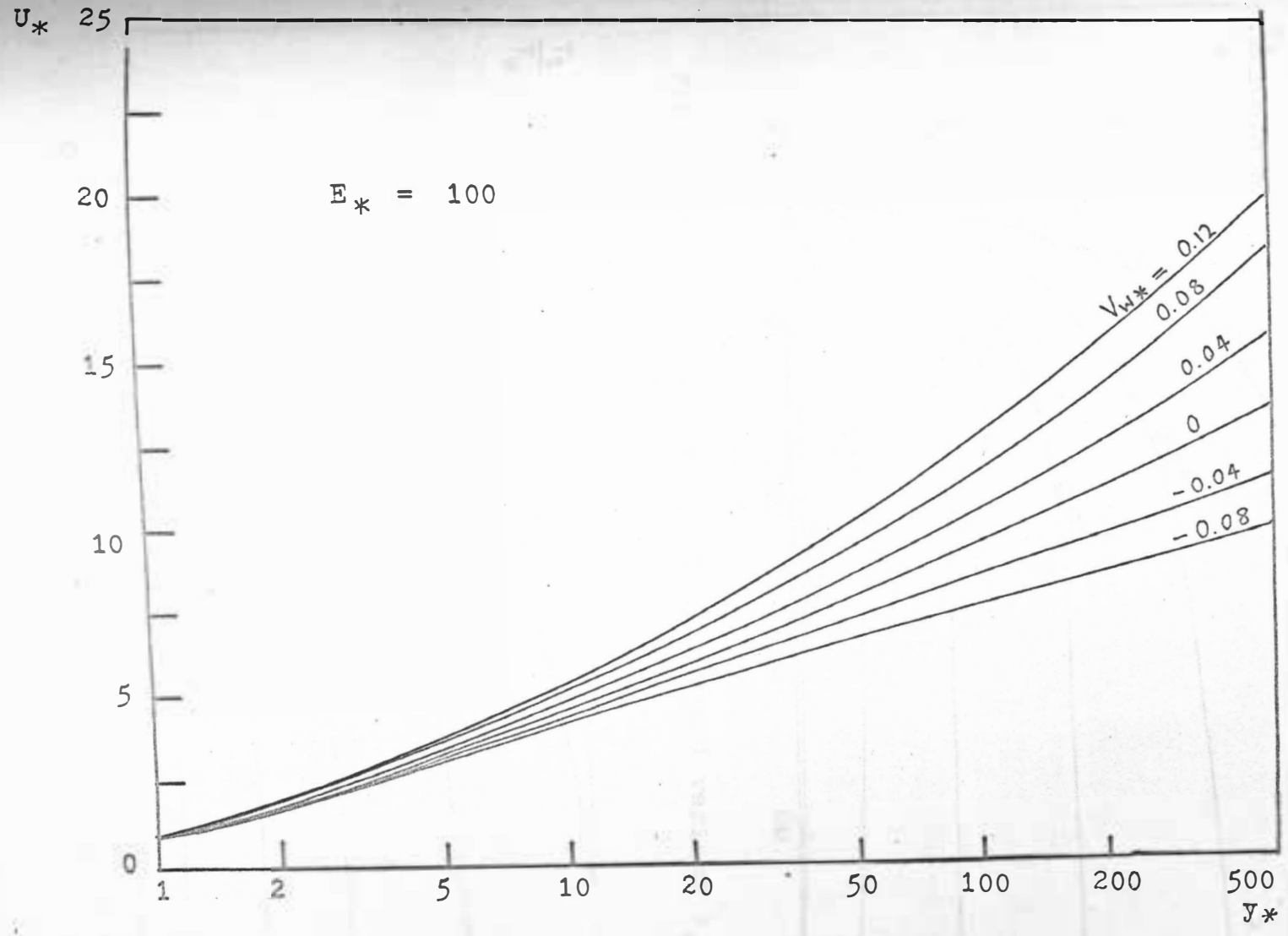

Fig. 4-9 Theoretical velocity distribution at various V_{W*} with $E_* = 100$

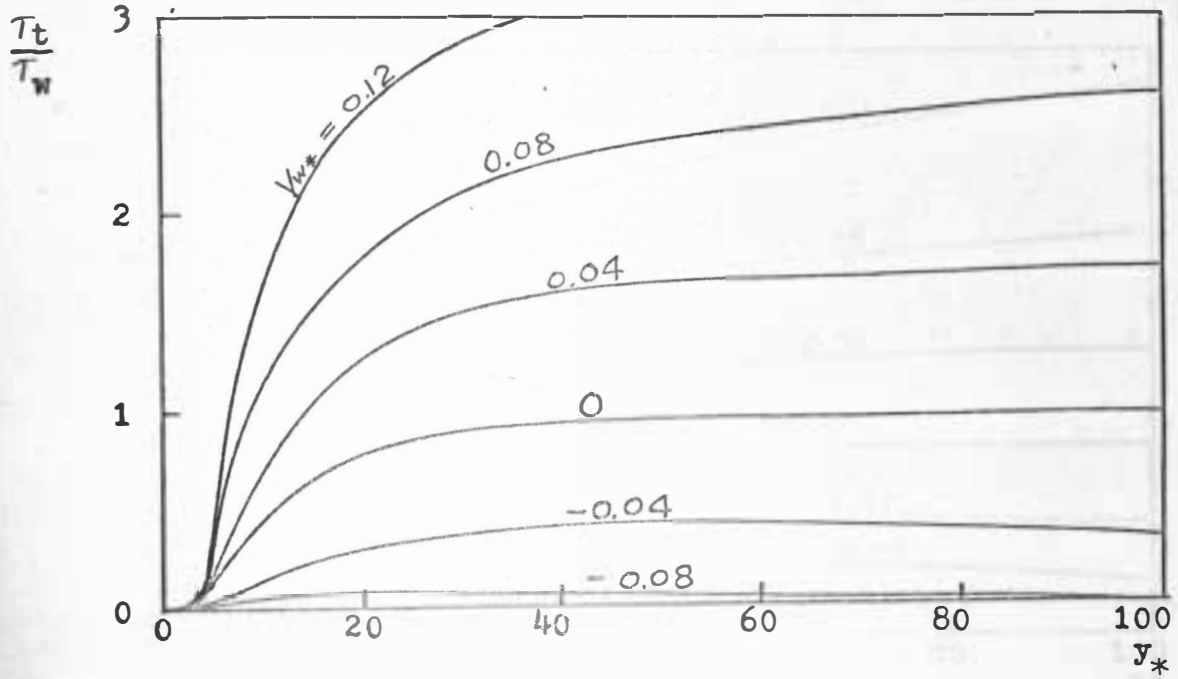

Fig. 4-10 τ_t/τ_w versus y_* at $E_* = 0$ and various V_{w*}

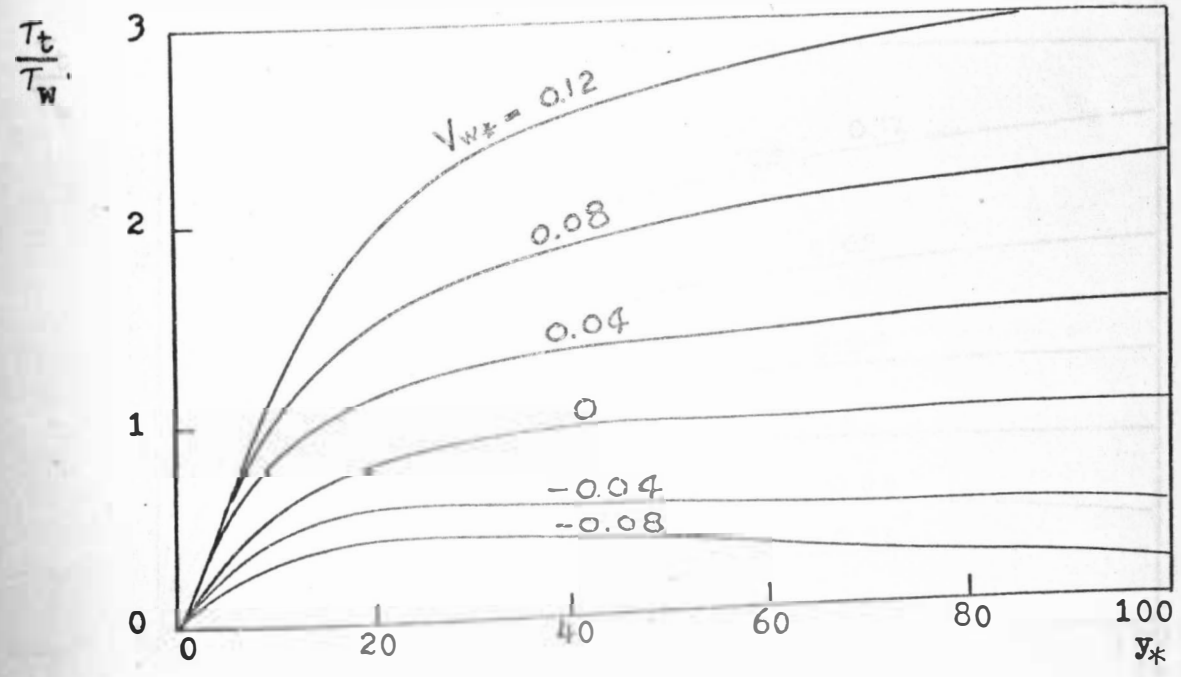

Fig. 4-11 τ_t/τ_w versus y_* at $E_* = 20$ and various V_{w*}

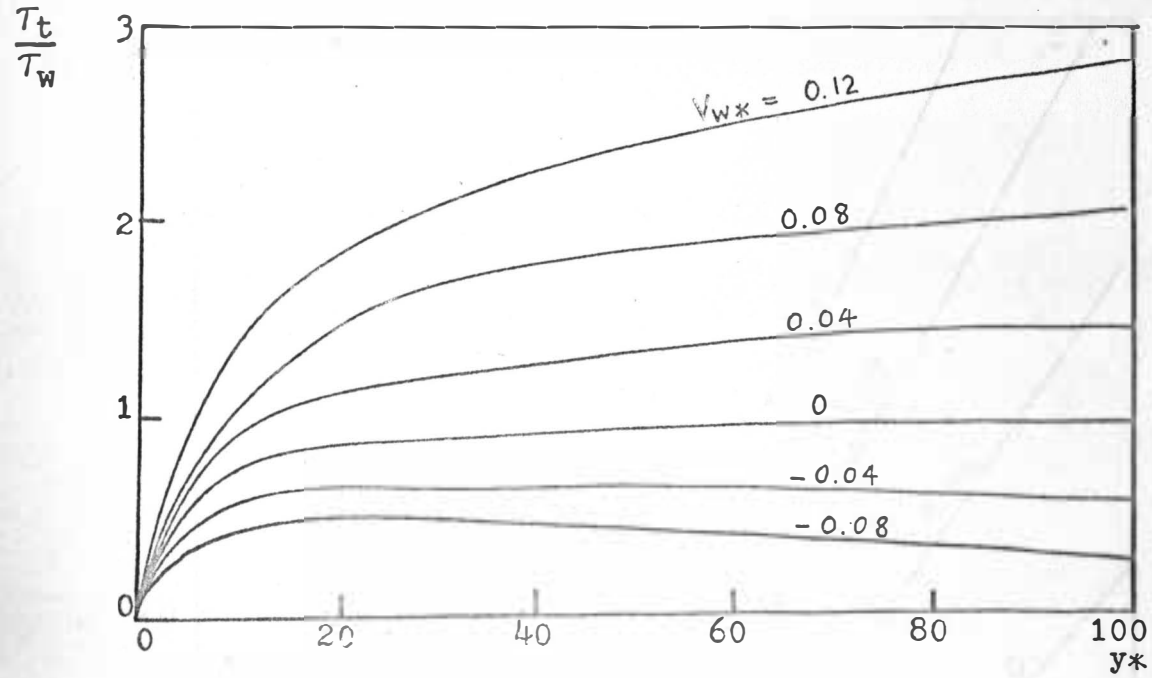

Fig. 4-12 τ_t/τ_w versus y_* at E_* = 40 and various V_{w*}

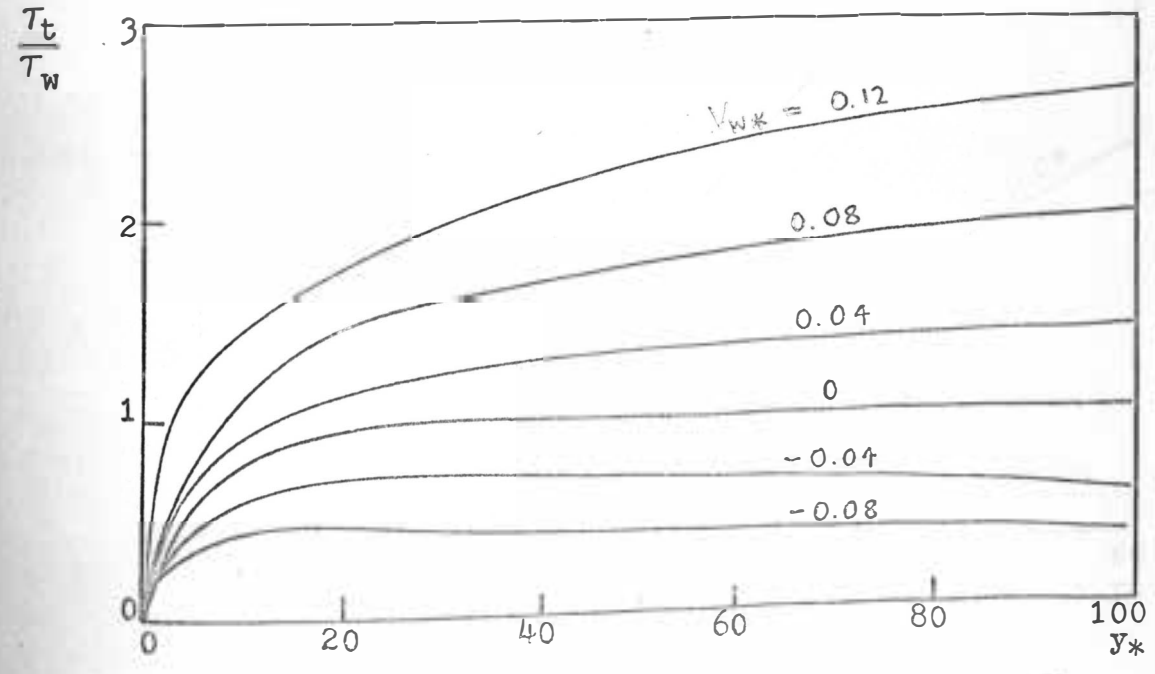

Fig. 4-13 τ_t/τ_w versus y_* at E_* = 60 and various V_{w*}

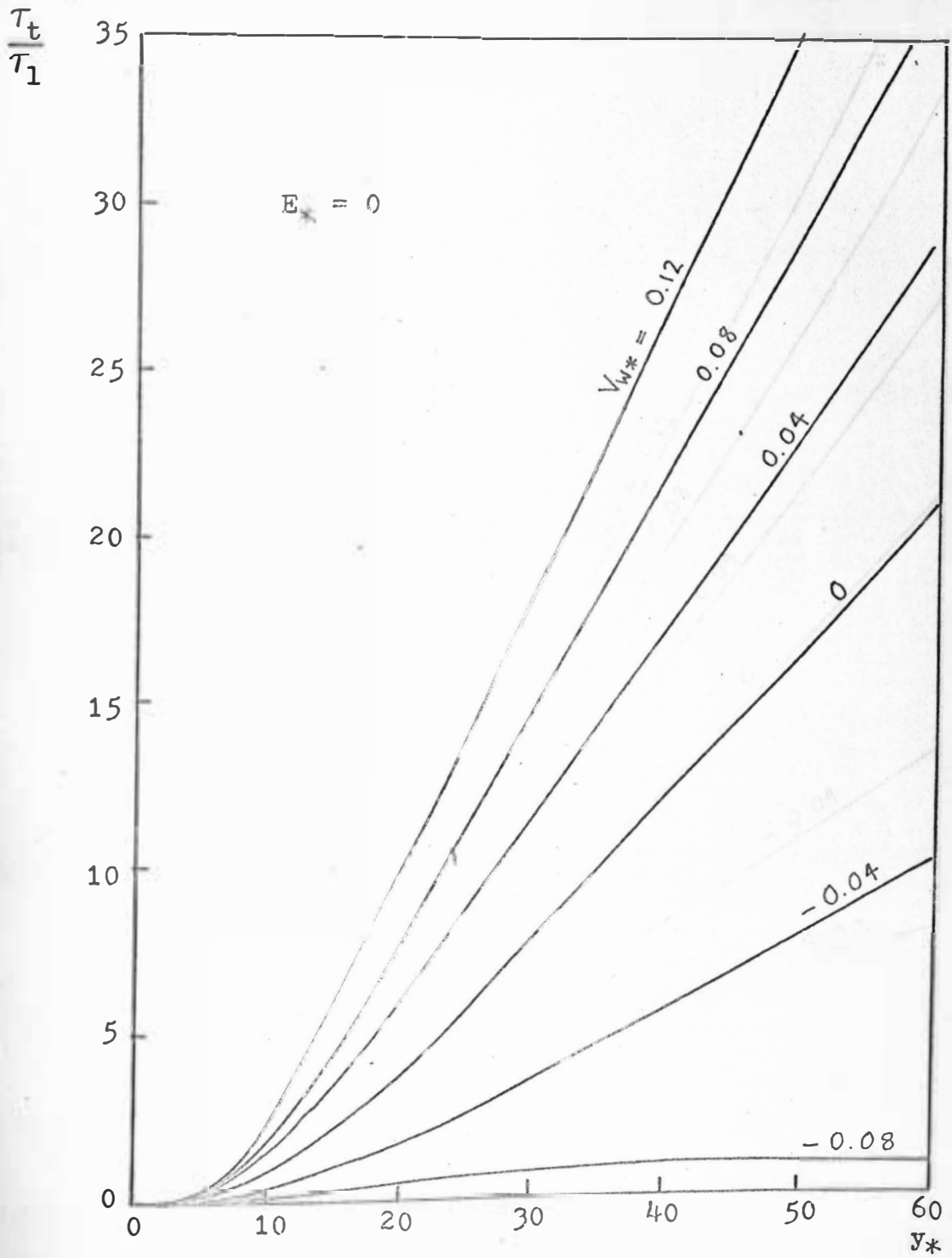

Fig. 4-14 τ_t/τ_w versus y_* at $E_* = 0$ and various V_{w*}

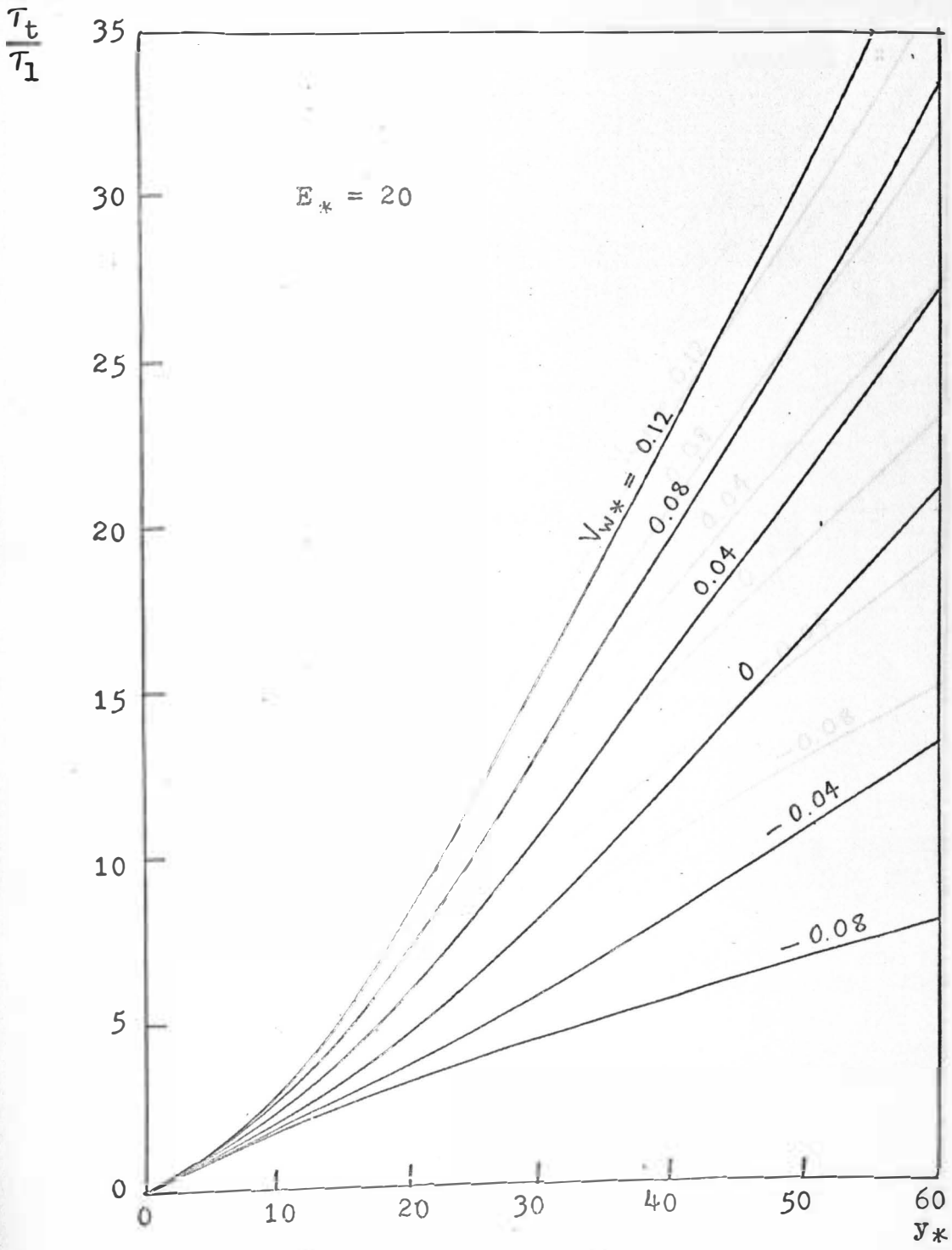

Fig. 4-15 τ_t/τ_w versus y_* at $E_* = 20$ and various V_{w*}

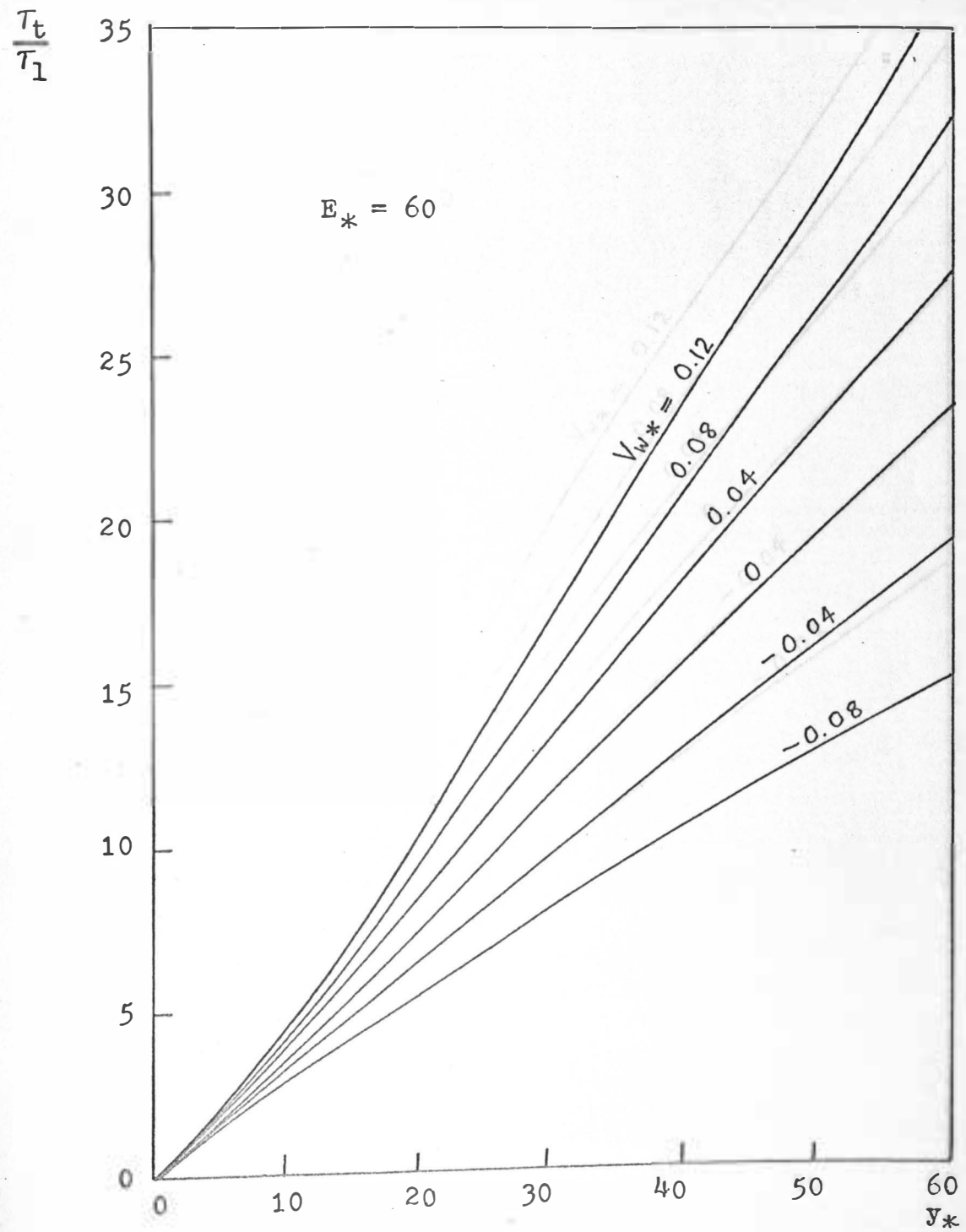

Fig. 4-16 τ_t/τ_w versus y_* at $E_* = 60$ and various V_{w*}

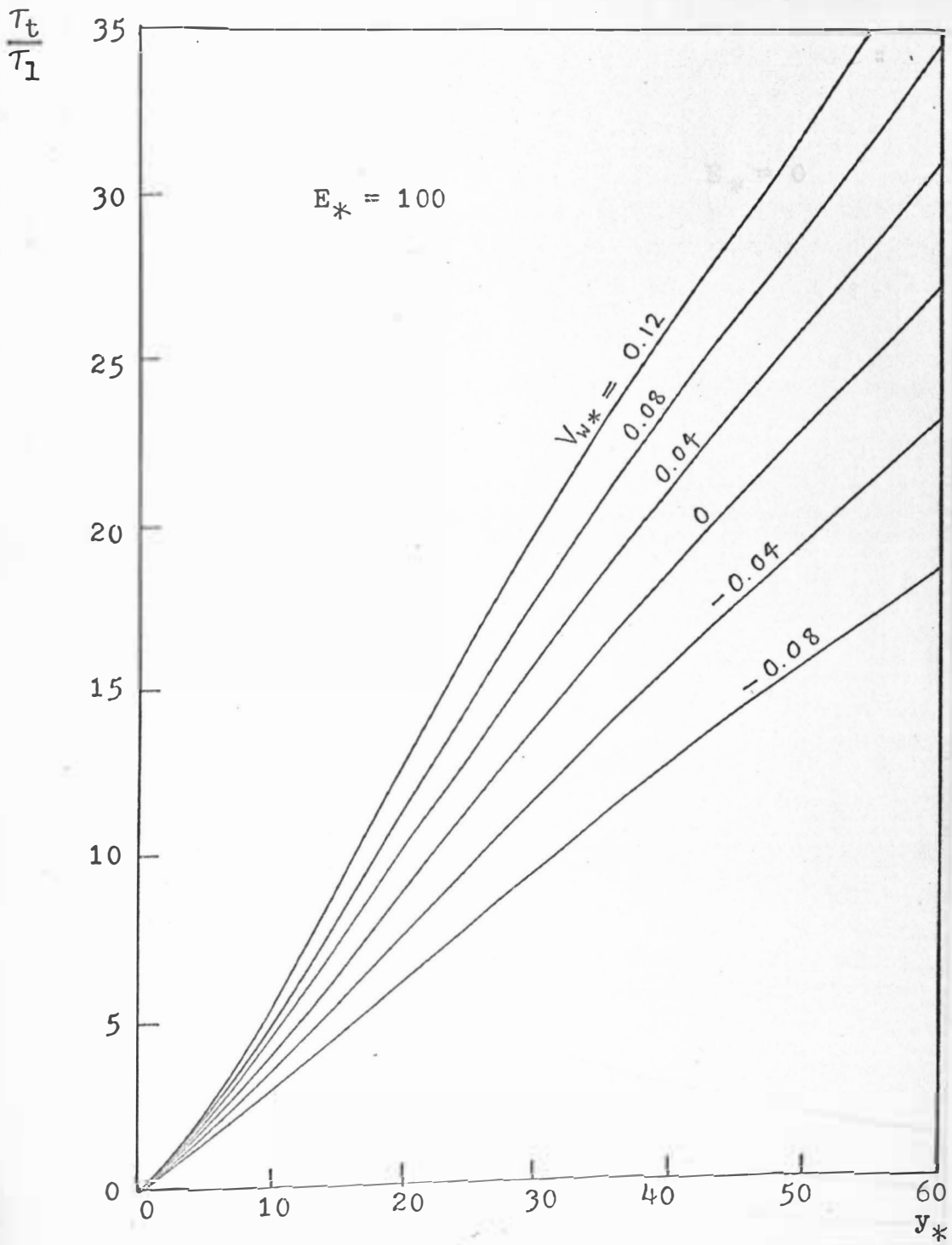

Fig. 4-17 τ_t/τ_w versus y_* at $E_* = 100$ and various V_{w*}

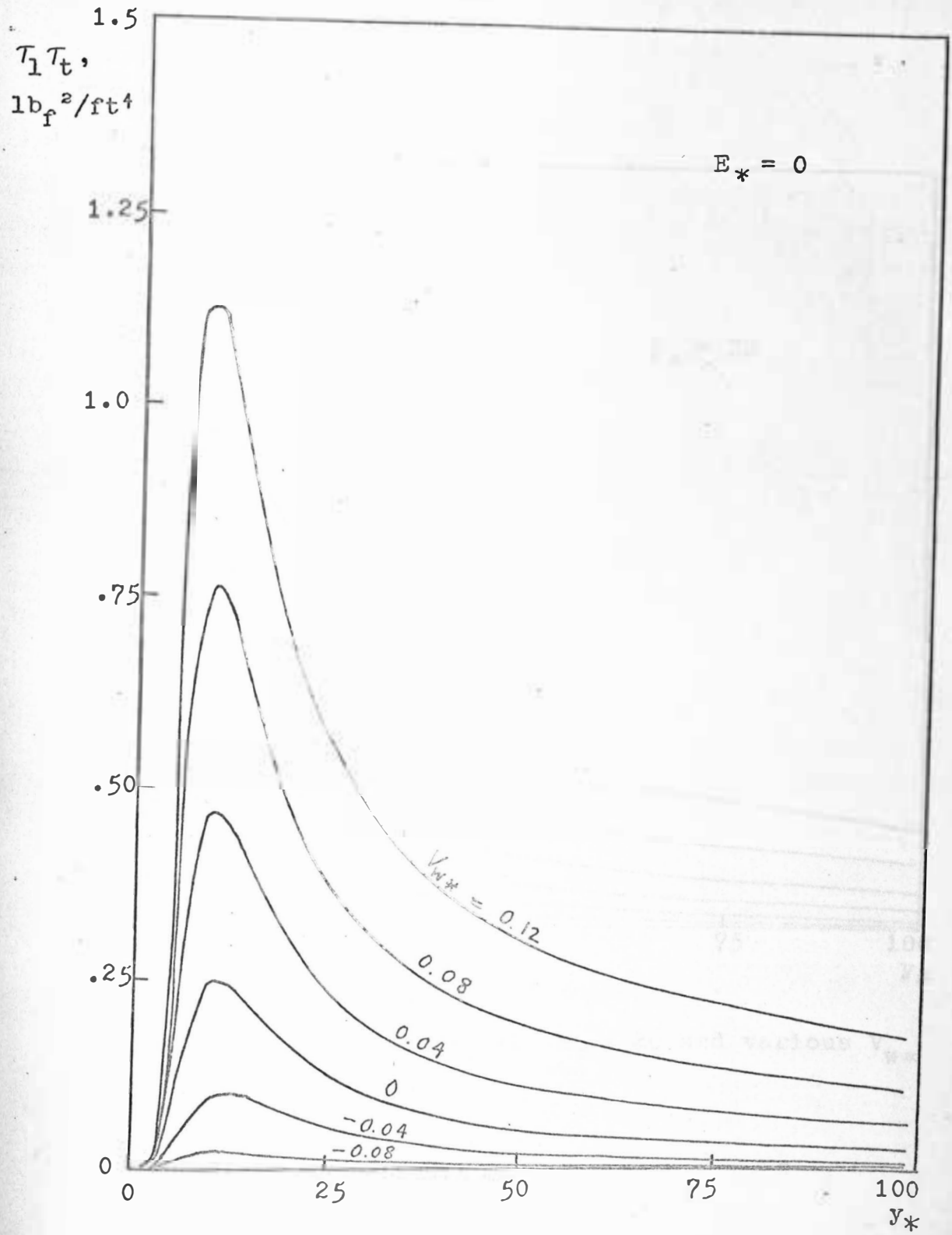

Fig. 4-18 $\tau_l \tau_t$ versus y_* at $E_* = 0$ and various V_{w*}

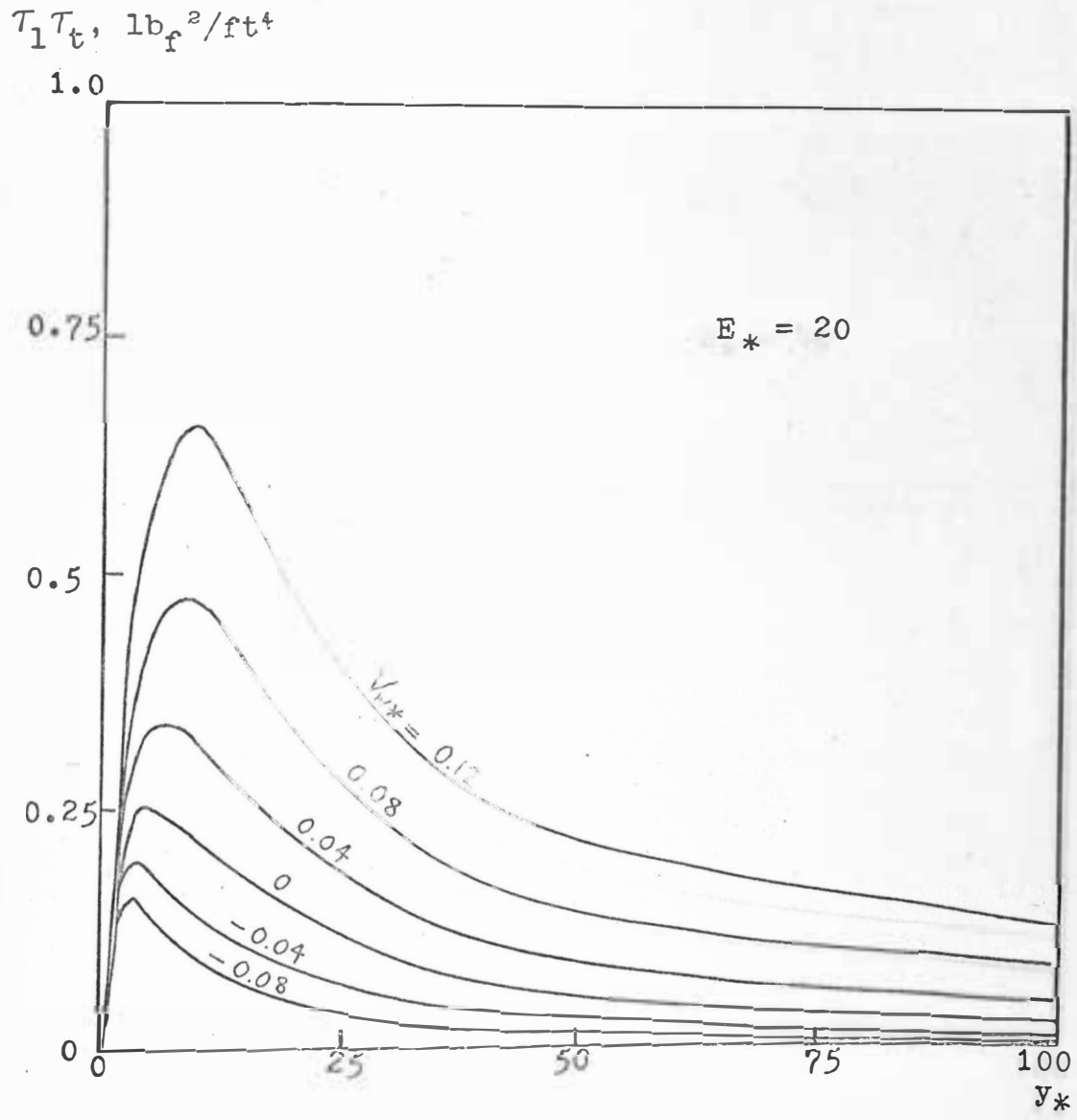

Fig. 4-19 $\tau_l \tau_t$ versus y_* at $E_* = 20$ and various V_{w*}

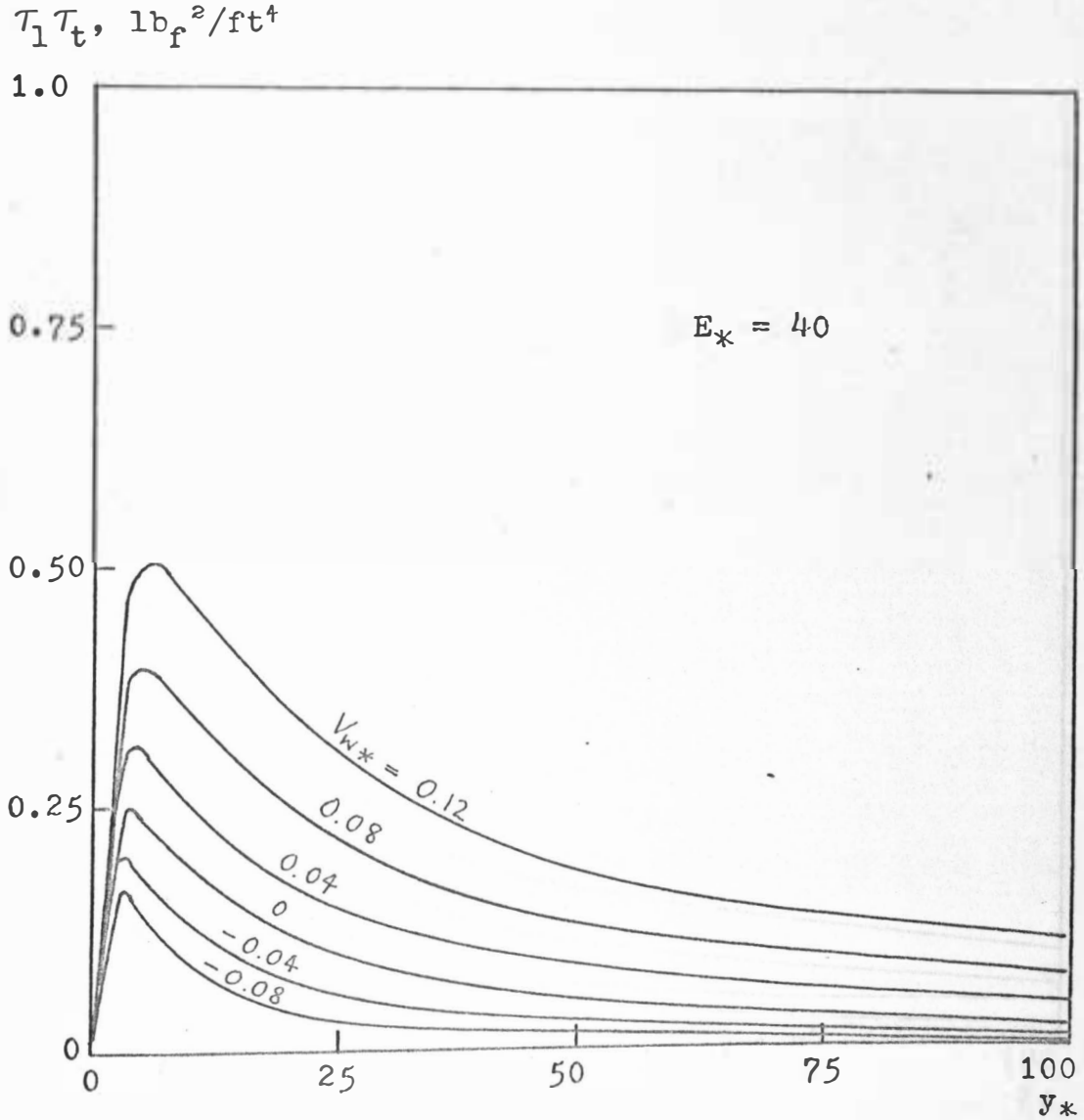

Fig. 4-20 $\tau_l \tau_t$ versus y_* at $E_* = 40$ and various V_{w*}

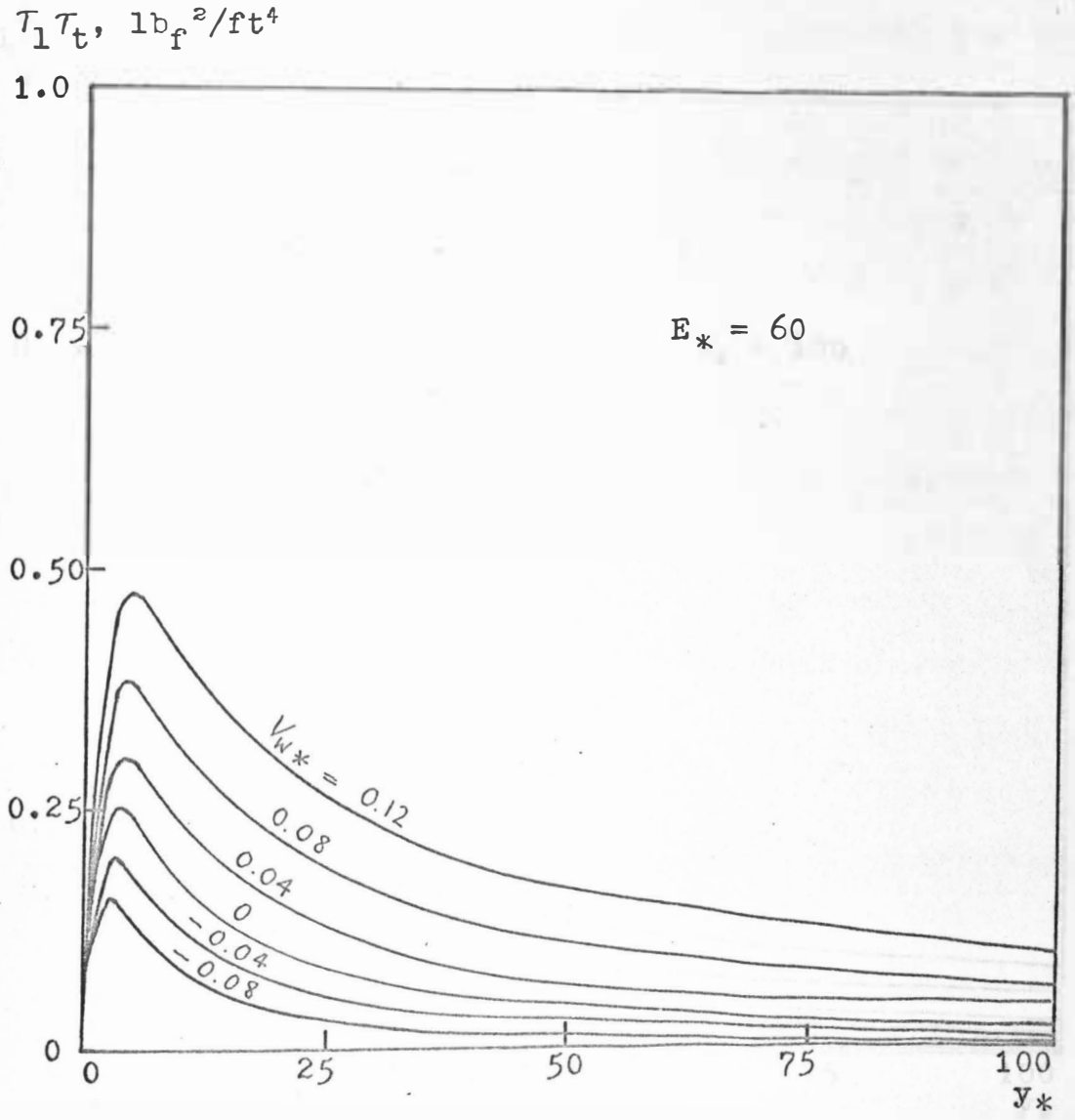

Fig. 4-21 $\tau_l \tau_t$ versus y_* at $E_* = 60$ and various V_{w*}

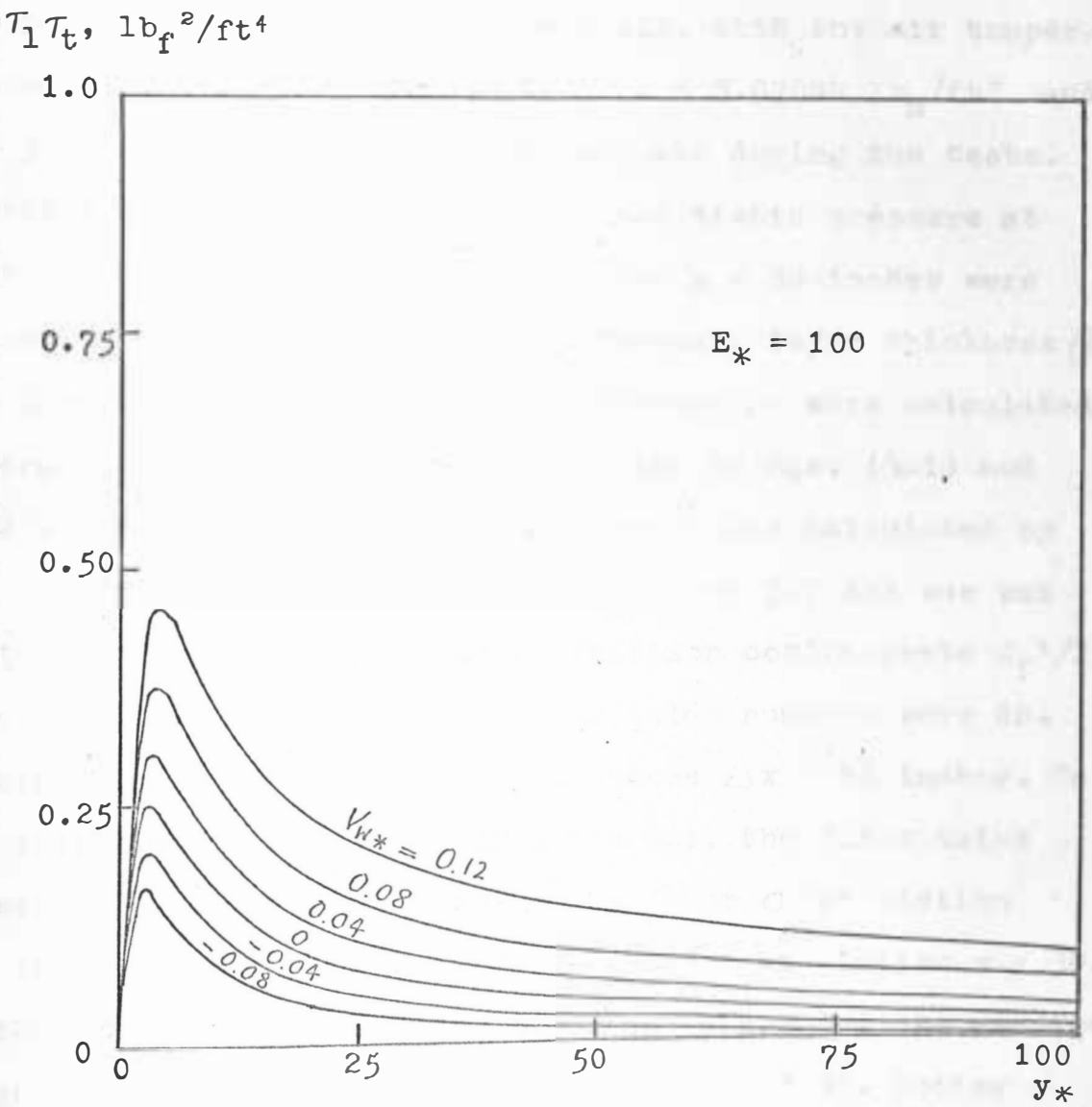

Fig. 4-22 $\tau_l \tau_t$ versus y_* at $E_* = 100$ and various V_{w*}

B. Experimental Results

Series of tests for each panel were run according to the procedures outlined in Chapter III, with the air temperature at 100 °F. This implies that $\rho = 0.07044$ lb_m/ft^3 and $\mu = 3.97 \times 10^{-7}$ lb_f-sec/ft^2 for the air during the tests. Velocity profiles, total pressure, and static pressure at both station x = 12 inches and station x = 30 inches were measured and calculated. Momentum boundary layer thickness θ and displacement boundary layer thickness σ were calculated according to measured velocity profiles by Eqs. (3-1) and (3-2). Also, the roughness of each panel was calculated by the comparison method mentioned in Chapter III and was put in terms of U_oE/ν. The average friction coefficients $C_f'/2$ were tabulated in Table 4-1. The Reynolds numbers were determined using the differential distance $\Delta x = 18$ inches. In the third and fourth column of Table 4-1, the first value refers to boundary layer thicknesses θ or σ at station x = 12 and the second one refers to those at station x = 30. In the eighth column of Table 4-1, the values for the average friction coefficient were derived from Eq. (3-3). Notice that for a smooth plate (RAYL = $U_oE/\nu = 0$) at $R_x = 5.52 \times 10^5$, the value of $C_f'/2 = 1.85 \times 10^{-3}$ is 0.65×10^{-3} lower than the value obtained by Schlichting [10]. This error is due to a slight favorable pressure gradient because of a misadjustment on the adjustable plate. Since this pressure gradient was not measured, an assumption is made to adjust

the reference value (smooth plate) to coincide with standard values. The remaining coefficients are adjusted by the same factor. The corrected average friction coefficients are listed in Table 4-1 and are used for calculating roughness E.

The local friction coefficients $C_f/2$ which were obtained by Eq. (3-4) were tabulated in Table 4-2. The values of $C_f/2$ for smooth plates shown in Table 4-2 are also not consistent with those given by Schlichting [10], but vary irregularly. It is conjectured from this that the Preston tube is not a reliable instrument for obtaining wall shear data under conditions of mass transfer at the wall boundary. In fact, all values for $C_f'/2$ and $C_f/2$ in Tables 4-1 and 4-2 are not very accurate because of instrumentation difficulties. The ordinary manometer cannot read out very small pressure changes and is certainly not sensitive enough to measure total pressure changes in the sublayer. Another complication is the initial measurement point at $y = 0$ or very close to the wall, say, at $y = 0.002$ inches. This is not actually the zero point of the velocity profile except on a smooth plate.

The effects of wall roughness on velocity distribution explained by Pao [12] are given in Fig. 4-23. When roughness of the wall exists, the pressure tube lies on the surface of the wall and does not measure the actual total pressure.

Deviations in measurement due to this mislocation of the pressure tube is not considered at present. Its effects are also in no way predictable. A further difficulty is bringing the pressure tube in contact with the test panel to start the measurement. At present, the contact was made by the observation and feeling of the operator. The reproductivity of $y = 0$ is almost impossible to obtain. Deviations in the measurement of each run are thus expected. Nevertheless, the experimental results listed in Table 4-1 are still reasonable enough to be useful.

The dimensionless velocity profiles at stations $x = 12$ and $x = 30$ in each run were plotted in Figs. 4-24 to 4-28 with y/σ and U/U_o as coordinates. Each curve represents a main stream velocity profile under a specified V_w as indicated in each figure. Only limited runs were made for each panel, and only five panels were studied. No definite conclusions can be drawn from the collected data. However, the trend that injection and roughness increase the boundary layer thickness and that suction decreases the boundary layer thickness can be seen in Tables 4-1 and 4-2. Also that injection delays the dimensionless velocity profile and that suction flattens the dimensionless velocity profile can be observed from the data on Figs. 4-24 to 4-28.

U_o, fps	R_x	θ, in.	σ, in.	V_w/U_o	RAYL	U_oE/ν	$C_f'/2$ by Eq. 3-3	$C_f'/2$ corrected
66.87	5.52×10^5	0.031 0.064	0.0358 0.0749	0	0	0	1.85×10^{-3}	2.5×10^{-3}
68.22	5.64	0.0308 0.0741	0.036 0.0864	0	5	270	2.41	3.06
69.24	5.72	0.112 0.225	0.149 0.316	5.05×10^{-3}	5	274	1.28	1.93
68.74	5.69	0.0154 0.0157	0.0223 0.0232	-2.18	5	272	2.20	2.85
70.25	5.8	0.0566 0.1031	0.0755 0.1356	0	16	300	2.58	3.2
71.79	5.93	0.1396 0.2578	0.2087 0.3837	5.29	16	306	1.27	1.92
68.48	5.6	0.0117 0.0125	0.0186 0.0284	-2.19	16	293	2.24	2.89
70.9	5.87	0.0573 0.1039	0.0758 0.141	0	25	310	2.59	3.24

$\triangle x$ = 18 in.

(continued)

Table 4-1 Experimental Data and Results I

$\triangle x$ = 18 in. (continued)

U_o, fps	R_x	θ, in.	σ, in.	V_w/U_o	RAYL	U_oE/ν	$C_f'/2$ by Eq. 3-3	$C_f'/2$ corrected
71.48	5.91×10^5	0.1283 0.229	0.1862 0.3367	3.5	25	312	2.35	3.0
67.71	5.58	0.0121 0.014	0.0202 0.0216	-2.22	25	296	2.32	2.97
69.25	5.71	0.0657 0.1162	0.0879 0.1527	0	40	380	2.81	3.45
70.37	5.82	0.1478 0.2387	0.2183 0.3617	3.69	40	386	1.37	2.02
69.05	5.7	0.0373 0.032	0.0498 0.0503	-2.17	40	379	2.17	2.82

Table 4-1 (continued) Experimental Data and Results I

x, in.	U_o, fps	R_x	V_w/U_o	RAYL	$C_f/2$ by Eq. 3-4
12	66.87	3.68×10^5	0	0	2.1×10^{-3}
30		9.21			1.99
12	68.22	3.76	0	5	2.35
30		9.388			2.397
12	69.24	2.81	5.05×10^{-3}	5	1.95
30		9.54			1.8
12	68.74	3.79	-2.18	5	2.074
30		9.5			2.03
12	70.25	3.95	0	16	2.52
30		9.89			2.24
12	71.79	3.95	5.29	16	1.88
30		9.67			1.80
12	68.48	3.73	-2.19	16	2.34
30		9.43			2.14
12	70.9	3.91	0	25	2.55
30		9.78			2.14

(continued)

Table 4-2 Experimental Results and Data II

(continued)

x, in.	U_o, fps	R_x	V_w/U_o	RAYL	$C_f/2$ by Eq. 3-4
12	71.48	3.94×10^5	3.5	25	2.038×10^{-3}
30		9.85			1.75
12	67.71	3.73	-2.22	25	2.33
30		9.32			1.998
12	69.25	3.81	0	40	2.25
30		9.54			2.13
12	70.37	3.88	3.69	40	1.9
30		9.69			1.79
12	69.05	3.8	-2.17	40	2.22
30		9.51			2.04

Table 4-2 (continued) Experimental Results and Data II

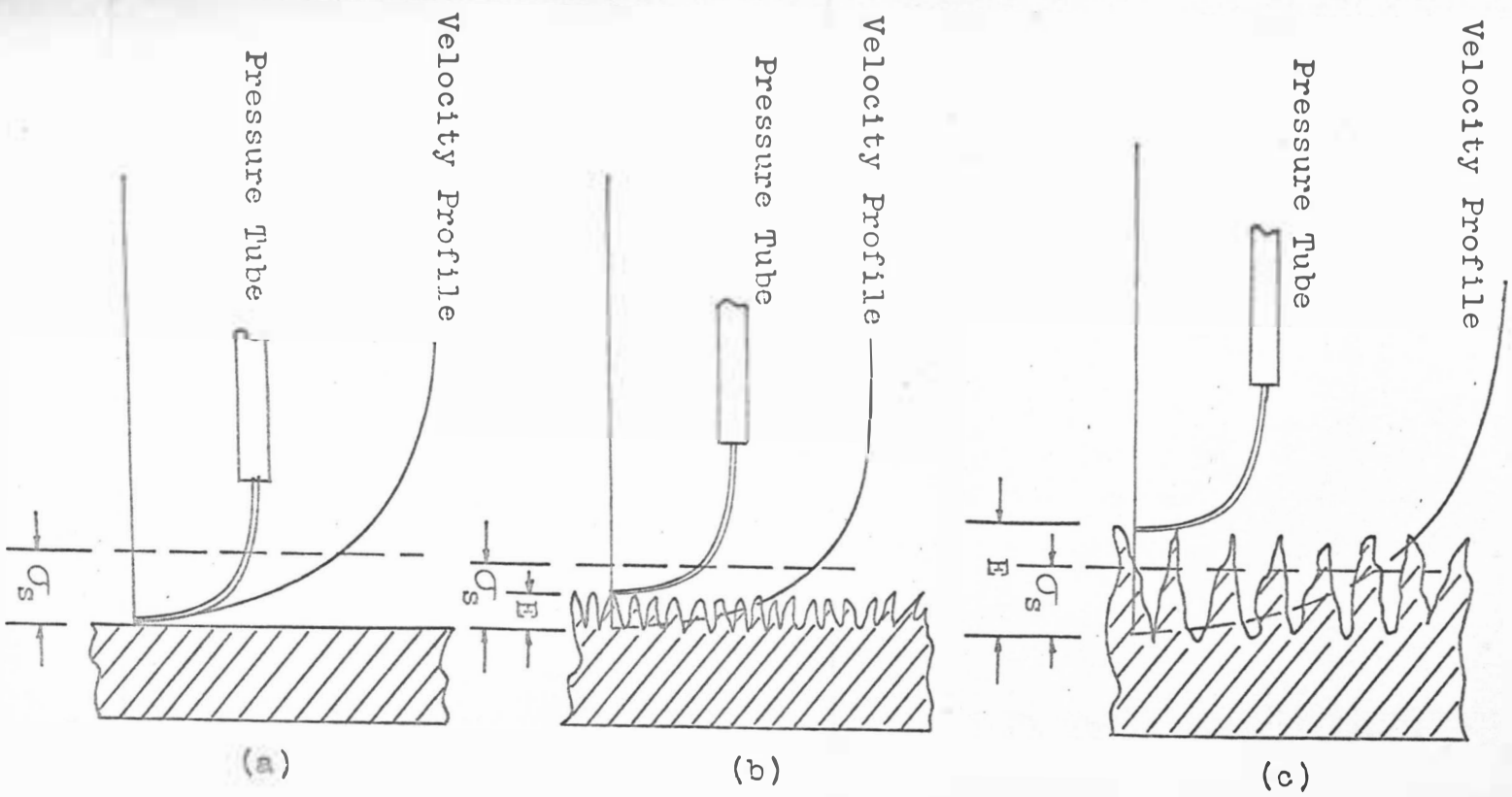

Fig. 4-23 Effect of wall roughness on the measurement of the velocity profile

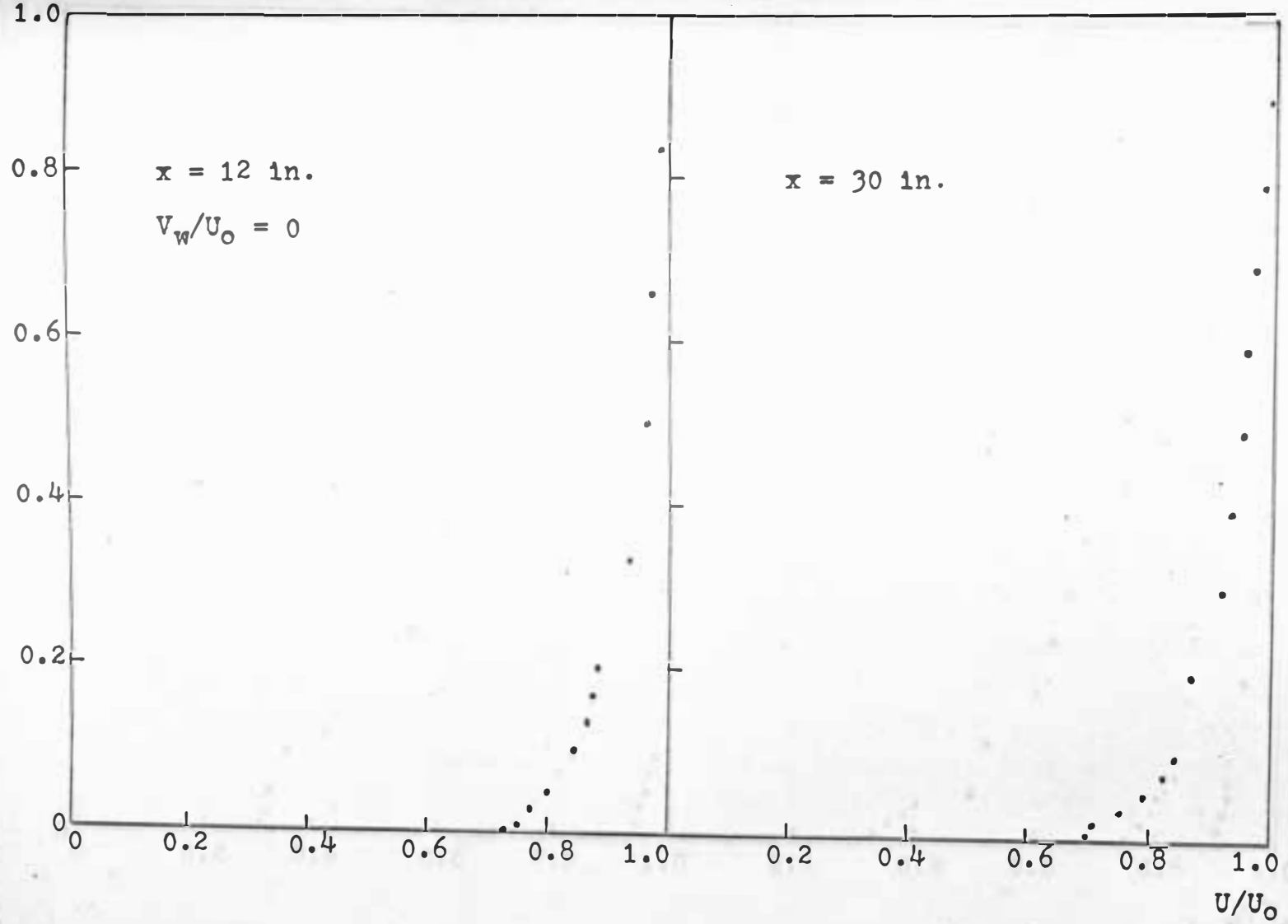

Fig. 4-24 Dimensionless velocity profile of a smooth flat plate

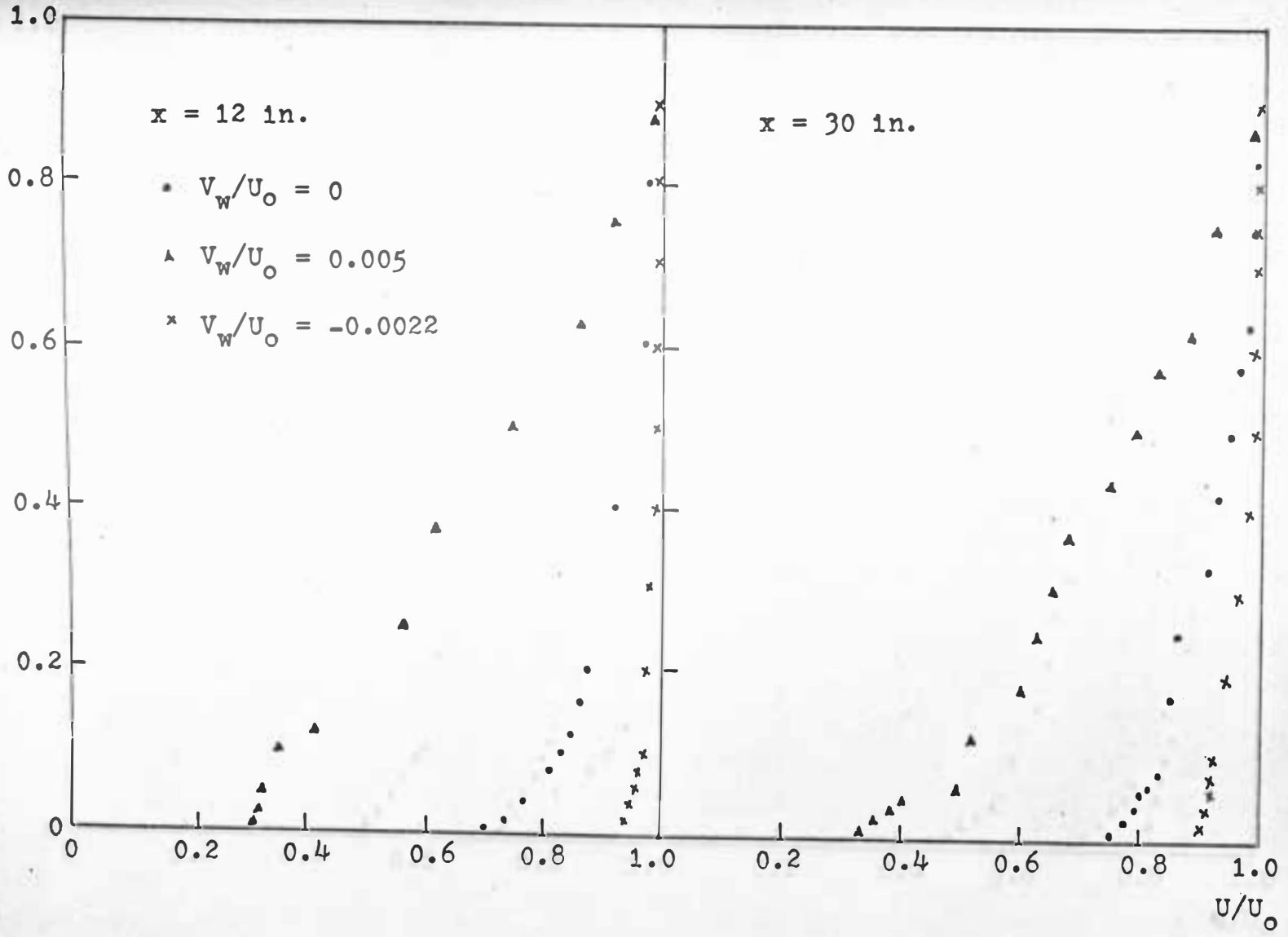

Fig. 4-25 Dimensionless velocity profile of a 5-RAYL panel

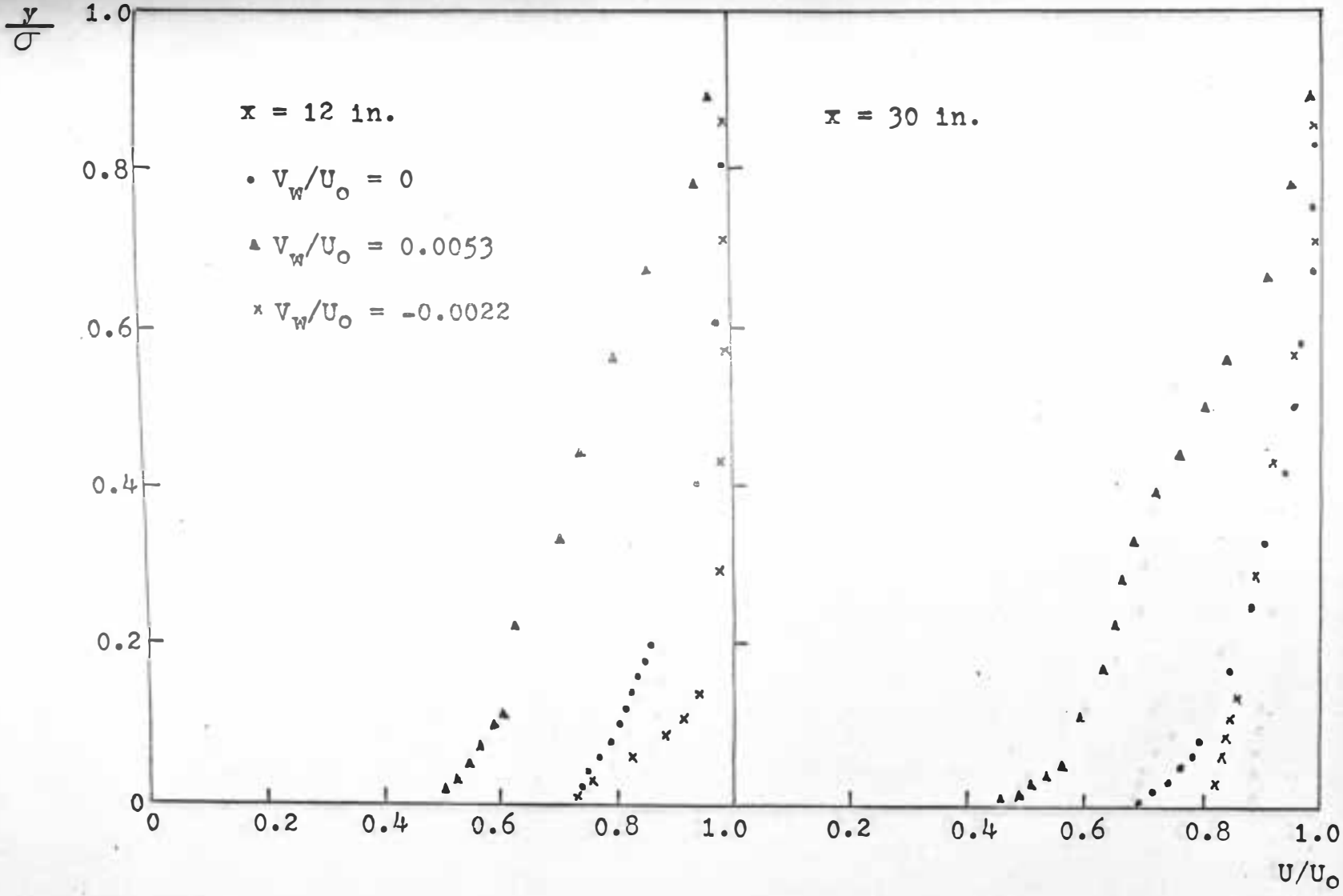

Fig. 4-26 Dimensionless velocity profile of a 16-RAYL panel

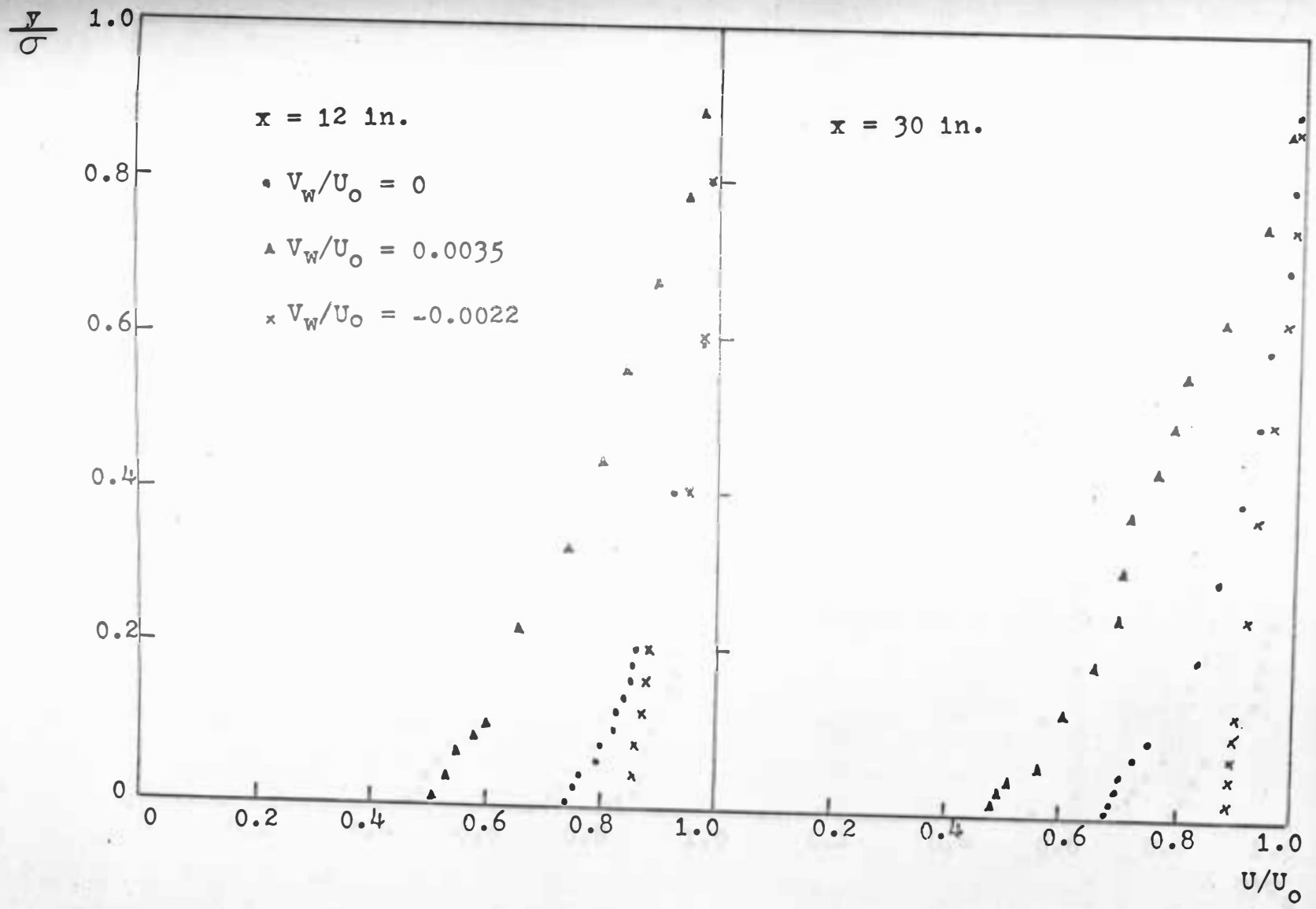

Fig. 4-27 Dimensionless velocity profile of a 25-RAYL panel

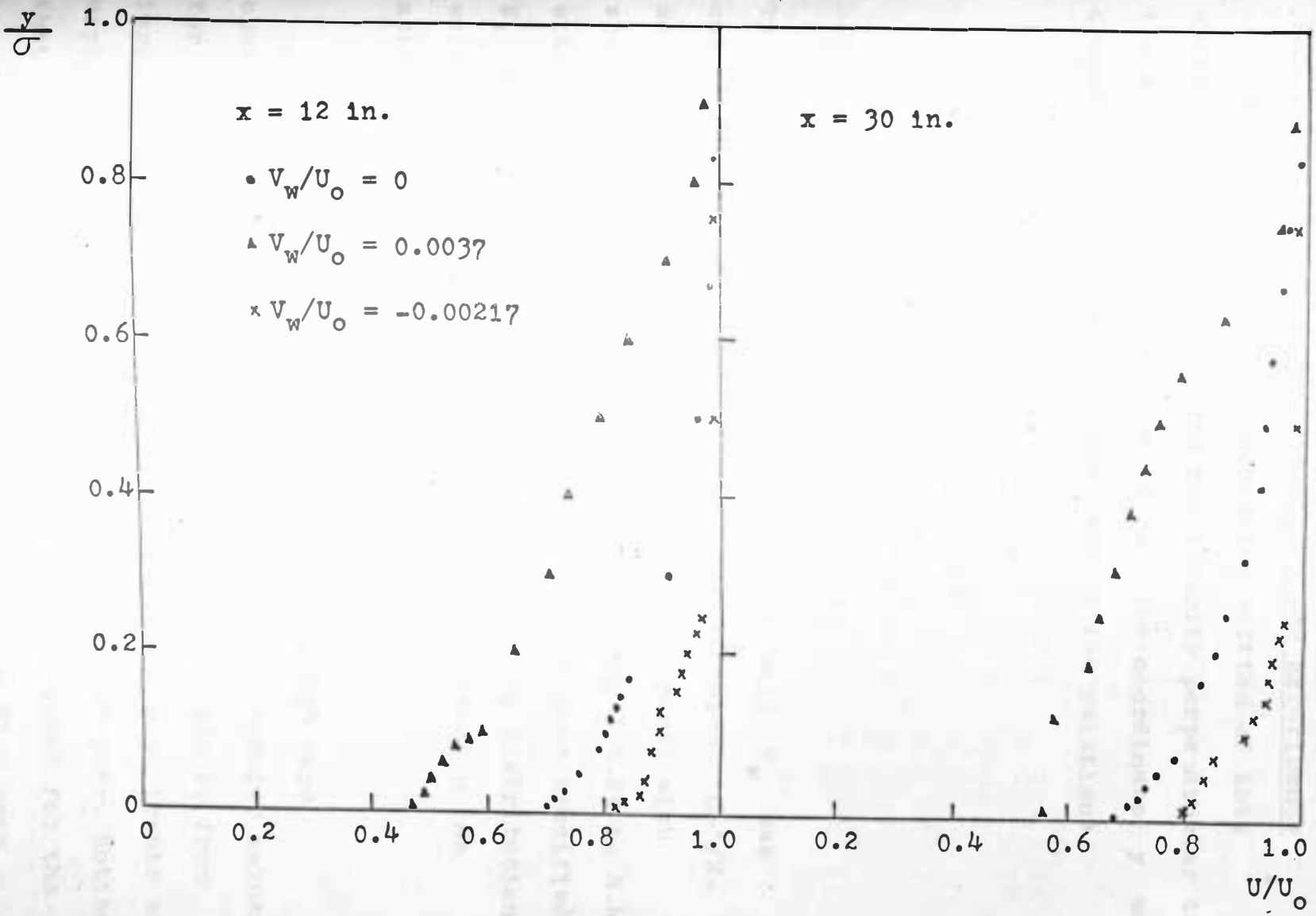

Fig. 4-28 Dimensionless velocity profile for a 40-RAYL panel

C. Comparison Between Theory and Experiments

Based on data in the preceeding section of this chapter, the velocity U and the velocity perpendicular to the wall V_w, the roughness E and the coordinate y were transformed into dimensionless form by the relations

$$U_* = U/\sqrt{\tau_w/\rho}$$

$$V_{w*} = V_w/\sqrt{\tau_w/\rho}$$

$$E_* = \sqrt{\tau_w/\rho}\, E/\nu$$

$$y_* = \sqrt{\tau_w/\rho}\, y/\nu$$

by employing Program V. The shear at the wall τ_w was calculated from the average friction coefficient $C_f'/2$. Results corresponding to each run for each panel with specified E_* and V_{w*} were plotted in Figs. 4-29 to 4-41 with U_* and y_* as coordinates. With the same specified E_* and V_{w*}, theoretical universal velocity distributions were obtained with Program I; they were plotted in the appropriate figures.

Deviations between theory and experiments were observed. Those deviations may be caused by improper values for A_*, D_* or χ in the theoretical analysis or from improperly measured data obtained during the experiments as explained in the preceeding section of this chapter. Notice that the deviations between theory and experiment for the suction case are very small. This is because flow over

porous plates with suction is more stable than flow with injection or flow with neither injection nor suction, and less errors exist during measurements. This also implies that the deviations between theory and experiments can be attributed mostly to the experiments and only to a minor degree to the theory. These deviations might be decreased and the results improved by resolving the existing difficulties in instrumentation. Another point to support the correctness of the theory is that the shear within the boundary layer should increase under injection, which is shown by the theory, whereas the experimental values indicate only a negligible increase in shear. Therefore, the present theory seems to provide an acceptable means of obtaining the velocity distribution and turbulent shear stress distribution of flow over rough porous plates.

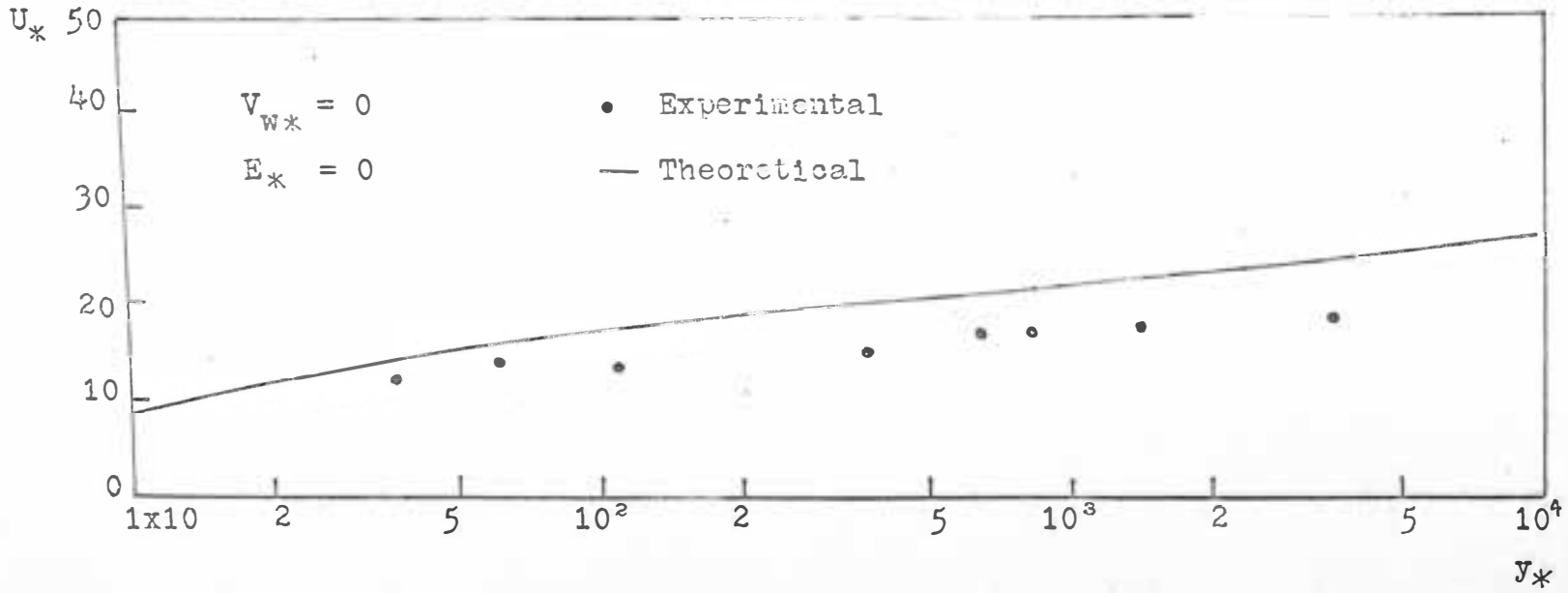

Fig. 4-29 Shear velocity profile of a smooth plate

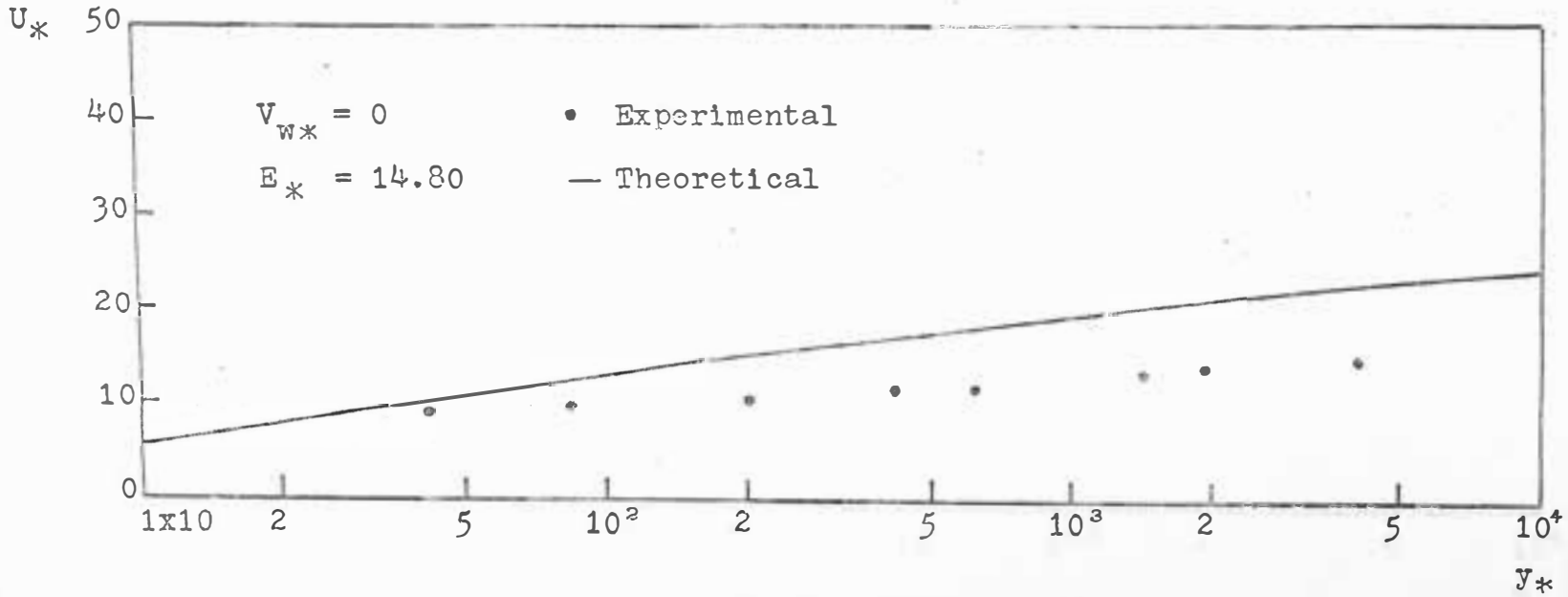

Fig. 4-30 Shear velocity profile of a 5-RAYL panel

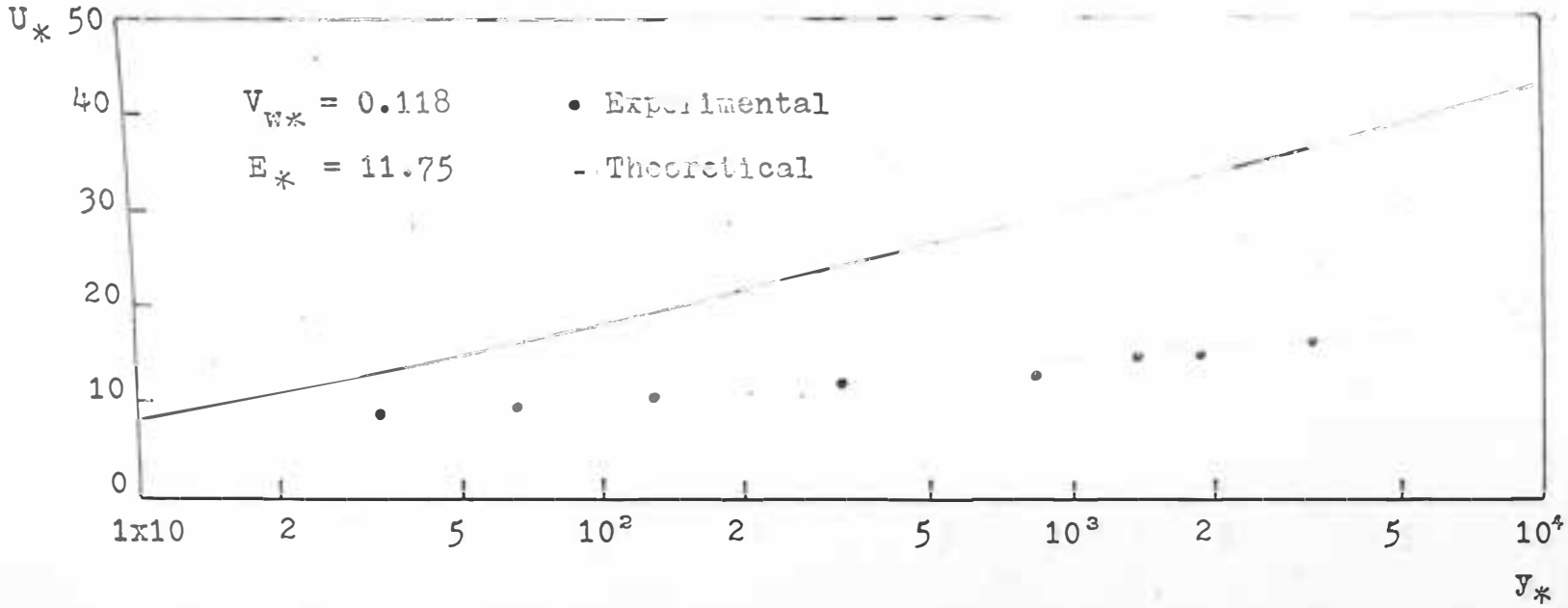

Fig. 4-31 Injection shear velocity profile of a 5-RAYL panel

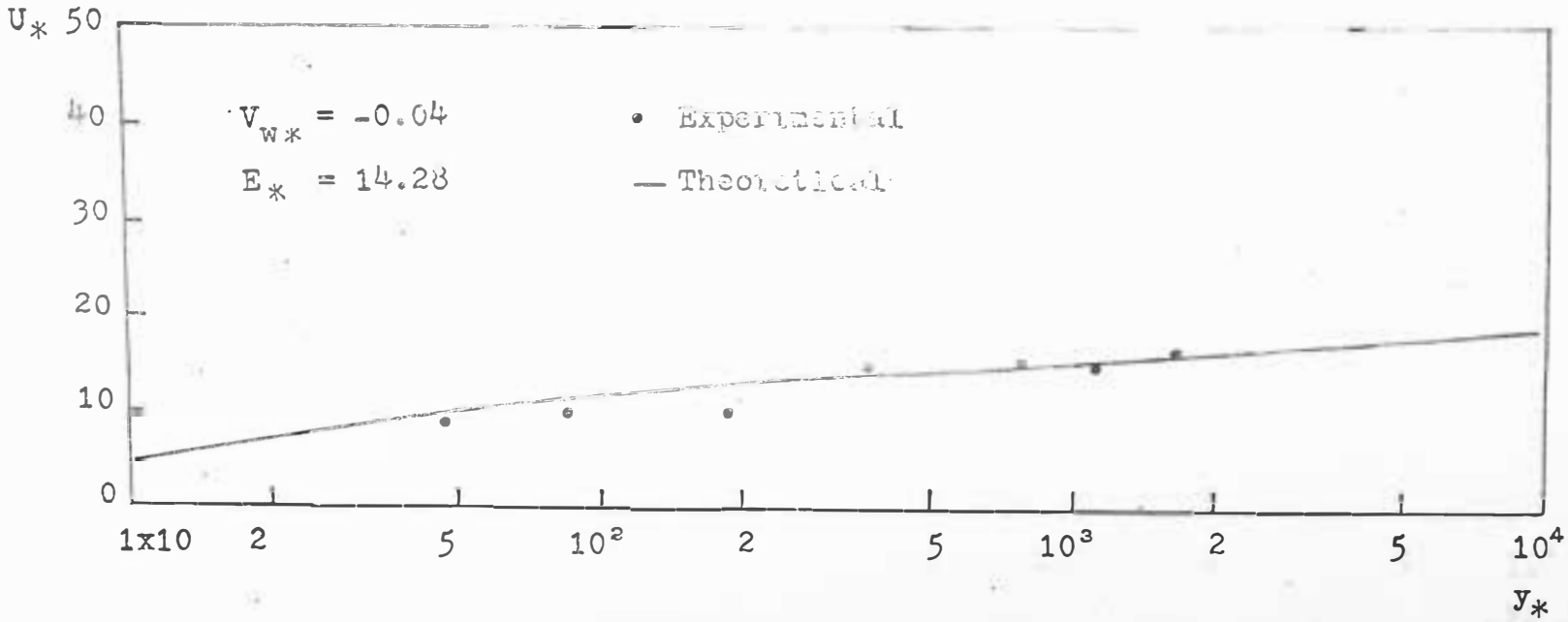

Fig. 4-32 Suction shear velocity profile of a 5-RAYL panel

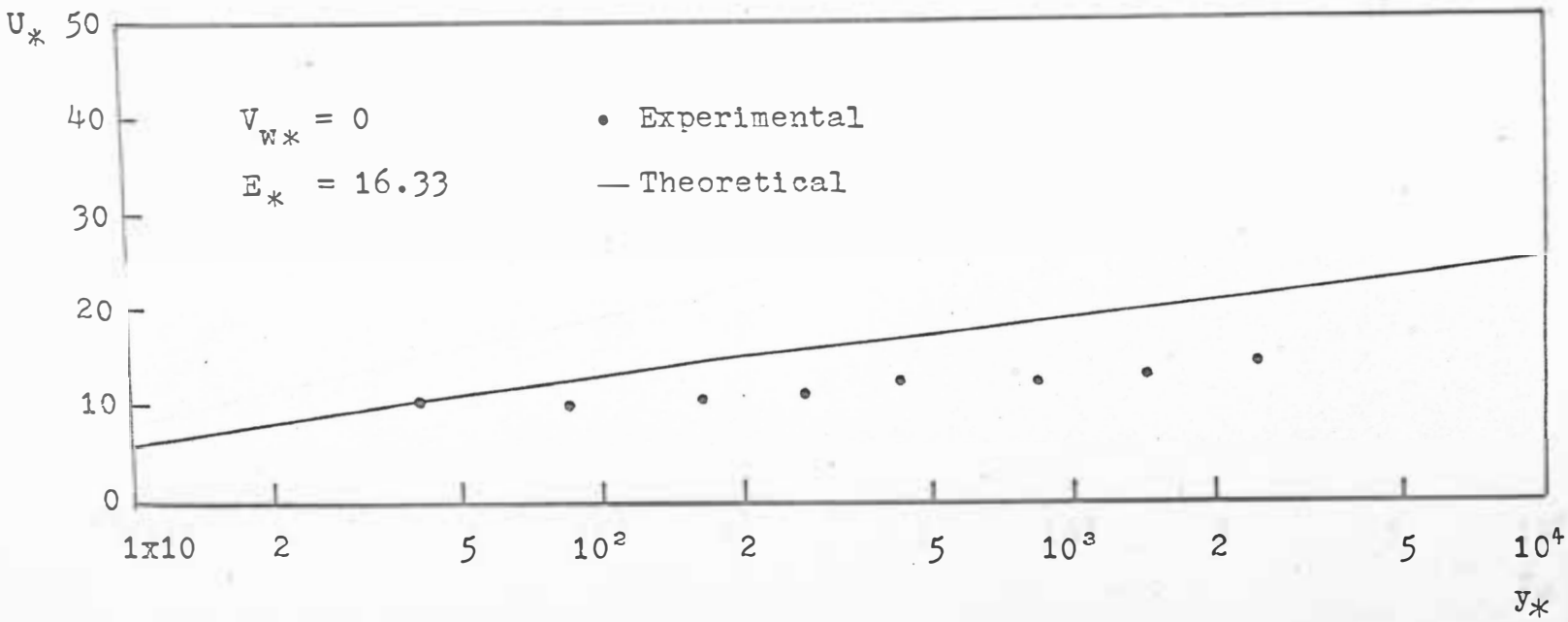

Fig. 4-33 Shear velocity profile of a 16-RAYL panel

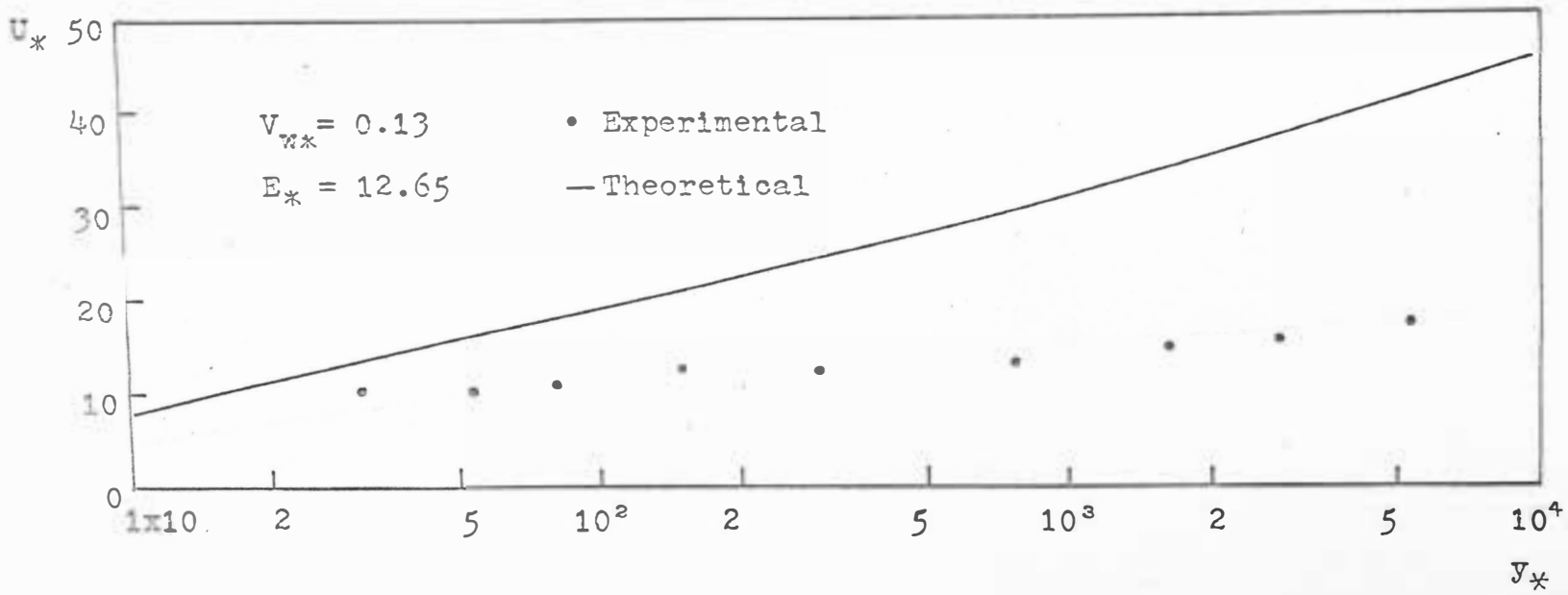

Fig. 4-34 Injection shear velocity profile of a 16-RAYL panel

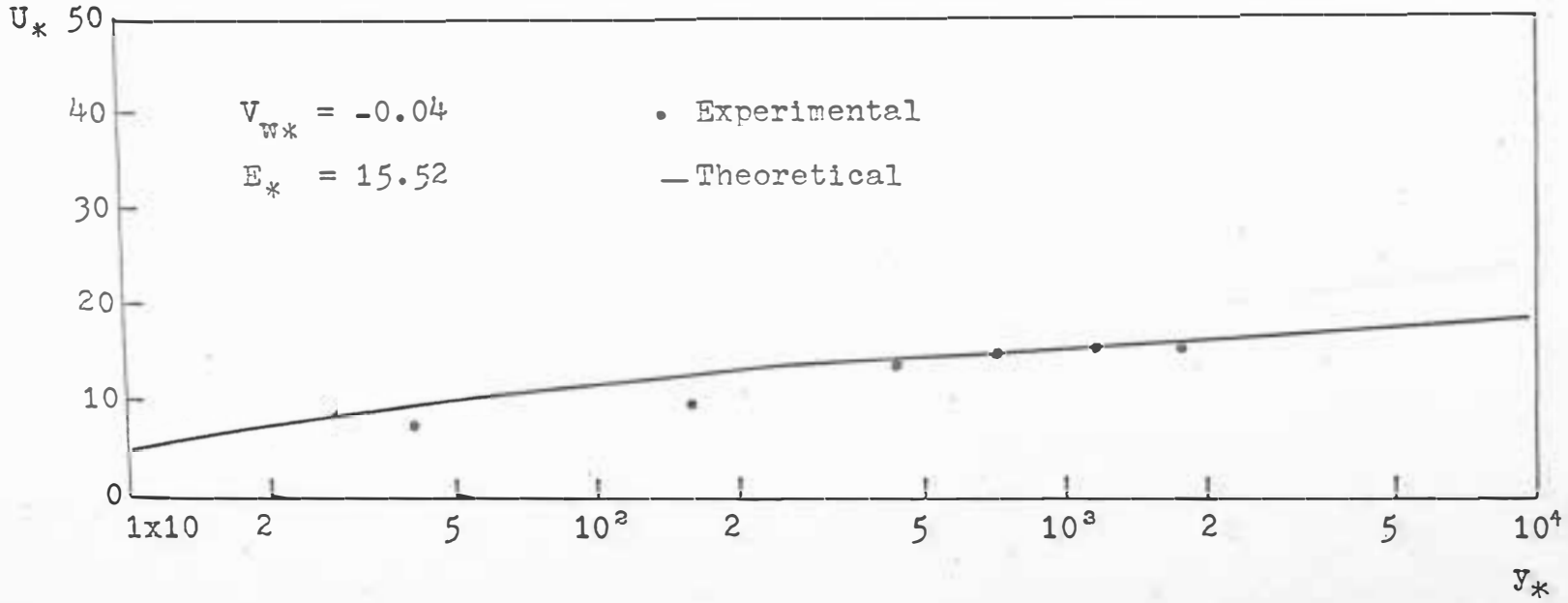

Fig. 4-35 Suction shear velocity profile of a 16-RAYL panel

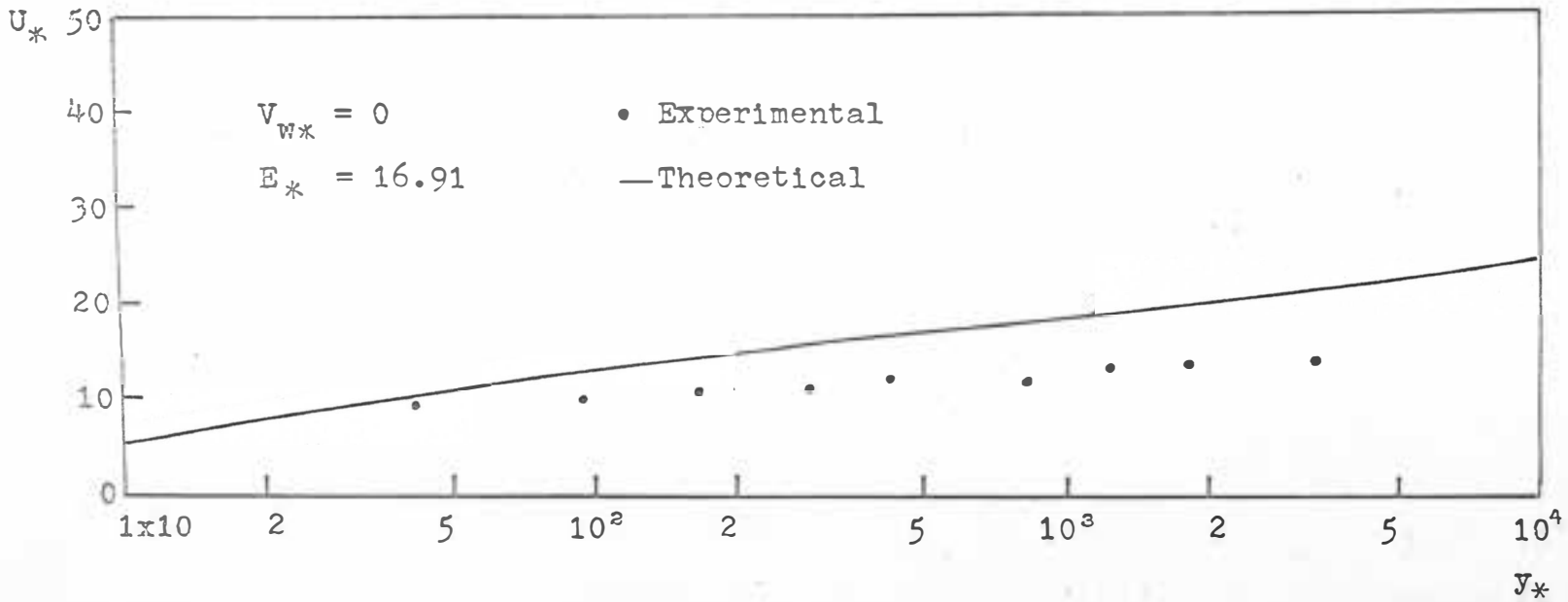

Fig. 4-36 Shear velocity profile of a 25-RAYL panel

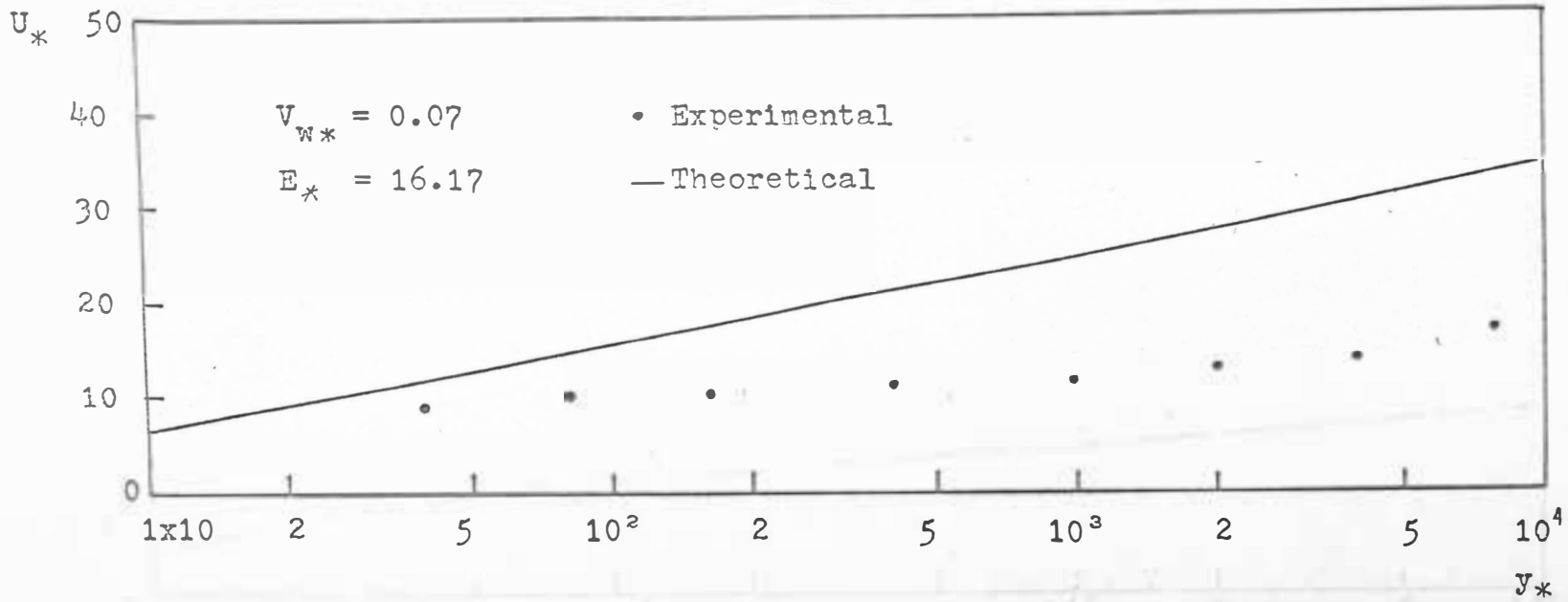

Fig. 4-37 Injection shear velocity profile for a 25-RAYL panel

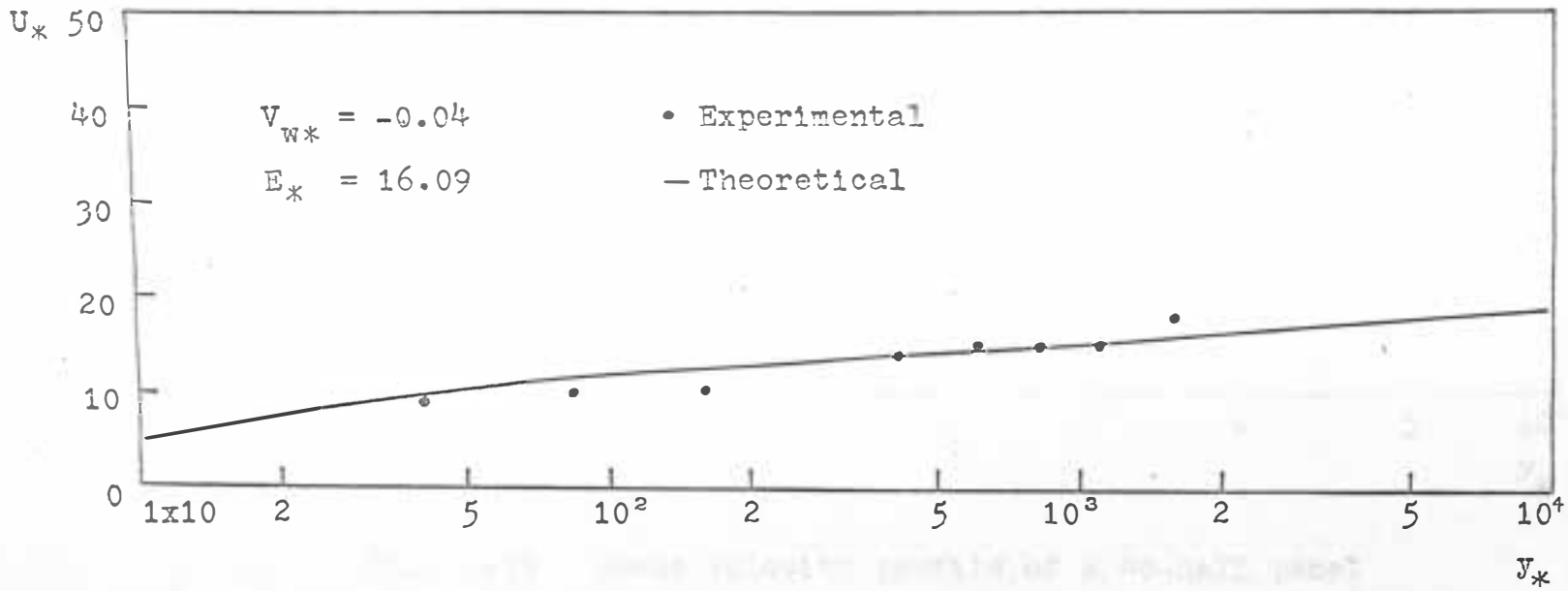

Fig. 4-38 Suction shear velocity profile of a 25-RAYL panel

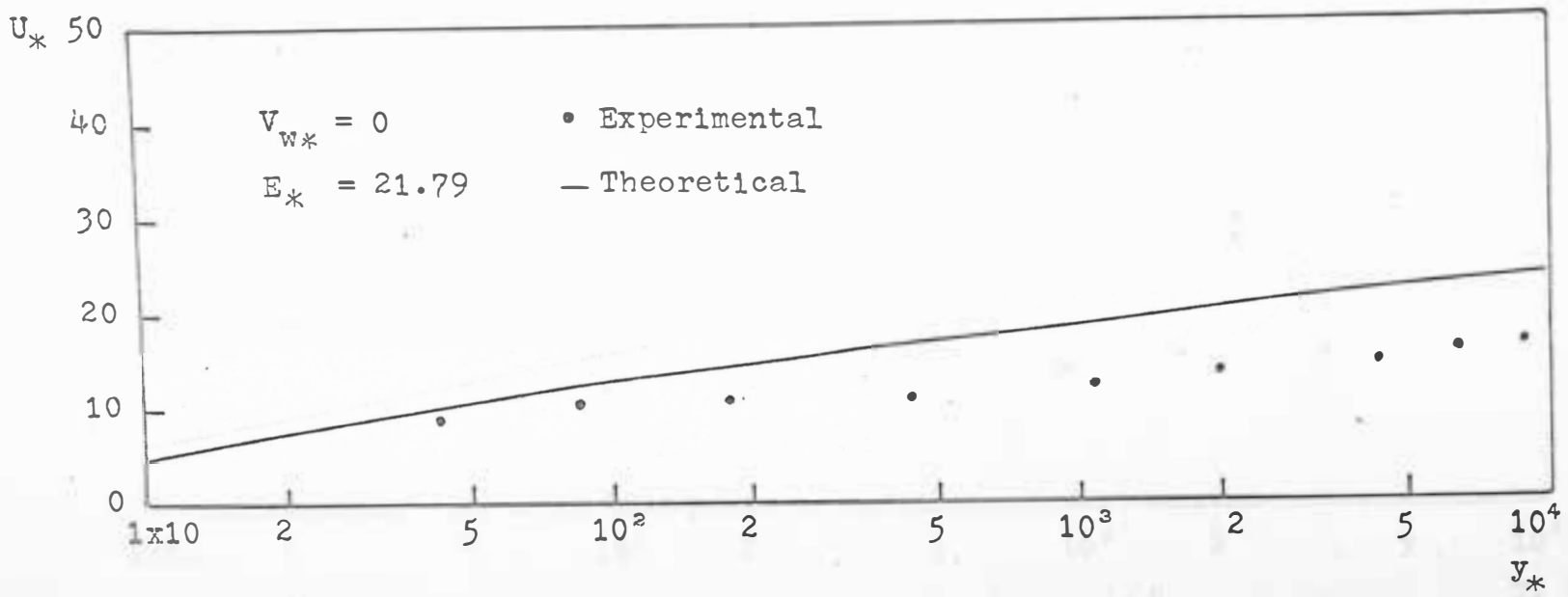

Fig. 4-39 Shear velocity profile of a 40-RAYL panel

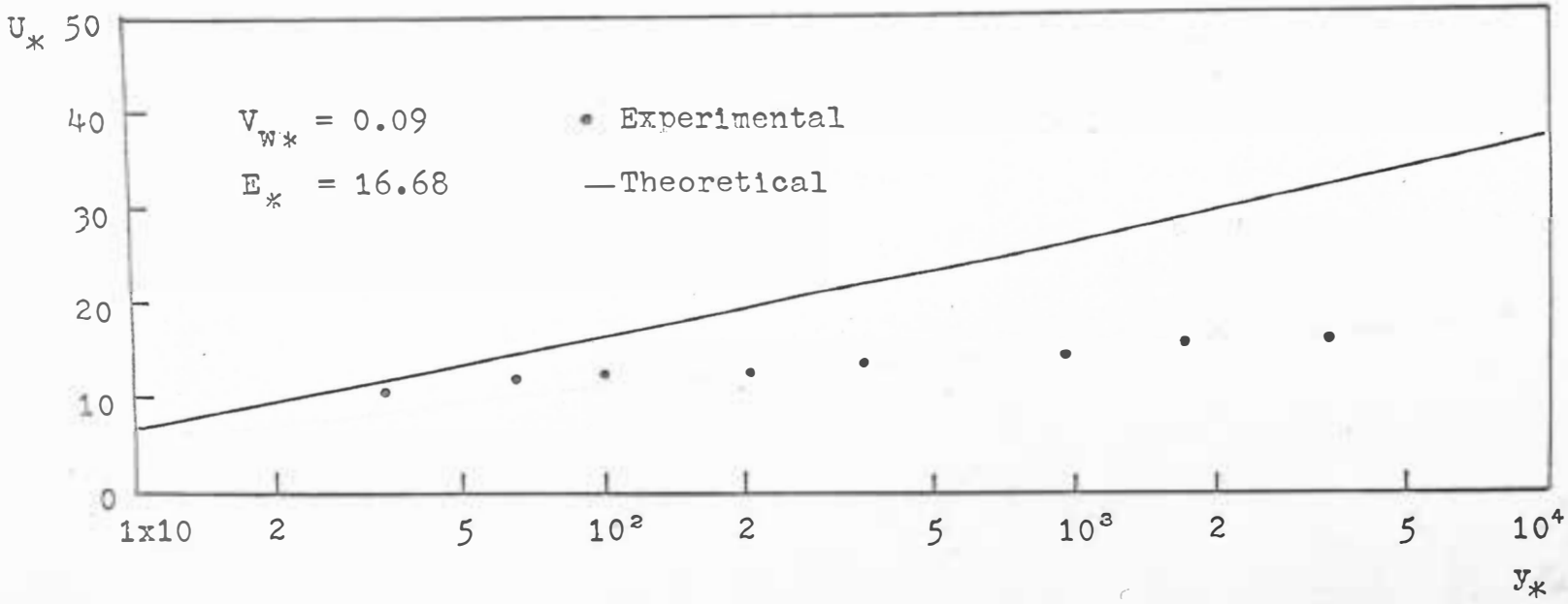

Fig. 4-40 Injection shear velocity profile of a 40-RAYL panel

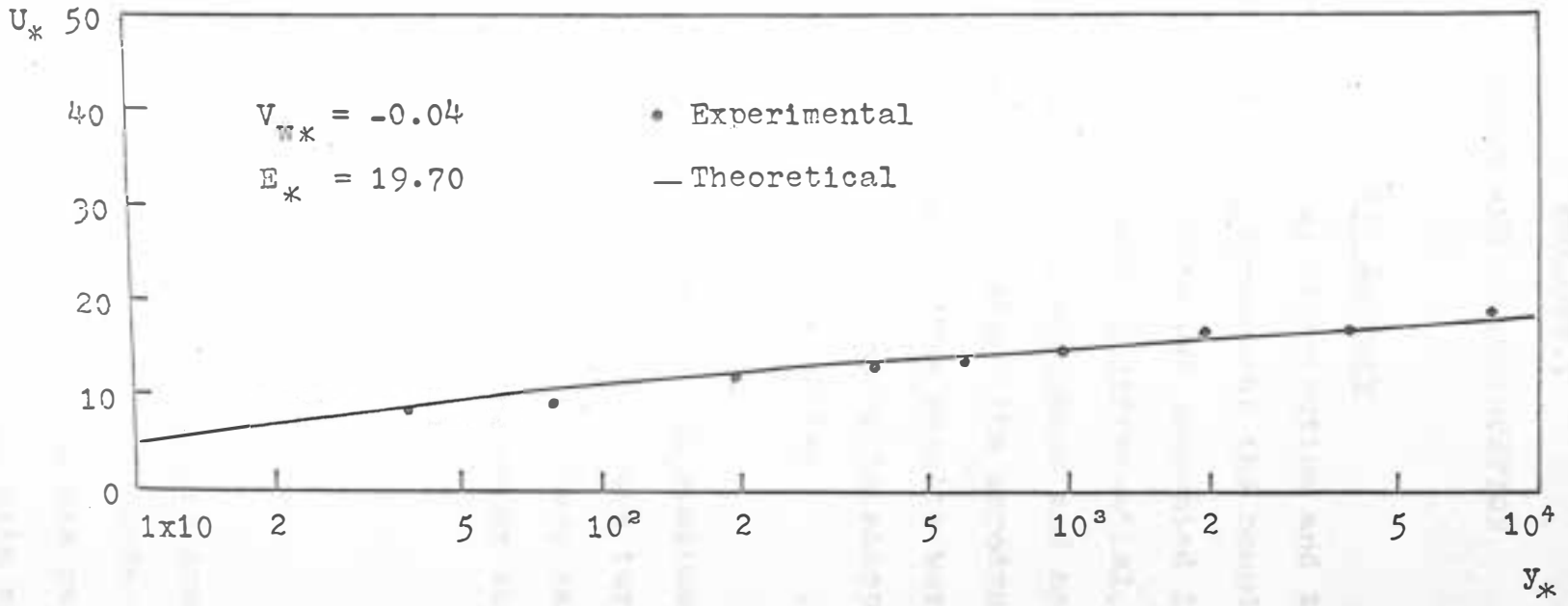

Fig. 4-41 Suction shear velocity profile of a 40-RAYL panel

CHAPTER V

SUMMARY AND RECOMMENDATION

A. Summary

The universal velocity distribution and the turbulent shear stress distribution throughout the boundary layer of flow over a rough porous plate was presented in Chapter II by solving the governing partial differential equation. In Chapter III, the experimental equipment and methods were discussed which were used to study the aerodynamic properties of acoustic panels. The results were examined in Chapter IV; they show that the theory is acceptable through a comparison with experimental results.

Effects of injection, suction and roughness on the universal velocity distribution and on the turbulent shear stress distribution throughout the boundary layer can be predicted by the theory. However, the shear stress at the wall must be determined experimentally.

B. Recommendation

1. In Theory

Present studies assumed zero pressure gradient and constant distribution of surface mass transfer along the plate. In practical use, however, cases are rarely like those which have been assumed. The flow with non-zero

pressure gradient and with variable surface mass transfer along the plate should be analyzed and descriptive equations developed.

2. In Experiments

Either a mechanical or electronic device should be used to improve the reproductivity of readings at $y = 0$. Also, a micro-manometer of the Prandtl type should be used to obtain more sensitive readings. Even though a hot-wire anemometer is good for measuring velocity fluctuations, it is not accurate for measuring small changes in the mean velocity profile. However, hot-wire anemometers should be employed to study the turbulent motion of the fluid throughout the boundary layer.

REFERENCES

1 Griffith, A.A., and Meredith, F.W., "The Possible Improvement on Aircraft Performance Due to the Use of Boundary Layer Suction," Rep. aero. Res. Coun., London, No. 2315, 1936.

2 Schlichting, H., "An Approximate Method for Calculation of the Laminar Boundary Layer with Suction for Bodies of Arbitrary Shape," Tech. Memor. nat. adv. Comm. Aero., Washington, No. 1216, 1948, pp. 201 - 220.

3 Kay, J.M., "Boundary-Layer Flow Along a Flat Plate with Uniform Suction," Rep. Memor. aero. Res. Coun., London, No. 2628, 1948.

4 Thwaites, B., "The Development of Laminar Boundaries Under Conditions of Continuous Suction," (Part II: Approximate Methods of Solution), Rep. aero. Res. Coun., London, No. 12699, 1949.

5 Ringleb, R.O., "Computation of the Laminar Boundary Layer with Suction," J. Aero. Sci., 19, 1952. pp. 48 - 54.

6 Mickley, H.S., and Davis, R.S., "Momentum Transfer for Flow Over a Flat Plate With Blowing," NACA Tech. Note 4017, 1957.

7 Rotta, J.C., "On the Velocity Distribution with Turbulent Flow in the Vicinity of Porous Walls," Deutsche Luft- und Raumfahrt, 1966.

8 Van Driest, E.R., "On Turbulent Flow Near a Wall," J. Aero. Sci., 23, 1956, pp. 1007 - 1011.

9 Stokes, G.G., "On the Effect of the Internal Friction of Fluids on the Motion of Pendulums," Trans. Cambridge Philos. Soc., Vol. 9, 1851.

10 Schlichting, H. Boundary Layer Theory, 6th ed., McGraw-Hill, New York, 1968 (Graph: p. 611).

11 Smith, D.W., and Walker, J.H., "Skin Friction Measurements in Incompressible Flow," Tech. Notes, nat. adv. comm. Aero., Washington, No. 4231, 1958.

12 Pao, R.H.F., Fluid Mechanics, McGraw-Hill, New York, 1961.

APPENDIX

I PROGRAM FOR CALCULATING VELOCITY DISTRIBUTION

Program Symbol	Analysis Symbol	Note
Input:		
AK	κ	= 0.4
VW	τ_{w*}	
C1		= 1
C2		= 0 (no roughness) = 1 (with roughness)
E	E_*	
Output:		
EPD	τ_t/τ_w	
EMU	μ_t/ρ	
Y(I)	y_*	
U(I)	U_*	
RDU	dU_*/dy_*	
I		Index belonging to Y(I)
TAUT	τ_t/τ_w	
YL		Last value y_* for which U_* was calculated
IL		Index belonging to YL

```
      DIMENSION Y( 50),Z( 50),U( 50),PH( 50),DU( 50)
    1 FORMAT (F11.7)
    2 FORMAT (3(F10.5))
    3 FORMAT (1H1,F11.7,F10.5)
    4 FORMAT (1H0,F10.5)
    5 FORMAT (1H ,I6,6(4X,E11.4))
    7 FORMAT (1H0,I6,6HMAX Y=,E11.4)
   11 READ (11,1) AK
   12 READ (11,1) VW
   13 READ (11,2) C1,C2,E
    8 WRITE (12,3) VW,E
      IF(E)14,14,15
   14 E=E+60.
   15 D=60.
      IF(VW)16,17,17
   16 A=26.-200.*VW
      GO TO 18
   17 A=26.-25.*VW
   18 WRITE (12,4) A
      DZ=0.1
      DZN=2.303*DZ/3.
      Z(1)=-0.8
      DO 20 J=2,4
      I=J
      Z(I)=Z(I-1)+DZ
      Y(I)=10.**Z(I)
      IF (ABS(VW)-0.0001)87,88,88
   88 DU(J)=Y(I)*EXP(VW*Y(I))
      U(I)=1./VW*(EXP(VW*Y(I))-1.)
      GO TO 19
   87 U(I)=Y(I)
      DU(J)=Y(I)
   19 IF (1.+VW*U(I))70,119,119
  119 YT=(-Y(I)*SQRT(1.+VW*U(I)))/A
   20 PH(I)=(1.-C1*EXP(YT)+C2*EXP(YT*D/E))**2
      M=1
      I=4
      J=I
      L=1
      GO TO 45
   31 I=I+1
      J=I
      IF (I- 50)32,32,70
   32 Z(I)=Z(I-1)+DZ
      Y(I)=10.**Z(I)
      GO TO (33,81),L
   81 IF (Y(I)-YL) 33,82,82
   33 DU(J)=3.*(DU(J-1)-DU(J-2))+DU(J-3)
```

```
40 U(I)=U(I-1)+DZN*(1.25*DU(J)+2.*DU(J-1)-DU(J-2)/4.)
   IF (1.+VW*U(I)) 70,41,41
41 YT=(-Y(I)*SQRT(1.+VW*U(I)))/A
   PH(I)=(1.-C1*EXP(YT)+C2*EXP(YT*D/E))**2
45 DU1=DU(J)
   ARG=1.+4.*(AK*Y(I))**2*PH(I)*(1.+VW*U(I))
   IF (ARG)70,46,46
46 ROT=SQRT(ARG)
   DUY=(2.*(1.+VW*U(I))*Y(I))/(1.+ROT)
   IF (DUY-0.001)70,47,47
47 DF1=DUY-DU1
   GO TO (48,51),M
48 DU(J)=DUY
   M=2
   GO TO 52
51 DU(J)=(DU2-DU1)/(DF1-DF2)*DF1+DU(J)
52 DF2=DF1
   DU2=DU1
   IF(ABS(DF1/DU1)-0.0001)55,55,40
55 RDU=DUY/Y(I)
   TAUT=1.-RDU+VW*U(I)
   WRITE (12,5) I,Y(I),U(I),RDU,TAUT,EPD,EMU
   M=1
   GO TO 31
70 IL=I-1
   YL=Y(I-1)
   L=2
   WRITE (12,7) IL,YL
   GO TO 12
82 IF (C2)12,12,71
71 E=E+10
   IF (E-60.)8,8,12
   END
```

II PROGRAM FOR PLOTTING EXPERIMENTAL VELOCITY PROFILES FOR DATA SMOOTHING

Program Symbol	Analysis Symbol	Note
Input:		
ILANK		= "blank"
IOT		= . (period)
IX		= x
AIO		= 0.826 specific gravity
CO		= 20 ° tilting angle of manometer
N		Number of data points
FV	$P_t - P_s$	Manometer reading, in.
YL	y	
Output:		
Y(I)	y	
B(I)	y/σ	
VB(I)	U/U_o	

```
      DIMENSION V(52),Y(52),B(52),VB(52),L(101),VBN(101)
    1 FORMAT (3A1)
    2 FORMAT (2F10.5,I2)
    3 FORMAT (2F10.5)
    4 FORMAT (1H ,2F16.6)
    5 FORMAT (1H ,8X,101I1)
    6 FORMAT (1H ,8X,101A1)
    7 FORMAT (1H ,F8.4,101A1,F8.5)
    8 FORMAT (1H ,10X,52I1)
    9 FORMAT (1H ,10X,52A1)
   10 FORMAT (1H ,F10.5,52A1,5F8.5)
  101 FORMAT (1H1,20X,8HPLOTTING//)
  102 FORMAT (1H1,20X,10HTABULATING///)
  103 FORMAT (1H1,20X,24HDIMENSIONLESS TABULATING///)
  104 FORMAT (1H+,11X,51A1)
  105 FORMAT (1H0,7HNEW SET/)
   11 READ (11,1) ILANK,IOT,IX
   12 READ (11,2) AIO,CO,N
   13 READ (11,3) FV,YL
      CO=3.14159*CO/180.
      FV=FV/1.53
      FV=SQRT(FV*SIN(CO)*AIO*62.2*64.4/(12.*0.07044))
      WRITE (12,102)
      DO 14 I= 1,N
      READ (11,3) Y(I),V(I)
      V(I)=V(I)/1.53
      V(I)=SQRT(V(I)*SIN(CO)*AIO*62.2*64.4/(12.*0.07044))
      WRITE (12,4) Y(I),V(I)
   14 CONTINUE
      WRITE (12,103)
      WRITE (13,105)
      DO 15 I=1,N
      B(I)=Y(I)/YL
      VB(I)=V(I)/FV
      WRITE (12,4) B(I),VB(I)
      WRITE (13,4) Y(I),VB(I)
   15 CONTINUE
      WRITE (12,101)
      DO 16 I=1,100
   16 L(I)=0
      L(101)=1
      WRITE (12,5)  (L(I), I=1,101)
      DO 17 I=1,101
   17 L(I)=IOT
      WRITE (12,6)  (L(I), I=1,101)
      N1=1
      N2=10
      NN=0
```

```
 18 DO 19 I=N1,N2
 19 L(I)=NN
    N1=N1+10
    N2=N2+10
    NN=NN+1
    IF (N2-100) 18,18,20
 20 L(101)=0
    WRITE (12,5) (L(I), I=1,101)
    N1=1
    N2=10
 23 NN=0
 21 DO 22 I=N1,N2
    L(I)=NN
 22 NN=NN+1
    N1=N1+10
    N2=N2+10
    IF (N2-100) 23,23,24
 24 WRITE (12,5) (L(I), I=1,101)
    DO 80 I=1,101
 80 VBN(I)=0.
    NB=1
    UD=0.01
 84 I=1
 25 F=B(I)-UD
    IF (F) 27,30,28
 27 IF (ABS(F)-0.005) 30,30,29
 28 IF (ABS(F)-0.005) 30,29,29
 29 VBN(NB)=0.
    I=I+1
    IF (I-N) 25,25,86
 30 VBN(NB)=VB(I)
    I=I+1
    IF (B(I)-UD+0.002) 25,25,86
 86 UD=UD+0.01
    NB=NB+1
 31 IF (NB-100) 84,84,32
 32 UD=0.01
    VBN(100)=1.
 33 DO 40 I=1,100
    F=VBN(I)-UD
    IF (F) 34,37,36
 34 IF (ABS(F)-0.005) 37,37,38
 36 IF (ABS(F)-0.005) 37,38,38
 37 L(I)=IX
    NB=I
    GO TO 40
 38 L(I)=ILANK
 40 CONTINUE
```

```
      WRITE (12,7) UD,IOT,(L(I), I=1,100),VBN(NB)
      NB=101
      UD=UD+0.01
      IF (UD-1.0) 33,33,41
   41 WRITE (12,101)
      DO 42 I=1,23
   42 L(I)=0
      N1=24
      N2=28
      NN=1
   43 DO 44 I=N1,N2
   44 L(I)=NN
      NN=NN+1
      N1=N1+5
      N2=N2+5
      IF (N2-53) 43,43,45
   45 WRITE (12,8) (L(I), I=1,52)
      DO 46 I=1,52
   46 L(I)=IOT
      WRITE (12,9) (L(I), I=1,52)
      DO 47 I=1,14
   47 L(I)=0
      NN=1
      DO 48 I=15,23
      L(I)=NN
   48 NN=NN+1
      N1=24
      N2=28
   49 NN=0
      DO 50 I= N1,N2
      L(I)=NN
   50 NN=NN+2
      N1=N1+5
      N2=N2+5
      IF (N2-53) 49,49,51
   51 WRITE (12,8) (L(I), I=1,52)
      DO 52 I=1,5
   52 L(I)=0
      NN=1
      DO 53 I=6,14
      L(I)=NN
   53 NN=NN+1
      DO 54 I=15,52
   54 L(I)=0
      WRITE (12,8) (L(I), I=1,52)
      NN=0
      DO 55 I=1,5
      L(I)=NN
```

```
 55 NN=NN+2
    DO 56 I=6,52
 56 L(I)=0
    WRITE (12,8) (L(I), I=1,52)
    ML=1
    NN=N+1
    DO 57 I=NN,52
 57 L(I)=ILANK
    MM=1
    UD=0.001
 64 DO 63 I=1,5
 63 VBN(I)=0.
    N1=1
 58 DO 70 I=1,N
    F=VB(I)-UD
    IF (F) 59,60,61
 59 IF (ABS(F)-0.0005) 60,60,62
 61 IF (ABS(F)-0.0005) 60,62,62
 62 L(I)=ILANK
    GO TO 70
 60 L(I)=IX
    ML=2
    VBN(N1)=VB(I)
    N1=N1+1
    MM=2
 70 CONTINUE
    GO TO (72,71),MM
 71 WRITE (12,10) UD,IOT,(L(I), I=1,51),(VBN(I), I=1,5)
    GO TO (72,90),ML
 90 DO 91 I=1,N
 91 L(I)=IOT
    WRITE (12,104) (L(I), I=1,N )
 72 UD=UD+0.001
    ML=1
    IF (UD-1.0) 64,64,12
    END
```

III PROGRAM FOR CALCULATING θ, σ AND $C_f'/2$ BY EQ.(3-3)

Program Symbol	Analysis Symbol	Note
Input:		
X(I)	x	= 6, 12, 18, 24, 30, 36, 42, 48, 54, 60
UA	U_o	
VWX	V_w	
RAYL	RAYL	
DUA	dU_o/dx	
N		Numbers of velocity profile points
NS		Position of x
NSS		Numbers of sets of data
Output:		
XXX	x	
REY	R_x	
UAU	V_w/U_o	
RAYL	RAYL	
CF(I)	$C_f'/2$	
TAW(I)	τ_w	
PGRD	dU_o/dx	

```
      DIMENSION X(10),Y(52),U(52),CF(10),TAW(10),FN(620)
      DIMENSION XN(10),SIM(10),F(52),GN(620),GI(5)
      DIMENSION GIM(10),G(52),SI(5)
    1 FORMAT (10F7.3)
    2 FORMAT (F17.6,F16.6)
    3 FORMAT (3I3)
    4 FORMAT (4F10.5)
    5 FORMAT (1H0,7(2X,E10.3)///)
    6 FORMAT (1H ,3(4X,E12.5))
   11 READ (11,1) (X(I) ,I=1,10)
      DO 50 I=1,10
   50 X(I)=X(I)/12.
      RO=0.07044/32.2
      AMU=3.97/10.**7
   12 READ (11,4) UA,VWX,RAYL,DUA
      ND=1
      UAV=VWX/UA
   13 READ (11,3) N,NS,NSS
      II=1
   14 DO 15 I=1,N
      READ (11,2) Y(I),U(I)
      G(I)=(1.-U(I))
      F(I)=U(I)*G(I)
   15 CONTINUE
      FN(1)=0.
      GN(1)=0.
      FN(2)=F(1)/2.
      GN(2)=G(1)/2.
      NN=2
      DO 16 I=1,5
      J=I+NN
      FN(J)=F(I)
      GN(J)=G(I)
   16 NN=NN+1
      NN=3
      DO 17 I=1,4
      J=I+NN
      FN(J)=(F(I+1)+F(I))/2.
      GN(J)=(G(I+1)+G(I))/2.
   17 NN=NN+1
      SUM1=0.
      SUM2=0.
      GUM1=0.
      GUM2=0.
      DO 18 I=2,10,2
      GUM1=GUM1+4.*GN(I)
   18 SUM1=SUM1+4.*FN(I)
      DO 19 I=3,9,2
```

```
      GUM2=GUM2+2.*GN(I)
   19 SUM2=SUM2+2.*FN(I)
      K=1
      SI(1)=0.001*(FN(1)+SUM1+SUM2+FN(11))/(36.)
      GI(1)=0.001*(GN(1)+GUM1+GUM2+GN(11))/(36.)
      F(4)=0.
      G(4)=0.
      N1=1
      N2=10
      I=5
      H=0.01
   20 YD=0.
      DO 21 J=N1,N2
      FN(J)=F(I)+(YD/H)*(F(I+1)-F(I-1))/2.+(YD/H)**2*(F
     1      (I+1)-2.*F(I)+F(I-1))/2.
      GN(J)=G(I)+(YD/H)*(G(I+1)-G(I-1))/2.+(YD/H)**2*(G
     1      (I+1)-2.*G(I)+G(I-1))/2.
   21 YD=YD+0.001
      I=I+1
      IF (I-N) 51,52,52
   52 II=2
      GO TO 53
   51 IF (I-13) 60,60,221
   60 N1=N1+10
      N2=N2+10
      GO TO 20
  221 FN(91)=F(14)
      GN(91) =G(14)
   53 SUM1=0.
      SUM2=0.
      GUM1=0.
      GUM2=0.
      DO 22 I=2,N2,2
      GUM1=GUM1+4.*GN(I)
   22 SUM1=SUM1+4.*FN(I)
      N2=N2-1
      DO 23 I=3,N2,2
      GUM2=GUM2+2.*GN(I)
   23 SUM2=SUM2+2.*FN(I)
      K=K+1
      GO TO (54,55),II
   55 SI(2)=0.001*(FN(1)+SUM1+SUM2+F(N  ))/36.
      GI(2)=0.001*(GN(1)+GUM1+GUM2+G(N  ))/36.
      GO TO 40
   54 SI(2)=0.001*(FN(1)+SUM1+SUM2+FN(91))/36.
      GI(2)=0.001*(GN(1)+GUM1+GUM2+GN(91))/36.
      F(13)=0.
      G(13)=0.
```

```
      N1=1
      N2=10
      I=14
      H=0.1
   24 YD=0.
      DO 25 J=N1,N2
      FN(J)=F(I)+(YD/H)*(F(I+1)-F(I-1))/2.+(YD/H)**2*(F
     1       (I+1)-2.*F(I)+F(I-1))/2.
      GN(J)=G(I)+(YD/H)*(G(I+1)-G(I-1))/2.+(YD/H)**2*(G
     1       (I+1)-2.*G(I)+G(I-1))/2.
   25 YD=YD+0.01
      I=I+1
      IF (I-N) 26,131,131
  131 II=2
      GO TO 28
   26 IF (I-23) 27,28,28
   27 N1=N1+10
      N2=N2+10
      GO TO 24
   28 SUM1=0.
      SUM2=0.
      GUM1=0.
      GUM2=0.
      DO 29 I=2,N2,2
      GUM1=GUM1+4.*GN(I)
   29 SUM1=SUM1+4.*FN(I)
      N2=N2-1
      DO 30 I=3,N2,2
      GUM2=GUM2+2.*GN(I)
   30 SUM2=SUM2+2.*FN(I)
      GO TO (31,32),II
   32 K=K+1
      SI(K)=0.01*(FN(1)+SUM1+SUM2+F(N))/36.
      GI(K)=0.01*(GN(1)+GUM1+GUM2+G(N))/36.
      GO TO 40
   31 K=K+1
      SI(K)=0.01*(FN(1)+SUM1+SUM2+F(23))/36.
      GI(K)=0.01*(GN(1)+GUM1+GUM2+G(23))/36.
      F(22)=F(21)
      G(22)=G(21)
      N1=1
      N2=20
      I=23
      H=0.2
  132 YD=0.
      DO 33 J=N1,N2
      FN(J)=F(I)+(YD/H)*(F(I+1)-F(I-1))/2.+(YD/H)**2*(F
     1       (I+1)-2.*F(I)+F(I-1))/2.
```

```
      GN(J)=G(I)+(YD/H)*(G(I+1)-G(I-1))/2.+(YD/H)**2*(G
     1       (I+1)-2.*G(I)+G(I-1))/2.
   33 YD=YD+0.01
      I=I+1
      IF (I-N) 34,35,35
   34 N1=N1+20
      N2=N2+20
      GO TO132
   35 SUM1=0.
      SUM2=0.
      GUM1=0.
      GUM2=0.
      DO 36 I=2,N2,2
      GUM1=GUM1+4.*GN(I)
   36 SUM1=SUM1+4.*FN(I)
      N2=N2-1
      DO 37 I=3,N2,2
      GUM2=GUM2+2.*GN(I)
   37 SUM2=SUM2+2.*FN(I)
      K=K+1
      SI(K)=0.01*(FN(1)+SUM1+SUM2+F(N))/36.
      GI(K)=0.01*(GN(1)+GUM1+GUM2+G(N))/36.
   40 SIMP=0.
      GIMP=0.
      DO 41 I=1,K
      GIMP=GIMP+GI(I)
   41 SIMP=SIMP+SI(I)
      SIM(ND)=SIMP
      GIM(ND)=GIMP
      XN(ND)=X(NS)
      GIMND=GIM(ND)*12.
      SIMND=SIM(ND)*12.
      WRITE (12,6) SIMND,GIMND,XN(ND)
      ND=ND+1
      IF (ND-NSS) 13,13,42
   42 I=1
   43 CF(I)=(SIM(I+1)-SIM(I))/(XN(I+1)-XN(I))-UAV
     1       +(2.+GIM(I+1)/SIM(I+1))*SIM(I+1)*DUA/UA
      TAW(I)=RO*UA**2*CF(I)
      XXX=XN(I+1)
      REY=RO*UA*XXX/AMU
      PGRD=UA*DUA*RO
      WRITE (12,5) XXX,REY,UAV,RAYL,CF(I),TAW(I),PGRD
      I=I+1
      IF (I-(NSS-1)) 43,43,12
      END
```

IV PROGRAM FOR CALCULATING $C_f/2$ BY EQ. (3-4)

Program Symbol	Analysis Symbol	Note
Input:		
PSIN1	$P_{t_o} - P_s$	Free stream manometer reading, in.
CO		= 20° tilting angle
D	d	
PP	$P_t - P_s$	Boundary layer manometer reading, in.
X	x	
RAYL	RAYL	
Output:		
D	d	
UA	U_o	
TAW	τ_w	
CF	$C_f/2$	
REY	R_x	
RAYL	RAYL	

```
  1 FORMAT (F12.7)
  2 FORMAT (2F10.5)
  3 FORMAT (1H0,6(3X,E12.5))
 12 READ (11,1) PSIN1
    READ (11,1) CO
 11 READ (11,1) D
    READ (11,1) PP
    READ (11,2) X,RAYL
    RO=0.07044/32.2
    AMU=3.97/10**7
    ANU=AMU/RO
    PSIN1=     PSIN1*SIN(CO*3.14159/180.)/1.53
    UA=SQRT(2.*(PSIN1   )*0.826*62.2/(RO*12.))
    PP=PP*0.826*62.2/12.*SIN(CO*3.14159/180.)/1.53
    A=0.875*ALOG10((PP/144.)*D*D/(4.*RO*ANU**2))-1.396
    TAW=4.*RO*ANU**2*10.**A/(D*D)*144.
    REY=UA*X/(12.*ANU)
    CF=TAW/(RO*UA*UA)
    WRITE (12,3) D,UA,TAW,CF,REY,RAYL
    GO TO 12
    END
```

V PROGRAM FOR CALCULATING EXPERIMENTAL SHEAR VELOCITY DISTRIBUTION

Program Symbol	Analysis Symbol	Note
Input:		
UAO	U_o	Run with no injection or suction
UA	U_o	Run with injection or suction of same panel
RAYL	RAYL	
VW	V_w	
X	x	
UKS	$U_o E/\upsilon$	Run with no injection or suction
N		Numbers of velocity profile points
TAW	τ_w	
Y(I)	y	
U(I)	U/U_o	
Output:		
VWT	V_{w*}	
E	E_*	
UKS	$U_o E/\upsilon$	
RAYL	RAYL	
X	x	
YI(I)	y_*	
UT(I)	U_*	
YN	y	
U(I)	U/U_o	

```
      DIMENSION Y(52),U(52),YT(52),UT(52)
    1 FORMAT (5F10.5,2E10.3,I2)
    2 FORMAT (F17.6,F16.6)
    3 FORMAT (1H ,2(5X,E11.4))
    4 FORMAT (1H1,3(2X,E11.4),2(2X,F10.5)///)
    5 FORMAT (1H1,14HNONDIMENSIONAL///)
      AMU=3.97/10.**7
      RO=0.07044/32.2
   11 READ (11,1) UAO,UA,RAYL,VW,X,UKS,TAW,N
      DO 12 I=1,N
   12 READ (11,2) Y(I),U(I)
      UKS=UKS*UA/UAO
      ANU=AMU/RO
      TC=SQRT(TAW/RO)
      VWT=VW/TC
      E=UKS*TC/UA
      WRITE (12,4) VWT,E,UKS,RAYL,X
      DO 14 I=1,N
      YT(I)=Y(I)*TC/ANU
      UT(I)=U(I)*UA/TC
   14 WRITE (12,3) YT(I),UT(I)
      WRITE (12,5)
      DO 15 I=1,N
      YN=Y(I)/Y(N)
   15 WRITE (12,2) YN,U(I)
      GO TO 11
      END
```